UNIVERSITY OF CALIFORNIA, SAN DIEGO

Deconstruction of neural circuits provides insights into complex network function

A dissertation submitted in partial satisfaction of the requirements for the degree Doctor of Philosophy

in

Biology

by

Matthew John Sternfeld

Committee in charge:

Professor Samuel L. Pfaff, Chair
Professor Sreekanth Chalasani
Professor Nicholas C. Spitzer
Professor Mark H. Tuszynski
Professor Eugene W. Yeo

2016

The Dissertation of Matthew John Sternfeld is approved, and it is acceptable in quality and form for publication on microfilm and electronically:

_____

_____

_____

_____

_____

Chair

University of California, San Diego

2016

TABLE OF CONTENTS

LIST OF OF FIGURES

LIST OF ABBREVIATIONS

μV	microVolt
5-HT	Serotonin
ACSF	Artificial cerebrospinal fluid
ALS	Amyotrophic lateral sclerosis
bHLH	Basic helix–loop–helix transcription factor
BMP	Bone morphogenetic protein
C.V.	Coefficient of variation
CAG	CAG promoter
Chx10	Visual System Homeobox 2
CNQX	6-Cyano-7-nitroquinoxaline-2,3-dione
CNS	Central nervous system
CPG	Central pattern generator
Cre	Cre recombinase
dF/F	Change in fluorescence divided by baseline fluorescence
dhβe	Dihydro-β-erythroidine hydrobromide
dI1	Dorsal interneuron Class 1
dI2	Dorsal interneuron Class 2
dI3	Dorsal interneuron Class 3
dI4	Dorsal interneuron Class 4
dI5	Dorsal interneuron Class 5
dI6	Dorsal interneuron Class 6
dILA	Late-born dorsal interneuron class A
dILB	Late-born dorsal interneuron class B
DTA	Diptheria toxin subunit A
e	Mouse embryonic day
E/I	Excitatory-to-inhibitory ratio
En1	Engrailed Homeobox 1

ESC	Embryonic stem cell
ESC-MN	ESC-derived motor neuron
GABA	Gamma aminobutyric acid
Gata3	GATA Binding Protein 3
GCaMP3	Genetically encoded calcium indicator
GFP	Green fluorescent protein
Hb9	Motor Neuron And Pancreas Homeobox 1
HMC	Hypaxial motor column
I.C.V.	Interval coefficient of variation
iPS	Induced pluripotent stem cell
LIM-HD	LIM homeodomain transcription factor
LMC	Lateral motor column
LMCl	LMC lateral division
LMCm	LMC medial division
LSL	Lox-stop-lox
mESC	Mouse embryonic stem cell
Min	Minute
MMC	Medial motor column
MN	Motor neuron
MN+V1	Mixed networks of MNs and V1 interneurons
Neo	Neomycin
NMA	N-Methyl-DL-aspartic acid
NMDA	N-Methyl-D-aspartic acid
OLP	Oligodendrocyte precursor
P	Mouse postnatal day
p0	V0 interneuron progenitor domain
p1	V1 interneuron progenitor domain
p2	V2 interneuron progenitor domain
p3	V3 interneuron progenitor domain

PC	Principle component
PCR	Polymerase chain reaction
pdI1	dI1 dorsal interneuron progenitor domain
pdI2	dI2 dorsal interneuron progenitor domain
pdI3	dI3 dorsal interneuron progenitor domain
pdI4	dI4 dorsal interneuron progenitor domain
pdI5	dI5 dorsal interneuron progenitor domain
pdI6	dI6 dorsal interneuron progenitor domain
pdIL	dILA–dILB late-born interneuron progenitor domain
PGC	Preganglionic motor column
pMN	Motor neuron progenitor domain
polyA	Polyadenylation tail
R26	Rosa locus
R26/C	R26 with inserted CAG promoter
RA	Retinoic acid
ROI	Region of interest
SAG	Smoothened agonist
Sec	Second
Shh	Sonic hedgehog
Sim1	Single-minded family bHLH transcription factor 1
SMA	Spinal muscular atrophy
V0	Ventral interneuron Class 0
V1	Ventral interneuron Class 1
V2	Ventral interneuron Class 2
V3	Ventral interneuron Class 3
$V3^{-/-}$	Genetic ablation of V3 interneurons
V3+V1	Mixed networks of V3 and V1 interneurons

LIST OF SUPPLEMENTARY MATERIALS

ACKNOWLEDGEMENTS

Chapter 1, in full, is a reprint of the material as it appears in Gifford, W.D., Hayashi, M., Sternfeld, M.J., Tsai, J., Alaynick, W.A., & Pfaff, S.L. (2013). Chapter 7 - Spinal Cord Patterning. Pattering and Cell Type Specification in the Developing CNS and PNS: Comprehensive Developmental Neuroscience (Vol. 1). Academic Press. http://doi.org/10.1016/B978-0-12-397265-1.00047-2. The thesis author was the third author of this paper.

Chapter 2 is an adaptation of a manuscript being prepared for submission. The working citation is: Matthew J. Sternfeld, Christopher A. Hinckley, Matthew T. Pankratz, Kathryn L. Hilde, Shawn P. Driscoll, Samuel L. Pfaff. Differential roles for inhibitory neurons revealed through creation of cell-type specific *de novo* networks. The authors would like to thank Martyn Goulding and Kamal Sharma for providing interneuron Cre-recombinase mouse lines used for generating mESCs; Karen Lettieri for continuous mouse colony support; the Salk Institute FCCF run by Carolyn O'Connor and Conor Fitzpatrick; and Dario Bonanomi, Ariel Levine, and Marito Hayashi for support and advice.

Chapter 3 is a summary list of future directions that build upon the work described in Chapter 2. It is the hope that these initial experiments or concepts will be a starting block for those looking to continue my work as their own. For this chapter I would like to thank Matthew T. Pankratz for his work in demonstrating the neurite outgrowth capability of plated young and old neurospheres and Mark Tuszynski's lab for their work in injecting our cells into spinally injured animals.

In addition to the help of those in the chapters described above, I would like to thank several individuals for their help, guidance, and support while in graduate school. To my fellow graduate students – Marito, Kathryn, Neal, and Wes – thank you for all of the wonderful conversations, intellectual and otherwise, we've had. The years faced in graduate school were dramatically eased knowing you were all in "it" with me. Ariel, thank you for every piece of advice you've ever given me; you've helped my growth considerably. Pankratz, thank you for all of your support, both personal and professional, including, but certainly not limited to, working through every cell culture issue with me. It was relieving to know someone was in the trenches

with me. Chris, your help in fitting my work into the larger backdrop of the CPG literature, in addition to all your other insights were invaluable. Dario, our conversations have been incredible and I can't thank you enough for your kindness and patience in helping me organize my figures, presentations, and papers. You all have helped to make the time I've spent in the Pfaff lab a tremendously positive experience.

Finally, Sam. Thank you for all of the guidance, support, and freedom you have provided me. The culture of high quality science in our lab stems from you, down through the post-docs and graduate students you select to join your lab. It is because of you and this culture that I have grown as a scientist more than I ever thought possible. I promise to use everything I have learned from you in all my future endeavors.

VITA

2002-2006	Carleton College Bachelor of Arts - Neuroscience *Magna cum laude* *Phi beta kappa*
2008-2016	University of California, San Diego The Salk Institute for Biological Studies Doctor of Philosophy - Biology
2010	UCSD Neurosciences Training Grant (NIH)
2010-2012	Christopher and Dana Reeve Foundation
2012-2013	H.A. and Mary K. Chapman Foundation Charitable Trust Scholarship
2013-2015	Rose Hills Foundation Graduate Fellowship
2015-Present	Christopher and Dana Reeve Foundation

PUBLICATIONS

Peer Reviewed Original Research

Sternfeld, M.J., Hinckley, C.A., Pankratz, M.J., Hilde, K.L., Driscoll, S.P., Pfaff, S.L., Differential roles for inhibitory neurons revealed through creation of cell-type specific *de novo* networks (manuscript in preparation for *Cell*)

Amin, N.D., Bai, G., Klug, J.R., Bonanomi, D., Pankratz, M.T., Gifford, W.D., Hinckley, C.A., **Sternfeld, M.J.**, Driscoll, S.P., Dominguez, B., Lee, K., Jin, X., Pfaff, S.L., Loss of motoneuron-specific microRNA-218 causes systemic neuromuscular failure. *Science*, 350(6267), 1525–1529. http://doi.org/10.1126/science.aad2509

Peer Reviewed Literature Review

Gifford, W.D., Hayashi, M., **Sternfeld, M.J.**, Tsai, J., Alaynick, W.A., & Pfaff, S.L., Chapter 7 - Spinal Cord Patterning, *Patterning and Cell Type Specification in the Developing CNS and PNS*, edited by John L.R. Rubenstein Pasko Rakic, Academic Press, Oxford, 2013, Pages 131-149, http://dx.doi.org/10.1016/B978-0-12-397265-1.00047-2.

ABSTRACT OF THE DISSERTATION

Deconstruction of neural circuits provides
insights into complex network function

by

Matthew John Sternfeld

Doctor of Philosophy in Biology
University of California, San Diego, 2016
Professor Samuel L. Pfaff, Chair

The neuronal subtypes that compose the locomotor central pattern generator (CPG) are found in the ventral horn of the spinal cord. Numerous studies have ablated neuronal subtypes and observed the altered activity in an experimental design called fictive locomotion. These ablation studies have provided great insight into the locomotor CPG, but the remaining network is still complex, making it difficult to obtain deep insight into how the circuit actually functions. To simplify this network, we set out to generate an *in vitro* stand-in for the locomotor CPG that

involved differentiating mouse embryonic stem cells (mESCs) into the neurons that comprise the locomotor CPG.

This dissertation describes a series of original work that aims to elucidate the contributions that different cellular components play in the final output of the locomotor CPG. The first chapter is an introduction into the developmental processes of spinal cord development and the diseases that result when such patterning does not occur properly.

The second chapter proceeds from this review to describe a unique and powerful new technique that allows us to separate the complex locomotor CPG into its cardinal neuronal subtypes. From these component parts, we then generated highly defined *de novo* networks to determine how a network composed of individual neuronal subtypes behaved. Finally, we mixed one inhibitory neuronal subtype into different pure excitatory neuronal subtype based networks. From these mixing studies we were able to determine that this one inhibitory neuronal subtype has strikingly diverse functions in different excitatory networks.

The third chapter discusses future directions for the work described in Chapter 2. Initially I explain how an extension of the experiments conducted in Chapter 2 could be used to address remaining questions about the locomotor CPG. From there I move on to describe how alterations to the basic experimental designs from Chapter 2 would allow for new, diverse, and exciting experimental questions to be asked. All together, Chapter 3 expands upon the work I have conducted in graduate school and suggests different sets of experiments that I believe would result in many interesting works in their own right.

Chapter 1

Introduction:
Spinal cord pattering

CHAPTER

7

Spinal Cord Patterning

W.D. Gifford, M. Hayashi, M. Sternfeld, J. Tsai, W.A. Alaynick, S.L. Pfaff

Howard Hughes Medical Institute, La Jolla, CA, USA; Salk Institute for Biological Studies, La Jolla, CA, USA

OUTLINE

Nomenclature

ALS Amyotrophic lateral sclerosis
bHLH Basic helix–loop–helix transcription factor
BMP Bone morphogenetic protein
CNS Central nervous system
dI1 Dorsal interneuron Class 1
dI2 Dorsal interneuron Class 2
dI3 Dorsal interneuron Class 3
dI4 Dorsal interneuron Class 4
dI5 Dorsal interneuron Class 5
dI6 Dorsal interneuron Class 6
dIL$_A$ Late-born dorsal interneuron class A
dIL$_B$ Late-born dorsal interneuron class B
E9.5 Embryonic day 9.5
ESC Embryonic stem cell
ESC-MN ESC-derived motor neuron
HMC Hypaxial motor column
iPS Induced pluripotent stem cell
LIM-HD LIM homeodomain transcription factor
LMC Lateral motor column
LMCl LMC lateral division
LMCm LMC medial division
MMC Medial motor column
MN Motor neuron
OLP Oligodendrocyte precursor
p0 V0 interneuron progenitor domain
p1 V1 interneuron progenitor domain
p2 V2 interneuron progenitor domain
p3 V3 interneuron progenitor domain
pdI1 dI1 dorsal interneuron progenitor domain
pdI2 dI2 dorsal interneuron progenitor domain
pdI3 dI3 dorsal interneuron progenitor domain
pdI4 dI4 dorsal interneuron progenitor domain
pdI5 dI5 dorsal interneuron progenitor domain
pdI6 dI6 dorsal interneuron progenitor domain
pdIL dIL$_A$–dIL$_B$ late-born interneuron progenitor domain
PGC Preganglionic motor column

Patterning and Cell Type Specification in the Developing CNS and PNS: Comprehensive Developmental Neuroscience, Volume 1 http://dx.doi.org/10.1016/B978-0-12-397265-1.00047-2

pMN Motor neuron progenitor domain
Shh Sonic hedgehog
SMA Spinal muscular atrophy
V0 Ventral interneuron Class 0
V1 Ventral interneuron Class 1
V2 Ventral interneuron Class 2
V3 Ventral interneuron Class 3

7.1 INTRODUCTION

The vertebrate spinal cord serves two basic functions for the organism. First, it relays sensory information from the periphery along a number of white matter tracts to the brain, where it is processed and informs the organism about the internal state of the body and position in space (interoception, proprioception) and the influences of the outside world upon the body (somatosensation). Second, it transmits motor information from the brain along white matter tracts to control the stability and movement of the body in space. However, the concept of the spinal cord as simply a collection of axonal conduits between the brain and the periphery is both factually oversimplified and a poor metaphor because the spinal cord is a highly complex neuronal structure that actively processes and modulates ascending and descending information and mediates compound reflexes (Figure 7.1). In fact, the spinal cord performs a number of sensorimotor computations, most notably those required for the proper control of movement. Classical experiments have demonstrated that a decerebrated cat preparation, when suspended above a treadmill, is capable of coordinated locomotion despite loss of descending control from the brain (Brown, 1911). It is now well accepted that the spinal cord contains the basic circuitry responsible for proper species-specific coordination of left versus right, flexor versus extensor, and forelimb versus hindlimb movement. For recent reviews on spinal locomotor circuitry, the reader is referred elsewhere (Goulding, 2009; Grillner and Jessell, 2009).

How does the spinal cord develop in the embryo? While a full answer to this question requires extensive scientific characterization at the molecular, cellular, and circuit levels, as well as an understanding of the roles that neural activity and experience play on developmental processes, this chapter focuses primarily on the generation of the distinct cell types that are specified by patterns of morphogen gradients. This focus can be explained by the wealth of information that has come out of studies over the last 20 years that were aimed at describing the basis for behaviors mediated by the spinal cord at the cellular level. Because of this work, a framework that assigns neuronal identity and diversity in the spinal cord based upon expression of transcription factors has now reached a more mature state and can be used to inform studies of other central nervous system (CNS) regions (Alaynick et al., 2011). Other developmental neuroscience topics important for understanding spinal cord function, such as early neural tube formation, neurogenesis, axon guidance, and postnatal developmental processes, are discussed elsewhere.

FIGURE 7.1 The black box of spinal cord circuitry. The spinal cord receives descending input from the brain and ascending information from the periphery, which it can modulate or process accordingly. Additionally, it has been shown that the spinal cord has the ability to produce movements independently of these inputs. The capacity to carry out diverse functions relies on the generation of many cell types that arise from an elegant system of patterning and transcriptional control, which is described in this chapter. These findings have helped to illuminate many components in this black box.

The molecular mechanisms of neuronal specification in this chapter have been the product of over a century of research using a variety of model systems. The six most widely used organisms in this regard are mouse, chicken, frog, zebra fish, fly, and worm. Each of these model organisms provides unique experimental tools that can be leveraged to better understand spinal cord patterning, such as mammalian genetics in mouse and optically accessible vertebrate development in zebra fish. Importantly, while many findings made in these organisms apply to human spinal cord development, this has not been directly demonstrated in most cases. Future work using fetal material and human embryonic stem cells (ESCs) may prove informative in this regard.

7.2 MAJOR CONCEPTS OF SPINAL CORD PATTERNING

A fundamental concept of spinal cord patterning is that the early embryonic neural tube is comprised of a largely unspecified pool of immature cells that are

capable of differentiating into any one of the many unique cell types in the spinal cord. Spinal cord organization results from uncommitted progenitor cells responding to positional cues that come from neighboring tissues that instruct the cells. These instructions come first in the form of morphogen gradients along three orthogonal axes: mediolateral, dorsoventral, and rostrocaudal. In effect, these axes define a three-dimensional Cartesian coordinate system in which each 'point' represents an uncommitted spinal cord cell that receives a unique complement of signals based upon its particular point in space (Figure 7.2). While there is a biological basis for considering these axes independently, it should be remembered that there is a complex interplay of factors across these axes over time.

The signals that act on the naïve spinal progenitor cells take one of two general forms. First, there are long-range secreted factors that are released from neighboring tissues and diffuse to their targets. These factors include sonic hedgehog (Shh) from the ventral notochord, bone morphogenetic proteins (BMPs), and wingless MMTV integration site proteins (Wnts) from the overlying ectoderm, and retinoic acid (RA) produced by the activity of retinaldehyde dehydrogenase (*Raldh*) in the paraxial mesoderm. A second short-range signaling strategy arises from membrane-bound molecules that mediate local cell–cell interactions, such as the Notch–Delta pathway (Figure 7.4). Some factors, like Shh, induce different cellular responses in a graded, concentration-dependent manner. Others, like Notch signaling, function with a binary (on/off) mechanism. The consequence for a particular cell depends on (1) the unique combination and concentration of secreted and fixed signals it receives from its environment; and (2) the extent to which prior signaling has rendered the cell competent to receive or integrate new signals.

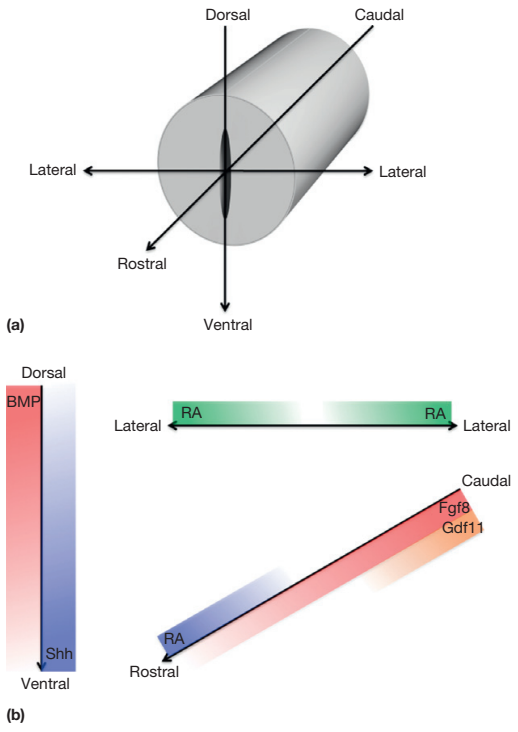

FIGURE 7.2 Cartesian coordinate system framework of spinal cord development. (a) The embryonic spinal cord tissue can be mapped in space along three axes: dorsoventral, rostrocaudal, and mediolateral. (b) Along these principal axes, gradients of morphogens induce cell-type-specific patterns of gene expression. High concentrations of Shh induce ventral cell fates while high concentrations of BMPs induce dorsal cell fates. Similarly, RA, FGF8, and Gdf11 regulate positional identity along the rostrocaudal axis.

These signaling molecules can exert lasting effects through signaling cascades that regulate the expression of transcription factors that produce gene expression changes capable of specifying cell fate. Borders between adjacent classes of cells (which receive roughly equivalent fate-instructive signals) must be clearly defined to avoid hybrid identities. This is accomplished by the elegant strategy of cross-repression, which has been well characterized in the ventral spinal cord. With this system, fate-specifying transcription factors of bordering cell types act to reciprocally repress one another. As a result, when a cell-type-specific transcription factor is expressed, it will directly inhibit the expression of other transcription factors that could serve to alter the identity of that cell. If two cross-repressive transcription factors are under the control of a single morphogen (such as Shh), then both factors may be briefly coexpressed. But the 'winner-takes-all' process of cross-repression ensures that only one specific cell identity is ultimately generated (Figure 7.7).

While signaling molecules set up a coarse coordinate system within the spinal cord that is refined by transcriptional cross-repression, generating a specific cell type results from the coactivation of a unique combination of transcription factors. Such combinations of transcription factors can interact at the protein level to form higher-order complexes that then recognize distinct DNA regulatory elements. This increased level of complexity, shaped by binding partners, allows for diverse transcription factor-binding characteristics and gene expression profiles.

The remainder of this chapter will survey research from many studies of spinal cord patterning with particular attention to features that are well studied. At the end of the chapter, human diseases of spinal cord patterning and the implications of the lessons learned from spinal cord patterning for regenerative medicine will be discussed.

7.3 DORSOVENTRAL PATTERNING

The dorsal portion of the spinal cord is primarily composed of interneurons that receive and process sensory input from peripheral neurons of the dorsal root ganglia, while the ventral spinal cord is generally thought to be dedicated to the processing of motor output. This gross dorsoventral division in sensory and motor function reflects the dorsoventral-patterning mechanisms in early spinal cord development. Within the ventricular zone of the spinal cord, many progenitor domains are established which give rise to distinct neuronal and glial lineages. As these progenitors mature during midgestion, they stop dividing, express further transcriptional programs important for differentiation, and migrate to stereotypic locations in the mantle layer (Jessell, 2000; Shirasaki and Pfaff, 2002).

Based on the expression patterns of various marker genes along the dorsoventral axis, six interneuron progenitor domains (dp1–6) have been designated in the dorsal spinal cord, while five progenitor domains have been designated in the ventral spinal cord (p0–3, pMN). Each of these progenitors then gives rise to a corresponding neuron population, dI1–dI6 interneurons in the dorsal spinal cord, and V0–V3 interneurons and motor neurons (MNs) in the ventral spinal cord (Alaynick et al., 2011; Goulding, 2009; Jessell, 2000; Shirasaki and Pfaff, 2002). This diversity in progenitor domains and their corresponding mature neural subtypes can be seen in Figures 7.6 and 7.9. The principle signals important for generating these diverse cell types along the dorsoventral axis are Shh, BMPs, and Wnts.

7.3.1 Dorsoventral Patterning: Shh

The transduction of morphogen signaling through second messenger systems to regulate specific gene expression programs is a general feature of spinal cord patterning. The most well-studied morphogen, Shh, is expressed and secreted from the notochord, which then induces Shh expression from the floor plate (Jessell, 2000). As a result of this secretion pattern, local Shh concentration is high in the ventral cord and diminishes dorsally. Many experiments have shown the importance of this Shh gradient. For example, studies conducted by Ericson and colleagues using spinal cord explants showed that induction of V1-specific genes required lower Shh concentrations than induction of V2- or MN-specific genes. These levels of Shh corresponded to the relative dorsoventral positions of the progenitor domains (Ericson et al., 1997a,b). Furthermore, studies of *Shh* knockout mice have shown that the floor plate fails to develop and genes that are normally transcribed only in the dorsal region of the spinal cord expand their expression domains into the ventral spinal cord (Chiang et al., 1996). More recent work has shown that, in addition to the Shh concentration gradient, the duration of exposure and an additional gene regulatory network appear to be critical for induction of downstream genes in response to Shh (Balaskas et al., 2012; Dessaud et al., 2007).

To signal downstream genes, in the canonical Shh pathway, Shh binds to its receptor, patched-1 (PTCH1). In the absence of Shh, PTCH1 inhibits the transmembrane protein, smoothened (SMO; Figure 7.4(a)). When Shh binds to PTCH1, SMO is released from inhibition by PTCH1, possibly mediated by transfer of an oxysterol from PTCH1 to SMO (Corcoran and Scott, 2006). SMO is then free to activate the transcription factors GLI1–GLI3, which, in turn, regulate the expression of downstream genes (Fuccillo et al., 2006; Rahnama et al., 2006).

The concentration gradient of Shh (high ventrally to low dorsally) causes differential expression of various downstream genes in progenitors along the dorsoventral axis, and this is thought to be a major factor responsible for the diversification of spinal cord progenitor domains. So how do the different local concentrations of Shh result in differing downstream gene expression effects? As described earlier, three GLI proteins serve as intermediaries in the Shh pathway. In the most ventral spinal cord, Shh is found at its highest levels. At this location, GLI1 and GLI2 transcriptionally activate their targets, while GLI3 repressor activity is low. In more dorsal regions, where Shh concentration is lower, GLI1 and GLI2 are not readily active, while GLI3 actively represses its targets. The combined activity of all three GLI proteins results in differential expression of downstream genes, based on the concentration of Shh (Figure 7.3; Fuccillo et al., 2006).

7.3.2 Dorsoventral Patterning: BMPs

In the dorsal spinal cord, BMPs and other TGFβ family members (Bmp2, 4, 7, growth differentiation factor 7, activin, dorsalin) are secreted from the overlying ectoderm (Liem et al., 2000; Liu and Niswander, 2005). Binding of BMPs to their receptors (BMPRs) results in receptor phosphorylation. Phosphorylated BMPRs subsequently phosphorylate Smad proteins which associate with additional Smad mediator proteins facilitate either activation or repression of downstream genes (Liu and Niswander, 2005).

The importance of TGFβ family proteins in determining dorsal fates of spinal cord progenitors during development was demonstrated experimentally in a manner similar to the Shh work. In BMPR knockout mice, the most dorsal interneuron population (dI1) was not present, the dI2 population was significantly reduced, and

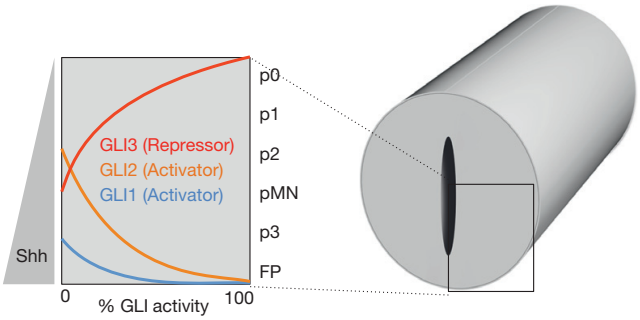

FIGURE 7.3 Shh regulates gene expression through modulation of GLI activity. Shh regulates the activity of the three GLI proteins. At the highest levels of Shh near the floor plate, for example, GLI1 and GLI2 transcriptionally activate their targets while GLI3 repressor activity is low. Reciprocally, at low levels of Shh, more dorsally, GLI1 and GLI2 are not readily active while GLI3 actively represses its targets. The net effect of differential GLI activity results in the induction of different sets of downstream genes. Gradients of other morphogens regulate their respective gene targets through similar intracellular machinery as that shown here for Shh. *Adapted with permission by Macmillan Publishers Ltd from Fuccillo M, Joyner AL, and Fishell G (2006) Morphogen to mitogen: The multiple roles of hedgehog signalling in vertebrate neural development.* Nature Reviews Neuroscience *7: 772–783.*

the dI3 and dI4 domains expanded dorsally, suggesting that BMP signaling is required for specification of the dorsal spinal cord (Wine-Lee et al., 2004). In a series of experiments, dorsal interneuron marker genes were shown to be upregulated in spinal cord explants by the application of various TGFβ family proteins (Liem et al., 1997). This was also observed when a constitutively active BMPR was ectopically expressed in chick spinal cords (Timmer et al., 2002).

Do the morphogens from the floor plate and roof plate specify the ventral cell fate and the dorsal cell fate independently, or do they interact to specify and refine cell fates? A study showed that in the presence of BMPs, ventral spinal cord marker genes induced by Shh were downregulated, and normally dorsal genes were upregulated, suggesting that Shh and BMPs interact (directly or indirectly) to specify progenitor cell fate. Furthermore, application of a BMP inhibitor together with Shh promoted greater expression of ventral marker genes than Shh alone (Liem et al., 2000).

7.3.3 Dorsoventral Patterning: Wnts

Apart from Shh, BMP and other TGFβ family members, Wnt signaling is also known to participate in cell specification in the spinal cord, particularly in the dorsal regions where Wnt1 and Wnt3a are found (Parr et al., 1993). In *Wnt1/3a* double knockout mice, the number of dI4–6 marker gene-positive neurons increased at the expense of dI1–3, suggesting that Wnt1 and Wnt3a are necessary for the specification of the dI1–3 dorsal progenitor domains. The intact expression patterns of BMP signaling components in this mutant mouse suggest that the changes in cell fate specification in this context were achieved directly by Wnt signaling rather than through modulation of BMP activity (Muroyama et al., 2002).

The role of Wnts in dorsal spinal cord patterning appears to be mediated by the canonical Wnt signaling pathway: once Wnt binds to its receptor Frizzled, initiating a downstream signaling cascade, β-catenin translocates into the nucleus where it interacts with TCF/LEF transcription factors to effect gene expression (Figure 7.4(b)). Consistent with this signaling pathway, ectopic expression of a constitutively active form of β-catenin in the chick spinal cord results in expansion of dorsal marker genes. Conversely, a dominant negative form of TCF3 facilitates the expression of the ventral marker genes, and was shown to suppress the expression of GLI3, a negative regulator of the Shh pathway. Taken together, these studies suggest that Wnt signaling specifies the dorsal spinal cord fate and can modulate Shh signaling (Alvarez-Medina et al., 2008).

7.3.4 Other Aspects of Dorsoventral Patterning

In addition to relative position with respect to Shh, BMP, and Wnt signaling centers, the timing of differentiation also contributes to the diversity of spinal neurons along the dorsoventral axis. For instance, the dIL spinal cord progenitor domain produces unique 'late-born' interneuron populations, dIL_A and dIL_B, between E12.0 and E13.5 in mice, while all other dorsal neural subtypes are generated between E10 and E11.5 (Mizuguchi et al., 2006). Furthermore, toward the end of neurogenesis, the progenitor cell programming switches from neurogenesis to gliogenesis, producing astrocytes and oligodendrocytes (Lee and Pfaff, 2001). A recent study suggests that the diversity of neurons along the dorsoventral axis may also be a general feature of glia subtypes (Hochstim

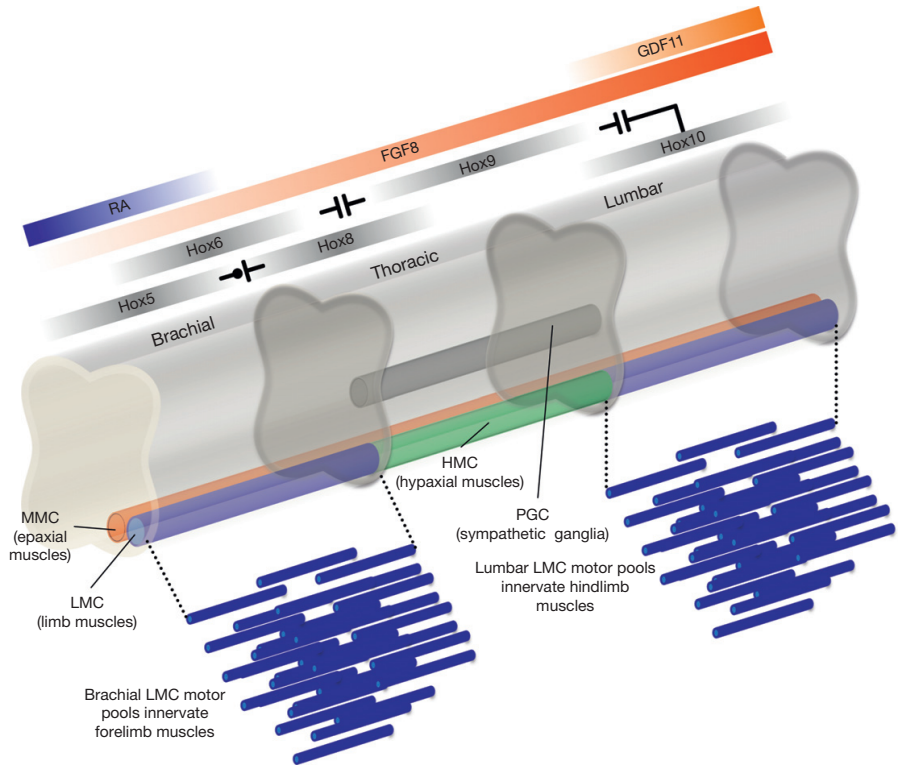

FIGURE 7.5 Rostrocaudal identity is defined by *Hox* genes. The morphogens FGF8, Gdf11, and RA are found in rostrocaudal gradients along the length of the spinal cord. These factors induce the expression of specific *Hox* genes, which serve to demarcate the spinal cord into rostrocaudal divisions. High levels of RA induce *Hox* genes that specify rostral spinal cord fates while high levels of FGF8 and Gdf11 induce *Hox* genes that specify caudal cell fates. Cross-repression between particular *Hox* genes defines the brachial, thoracic, and lumbar levels. This also specifies the rostrocaudal extent of each of the motor neuron columns. The MMC is found throughout the rostrocaudal extent of the spinal cord, the HMC is restricted to thoracic levels, the PGC is found in thoracic and upper lumbar levels, while the LMC is found at limb levels (brachial and lumbar spinal cord). The LMC is further subdivided into motor pools, each responsible for innervating a single limb muscle.

high concentrations of FGF to ensure the appropriate expression of specific *Hox* genes (Liu et al., 2001).

In addition to the Gdf11 and FGF signaling needed for proper spinal *Hox* expression caudally, RA drives the expression of *Hox* genes at rostral spinal levels (Dasen and Jessell, 2009). RA is expressed by somites in the paraxial mesoderm alongside the rostral spinal cord, influencing *Hox* patterning in the cervical and brachial levels (Figure 7.5; Liu et al., 2001). RA also affects hindbrain *Hox* expression, and it imposes its influence here by binding the nuclear hormone receptor, RAR (Dasen and Jessell, 2009; Duester, 2008). In addition to shaping *Hox* expression patterns in the rostral spinal cord, RA is also responsible for antagonizing FGF signals from the caudal mesoderm (Dasen and Jessell, 2009; Duester, 2008), possibly helping to define borders of *Hox* expression. The combined signaling of RA, Gdf11, and FGF leads to 3′ *Hox* expression (*Hox4–Hox8*) at cervical and brachial levels, *Hox8* and *Hox9* expression at thoracic levels, and 5′ *Hox* expression (*Hox10–Hox13*) at lumbar levels (Dasen and Jessell, 2009).

7.4.2 Rostrocaudal Patterning: *Hox* Expression in MNs

While systematic studies comparing interneurons of a single class across rostrocaudal levels in the spinal cord have not been conducted, the MN populations along the rostrocaudal axis have been shown to differ with respect to *Hox* gene expression. In the spinal cord, there are four different columns of MNs: the lateral motor column (LMC), the medial motor column (MMC), the hypaxial motor column (HMC), and the preganglionic motor column (PGC). The MMC runs the length of the cord and innervates dorsal epaxial musculature, while the LMC is limited to the brachial and lumbar levels where MNs innervate the limbs. The MNs of the HMC target intercostal and abdominal wall hypaxial musculature.

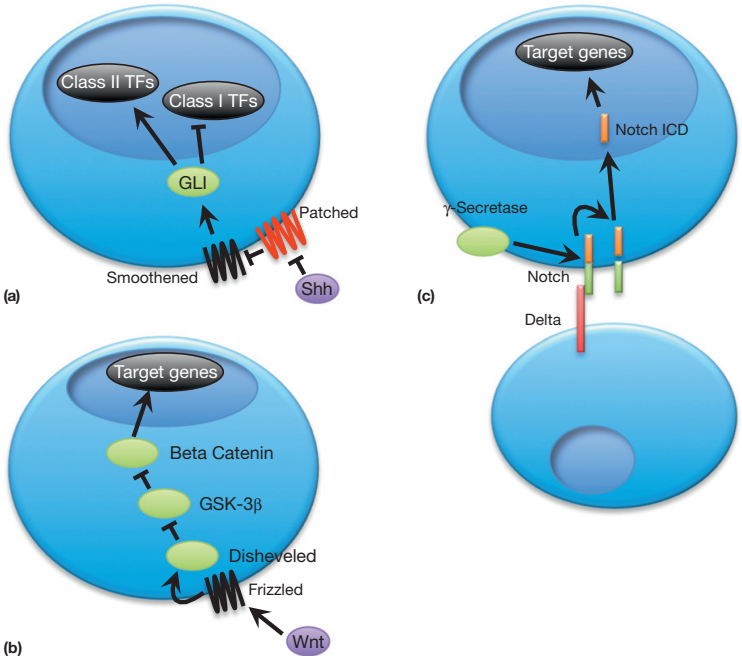

FIGURE 7.4 Examples of classical signaling cascades involved in spinal cord patterning. Several signaling pathways are induced by morphogen gradients or cell–cell interactions that induce the expression of target genes, such as transcription factors. These transcription factors and transcriptional modulators then express cell fate specification genetic programs. (a) The canonical Shh pathway. Shh binds to the patched receptor, thus disinhibiting Smoothened. This then activates GLI factors responsible for regulating downstream genes. (b) The canonical Wnt signaling pathway. Wnt binds to the Frizzled receptor and the following intracellular signaling cascade results in transcriptional changes. (c) The canonical Notch–Delta signaling pathway. Physical proximity of two adjacent cells allows the two transmembrane proteins Delta and Notch to interact. This binding event allows γ-secretase to cleave Notch, releasing the Notch intracellular domain (ICD), which then translocates into the nucleus to effect transcription.

et al., 2008). Future work is expected to uncover glial subtype-specific functions (see Section 7.7).

7.4 ROSTROCAUDAL PATTERNING

While many studies have focused on dorsoventral patterning of the spinal cord, much less effort has been put into understanding rostrocaudal diversity and specification. However, recent studies have shown that homeobox (*Hox*) transcription factor genes are differentially expressed along the spinal cord under the influence of RA, fibroblast growth factors (FGFs), and growth and differentiation factor 11 (Gdf11) (a TGFβ family member) (Figure 7.5).

7.4.1 Rostrocaudal Patterning: RA, FGFs, Gdf11, and the *Hox* Code

Hox genes are responsible for the rostrocaudal segmentation seen in animals. They are found arrayed in gene clusters, of which there are four in mammals. Typically, the *Hox* genes located at the 3′ end of a particular cluster are expressed in more rostral areas, while genes at the 5′ end of the cluster are most often active in caudal regions of the organism, though exceptions exist (Lemons and McGinnis, 2006). FGF signaling is responsible for the initial expression of *Hox* genes along the spinal cord and then continually influences their caudal expression through its secretion from the primitive knot (or Hensen's node/Spemann's organizer in various species) and the presomitic mesoderm. During development, these two areas move farther caudally, resulting in the caudal regions of spinal cord being exposed to higher concentrations of FGF, and for a longer period of time, relative to the rostral cord (Bel-Vialar et al., 2002; Dasen et al., 2003; Dubrulle and Pourquie, 2004; Liu et al., 2001). How FGF influences the expression of *Hox* genes is not clear, but altering expression of vertebrate caudal homeobox (*Cdx*) genes can mimic aberrant expression of FGF (Bel-Vialar et al., 2002). This finding, and the possibility that Cdx could bind directly to *Hox* regulatory elements, has led to the hypothesis that FGF may act through Cdx activity to regulate *Hox* gene expression (Dasen and Jessell, 2009).

Though FGF expression is responsible for *Hox* patterning in most regions of the spinal cord, it alone is insufficient to drive the entire *Hox* expression pattern seen in the spinal cord (Carpenter, 2002; Dasen and Jessell, 2009). For instance, in caudal areas of the spinal cord, Gdf11, a specific TGFβ family member, is required for proper *Hox* expression (Figure 7.5). Like FGF, Gdf11 is expressed by the primitive knot, which leads to its high caudal-to-rostral gradient (Dasen and Jessell, 2009). In these caudal regions, Gdf11 works in conjunction with

The MNs in the PGC, located in the thoracic and upper lumbar levels, target sympathetic ganglia (Dasen and Jessell, 2009). *Hox* genes appear to be responsible for setting up these columns as it has been found that *Hox6* is restricted to the brachial LMC neurons, *Hox9* to the thoracic PGC neurons, and *Hox10* to the lumbar LMC neurons (Choe et al., 2006; Dasen and Jessell, 2009; Dasen et al., 2003; Lance-Jones et al., 2001; Liu et al., 2001). Furthermore, *Hox9* is cross-repressive with both *Hox6* and *Hox10*, ensuring distinct boundaries between the brachial, thoracic, and lumbar segments (Dasen et al., 2003; Figure 7.5).

In addition to establishing rostrocaudal boundaries of motor columns, *Hox* genes can act with accessory factors to promote the diversification of MNs. Recently, it was discovered that *FoxP1*, whose expression is in part controlled by *Hox* genes, promotes MN segregation and motor pool specification. In studies by Dasen and colleagues (2008) and Rousso and colleagues (2008), formation of the LMC and PGC were found to be dependent on the expression of *FoxP1*. Elimination of *FoxP1* in mice resulted in the loss of the PGC and LMC, resulting in a more primitively structured spinal cord with a more homogeneous MN population throughout its length (Dasen et al., 2008). *FoxP1*'s effect on the generation of these columns appears to be expression-level-dependent, where a lower level of the protein promotes a PGC fate while the LMC is generated at higher levels of *FoxP1* (Dasen et al., 2008).

The loss of the LMC and PGC in *FoxP1* knockout mice is not because LMC and PGC progenitors are not generated, but rather due to a change in cell fate for these MNs as they differentiate (Rousso et al., 2008). Studies examining the axonal projections of these transformed neurons showed that gross nerve branches were still present and the proper muscles were still innervated. It was noted, however, that the normal arborization within specific muscles was lost. In addition, while dorsal and ventral projecting MNs normally tend to be found in a medial to lateral position, respectively, backfill labeling from limbs in *FoxP1* knockout mice showed this topography to be randomized (Dasen et al., 2008; Rousso et al., 2008). Further work has examined downstream effectors of *FoxP1*. One example, *Dab1*, appears to have a role in the migration of MN somata (Palmesino et al., 2010). Studies to identify other factors that control the expression of FoxP1 are ongoing and new layers of regulatory complexity are emerging. For instance, a miRNA, *miR-9* appears to play an important regulatory role (Otaegi et al., 2011).

In the brachial and lumbar LMCs, *FoxP1* acts as a permissive factor to gate the expression of additional *Hox* genes that drive motor pool formation. The specific combinations of *Hox* genes are a result of the unique rostrocaudal expression patterns of each *Hox* gene (Carpenter, 2002). However, these termination zones are not as well defined as those between *Hox9*, *Hox6*, and *Hox10* (Dasen and Jessell, 2009). One model states that LMC motor pool formation is due to the overlapping expression of more than one *Hox* gene within a MN. Because *Hox* genes can cross-repress and compete for dominance within each MN, a mosaic of MNs expressing distinct sets of transcription factors is produced. This model suggests that once a *Hox* expression profile has been established, similar neurons coalesce into a defined pool, with each pool dedicated to innervating a specific muscle (Dasen and Jessell, 2009; Dasen et al., 2005).

7.5 LIM/bHLH FACTORS AND THE COMBINATORIAL CODE

As mentioned earlier, several progenitor domains express unique sets of transcription factors in response to morphogen gradients. A 'map' that serves to catalog the various combinations of transcription factors expressed in each cell type is shown in Figure 7.6. Most of these transcription factors defining the progenitor domains are LIM homeodomain (LIM-HD) transcription factors, though some are basic helix-loop-helix (bHLH) proteins (Jessell, 2000; Shirasaki and Pfaff, 2002).

7.5.1 LIM Homeodomain Factors

LIM-HD proteins have two LIM domains, each composed of two zinc fingers at the N-terminal, allowing for protein–protein interactions responsible for modulating the function of transcription factors, while the homeodomain, located at the center of the amino acid sequence, specifies the DNA sequence motif to which it binds (Hunter and Rhodes, 2005). LIM-HD factors found within the spinal cord are classified as either Class I or Class II transcription factors depending on their response to Shh signaling (Briscoe and Novitch, 2008; Jessell, 2000; Shirasaki and Pfaff, 2002). Class I transcription factors are repressed by Shh, while Class II transcription factors are induced by Shh (Figure 7.7). Additionally, the expression of the transcription factors within each class is dependent on differential sensitivity to Shh signaling (mediated by GLI), resulting in distinct dorsal and ventral boundaries for transcription factors within the same class. One example of this is the differential expression of two Class I transcription factors, Pax6 and Irx3. Irx3 is more sensitive to repression by Shh, and therefore has a more dorsal boundary than Pax6. At the same time, Class II, Shh-activated, transcription factors that are less sensitive to Shh are less likely to be activated in more dorsal areas of the cord.

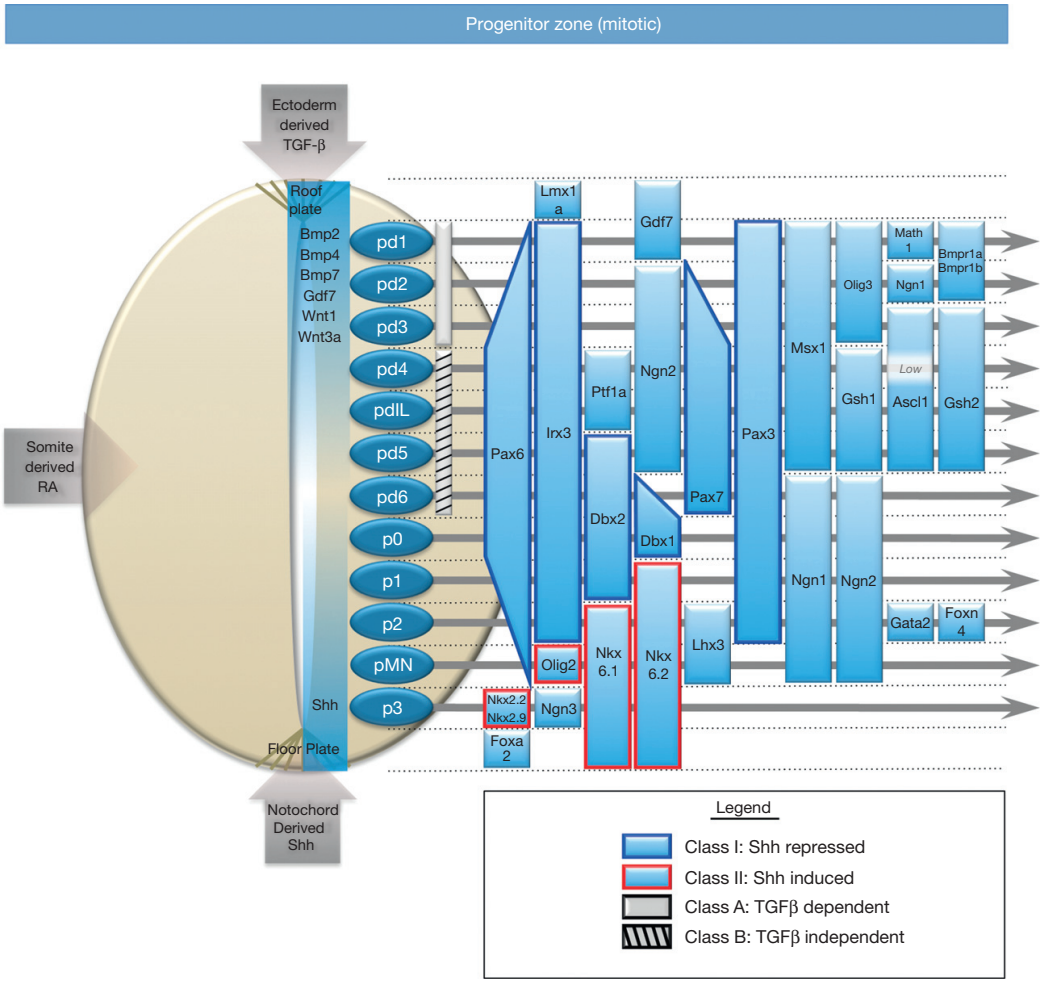

FIGURE 7.6 Generation of progenitor domains. At least 12 progenitor domains have been defined by their expression of unique combinations of transcription factors. This image depicts an idealized spinal cord section. As cells from these progenitor domains differentiate, they express additional, unique sets of postmitotic transcription factors, depicted in Figure 7.9. *Adapted with permission of Elsevier from Alaynick WA, Jessell TM, and Pfaff S (2011) SnapShot: Spinal cord development.* Cell *146: 178-178.e1.*

For example, Nkx2.2 and Nkx6.1, both Class II transcription factors, differ in their dorsal termination point because Nkx2.2 is less sensitive to Shh, preventing it from extending as far dorsally as the more sensitive Nkx6.1 (Figure 7.7).

Furthermore, when the ventral limit of a Class I transcription factor shares the dorsal limit of a Class II transcription factor, such as the Class I Dbx2 and Class II Nkx6.1, the two transcription factors have often been found to display reciprocal inhibition, a concept known as cross-repression (Figure 7.7; Briscoe and Novitch, 2008; Jessell, 2000; Lewis, 2006; Shirasaki and Pfaff, 2002). This cross-repression results by the binding of a transcription factor to a regulatory element of its opposing factor. Such cross-repression, also seen with *Hox* genes discussed earlier, leads to sharp, delineated boundaries between expression zones. The direct silencing action of many of these transcription factors is accomplished by Engrailed homology-1 (eh1) domains, a conserved region of the Engrailed transcriptional repressor (Muhr et al., 2001). Transcription factors containing the eh1 domain recruit Groucho/TLE corepressors to suppress transcription. Disruption of Groucho/TLE function leads to the loss of the sharp

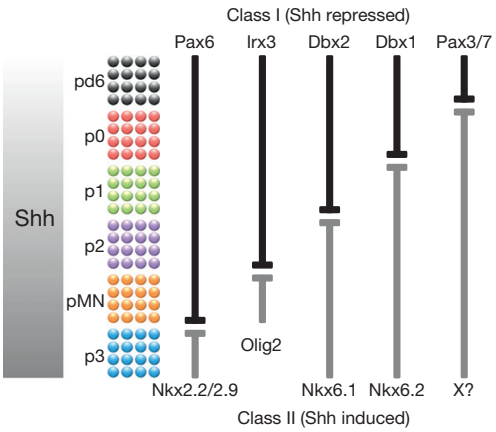

FIGURE 7.7 Transcriptional cross-repression sharpens boundaries between progenitor domains. Shh, found in a ventral to dorsal gradient, represses expression of Class I transcription factors and induces expression of Class II transcription factors. The Shh concentration needed to induce or repress each specific transcription factor defines their dorsal/ventral expression boundaries. Often the dorsal boundary of a Class II transcription factor is found at the ventral boundary of a Class I transcription factor. When this shared boundary is seen, these transcription factors typically inhibit each other's expression, which is termed cross-repression. Cross-repression ensures that only one of the competing factors is expressed in a particular cell, eliminating hybrid cell identities and sharpening the boundaries between the progenitor domains (pd6–p3). *Adapted by permission of Macmillan Publishers Ltd from Lee SK and Pfaff SL (2001) Transcriptional networks regulating neuronal identity in the developing spinal cord.* Nature Neuroscience *4 (supplement): 1183–1191.*

boundaries between progenitor domains of the spinal cord (Muhr et al., 2001).

7.5.2 bHLH Factors

In addition to LIM-HD transcription factors setting up distinct boundaries through cross-repression, bHLH factors can occasionally repress LIM-HD factors. For example, the bHLH factor *Olig2*, which is expressed by the pMN domain, has been found to repress the LIM-HD factor *Irx3* (Mizuguchi et al., 2001; Novitch et al., 2001; Zhou and Anderson, 2002). Furthermore, while LIM-HD proteins are thought to specify neuronal subtypes, bHLH proteins typically regulate generic neuronal traits such as promoting axon and dendrite outgrowth, but bHLH factors can also specify cell fate (Bertrand et al., 2002; Lewis, 2006). The dual role of bHLH factors is exemplified by *Olig2*, which is important during neurogenesis, as well for the specification of MNs and oligodendrocytes derived from the pMN domain (Mizuguchi et al., 2001; Novitch et al., 2001; Pfaff et al., 1985; Zhou and Anderson, 2002).

Other bHLH factors can play dual roles as well. For example, when *Ngn2* is replaced by *Mash1 (Ascl1)* by gene targeting, neuronal differentiation occurs normally, but the MN domain (which normally expresses *Ngn2*) is disrupted by the ectopic expression of V2 interneurons (which normally express *Mash1*), leading to the conclusion that *Mash1* and *Ngn2* specify different neuronal populations while functioning similarly in neurogenesis (Parras et al., 2002). The ability of *Mash1* to have the dual functions of promoting neurogenesis and specifying neuronal subtype was later attributed to the different helices of the protein, where Helix 1 is responsible for neurogenesis while both Helices 1 and 2 are responsible for neuronal subtype specification (Nakada et al., 2004). *Ngn2* has been found to function in neuronal specification through a different mechanism: phosphorylation of serine residues. While this phosphorylation is not needed for the neurogenic properties of *Ngn2*, it is required to promote MN specificity (Ma et al., 2008). It should also be noted that bHLH and LIM-HD factors do not necessarily work independently of each other; in some cases, bHLH and LIM-HD factors form heteromers to regulate neurogenesis and subtype specification (Lee and Pfaff, 2003).

7.5.3 Establishing Neural Identities through a Combinatorial Code

The transcription factors expressed in the progenitor domains drive expression of additional postmitotic transcription factors that further specify neuronal identity (Figure 7.9). V0 interneurons from the p0 domain express *Evx1*, V1 interneurons derived from the p1 domain express *En1*, the p2 domain gives rise to V2a (*Chx10+*) and V2b (*Gata3+*), *Hb9* is expressed by MNs from the pMN domain, and finally V3 interneurons from the p3 domain express *Sim1* (Goulding, 2009; Lewis, 2006). Loss of *Evx1* results in V0 interneurons taking on some phenotypic and genotypic characteristics of V1 interneurons, independently of upstream progenitor domain transcription factors (Moran-Rivard et al., 2001). Similarly, loss of *En1*, which is not required for early V1 interneuron differentiation, leads to pathfinding and functional defects in these neurons (Saueressig et al., 1999). Some of these transcription factors are sufficient for postmitotic cell-type specification as well. For instance, overexpression of *Hb9* is sufficient to drive ectopic MN development in the dorsal spinal cord (Tanabe et al., 1998).

Some of these transcription factors work in combination to specify neuronal subtypes. The proteins Lhx3, Isl1, and the nuclear LIM domain interactor (NLI) have been shown to form higher-order complexes. In this model, NLI dimers in the p2 domain are flanked by

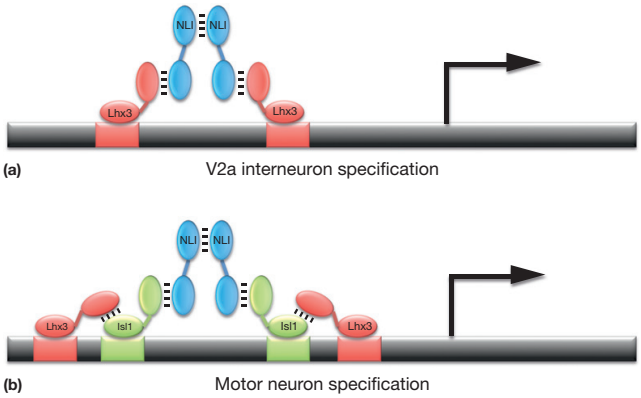

FIGURE 7.8 Example of a combinatorial transcription factor code. The expression of different combinations of transcription factors leads to specification of unique cell fates. In some cases, it has been shown that specific transcription factors physically interact to form higher-order transcriptional complexes that bind to novel regulatory sequences, which control distinct gene expression programs. (a) In the V2 progenitor domain, Lhx3 and NLI interact to form a tetramer that binds to specific DNA regulatory sequences, which results in specification of V2a interneuron identity. (b) In the pMN domain, Isl1 is coexpressed with Lhx3 and NLI. Isl1 prevents the formation of the V2a-specifying NLI–Lhx3 tetramer. Instead, an NLI–Isl1–Lhx3 hexamer forms. This new protein complex now binds to different DNA regulatory sequences, resulting in the expression of genes that specify motor neuron fate, instead of V2 interneurons. *Adapted with permission from Elsevier from Thaler JP, Lee SK, Jurata LW, Gill GN, and Pfaff SL (2002) LIM factor Lhx3 contributes to the specification of motor neuron and interneuron identity through cell-type-specific protein–protein interactions.* Cell *110: 237–249.*

Lhx3 to form a tetramer that drives V2a identity (Figure 7.8). In the adjacent pMN domain, two Isl1 proteins bind to two NLI and two Lhx3 proteins to form a hexamer that drives MN identity (Lee et al., 2008; Thaler et al., 2002). In certain contexts, the LIM-HD factors Lhx3 and Isl1 require modulation by the bHLH factors Ngn2/NeuroM as well, illustrating how combinatorial expression patterns of transcription factors specify many different cell fates in the spinal cord (Lee and Pfaff, 2003).

7.6 CELL–CELL INTERACTIONS

While diffusible factors expressed within and outside the spinal cord play large roles in its organization, emerging studies are showing that cell–cell interactions within the cord also help determine its patterning and can give rise to a diverse population of neuronal subtypes.

7.6.1 Notch–Delta Signaling

The specification of V2a and V2b interneurons in the ventral spinal cord provides an example of cell-to-cell signaling. V2a neurons, which express the transcription factor *Chx10*, make up a population of glutamatergic interneurons, whereas V2b neurons, marked by *Gata3*, are composed of GABAergic interneurons. Two groups provided evidence for the involvement of the Notch–Delta signaling pathway in generating Gata3+ V2b neurons from p2 at the expense of Chx10+ V2a cells (Del Barrio et al., 2007; Peng et al., 2007). In the canonical Notch–Delta pathway, Notch, a transmembrane receptor, binds the transmembrane ligand Delta/Jagged expressed by adjacent cells. Activated Notch is cleaved by the γ-secretase complex, and its intracellular domain (ICD) translocates into the nucleus. The ICD affects transcription of downstream genes in conjunction with CBF-1 and other proteins (Figure 7.4(c); Yoon and Gaiano, 2005). Studies performed primarily in *Drosophila* and *C. elegans* led to a model where lateral signaling mediated by the Notch–Delta interaction can generate cells with two distinct cell fates, despite coming from a population of progenitors with apparently equivalent cell fate (Greenwald and Rubin, 1992; Sprinzak et al., 2010).

In Presenilin (*PS1*) null embryos, where defective γ-secretase processing of Notch prevents ICD formation, Chx10+ cell numbers were increased while Gata3 expression was lost. Similarly, ectopic expression of either *Delta4* or the ICD of *Notch* in chick spinal cords resulted in an increase of V2b neurons at the expense of V2a neurons, providing further evidence that Notch signaling promotes generation of V2b neurons from p2 (Del Barrio et al., 2007; Peng et al., 2007).

In the dorsal spinal cord, Notch signaling also plays a role in the choice between excitatory and inhibitory interneuron fate. The superficial dorsal horn includes glutamatergic excitatory dIL_B interneurons and GABAergic inhibitory dIL_A interneurons, both of which are derived from the dIL progenitor domain. Mizuguchi and colleagues showed that, in *Mash1* mutant mice, Delta1 expression and the Notch ICD are reduced, suggesting a

role for Mash1 in regulating the Notch signaling pathway. In thesemice, dIL_A neuron markers were downregulated while dIL_B neuron markers were upregulated. Consistently, overexpression of *Mash1* in chick spinal cord upregulated dIL_A genes and downregulated dIL_B markers. Interestingly, overexpression of *Delta1* resulted in upregulation of dIL_B genes, while dIL_A genes appeared unchanged. Similarly, in both *PS1* and *Delta1* mutants, although dIL_B gene expression was decreased, dIL_A gene expression was unchanged (Mizuguchi et al., 2006).

7.6.2 Retinoid Signaling

Another example of a cell–cell interaction that regulates spinal cord patterning is retinoid signaling in MN pools. In the brachial and lumbar levels of the spinal cord, LMC neurons innervate muscles in the limb. The LMC has ventral limb muscle-innervating medial LMC neurons (LMCm) and dorsal limb-innervating lateral LMC neurons (LMCl). During development, LMCm cells differentiate first and migrate out from the ventricular zone into the mantle zone. Subsequently, LMCl neurons are born and migrate out through the existing LMCm in an 'inside-out'manner. Studies by Sockanathan and colleagues showed that retinaldehyde dehydrogenase 2 (*Raldh2*), an enzyme responsible for RA synthesis, is expressed specifically in LMCm MNs and subsequently acts on differentiating LMCl MNs. In these experiments, brachial and thoracic spinal cord explants were cultured with retinol, the RA precursor. This resulted in increased numbers of ventral progenitor cells and MNs in brachial explants, but was not observed in thoracic explants, which suggests that expression of *Raldh2* in the MN pool at the brachial level may account for generation of RA, subsequently resulting in an increase in MN numbers. Using LMCl marker genes, they further showed that the expansion in the MN pool was due to an increase in LMCl neurons. Furthermore, overexpression of *Raldh2* caused the ectopic expression of LMCl markers in surrounding neurons, suggesting that diffusible RA has a non-cell-autonomous role in motor column specification (Sockanathan and Jessell, 1998).

In addition to being expressed in LMC, *Raldh2* is also expressed in the paraxial mesoderm. Using a Cre-lox system in mice to reduce the levels of *Raldh2* in a tissue-specific manner, the functions of *Raldh2* in the paraxial mesoderm and LMC were studied independently. In a mouse line with paraxial mesoderm-specific loss of *Raldh2*, the population of LMCl was reduced, while the LMCm population remained unchanged. However, when *Raldh2* expression was reduced specifically in the LMC, both LMCm and LMCl populations became smaller, and the timing of this was later than that of *Raldh2* reduction in the paraxial mesoderm. These results imply that tissue-specific *Raldh2* may function in the specification of LMCl via paracrine RA signaling from the paraxial mesoderm as well as in the subsequent maintenance of both LMCm and LMCl populations through autocrine RA signaling from LMC MNs themselves (Ji et al., 2006).

7.7 GLIA IN THE SPINAL CORD

In addition to the different classes of neurons present in the spinal cord, there are two major types of glia: astrocytes and oligodendrocytes. Both cell types are found throughout the spinal cord. Historically, astrocytes have been thought of as cells which provide structural and metabolic support to their neuron neighbors, but additional astrocyte functions are continually being discovered. Oligodendrocytes are responsible for facilitating action potential conductance by myelinating axons.

7.7.1 Astrocytes

Traditionally, little effort has been put into the study of astrocyte diversity and any corresponding functional differences that arise from astrocytes derived from discrete progenitor domains. Recent work, however, has started to reveal that astrocyte diversity is much more extensive than previously appreciated (Hewett, 2009; Richardson et al., 2006). Astrocytes are generated in most of the spinal cord progenitor domains, with a notable exception of the pMN domain, which generates oligodendrocytes (Rowitch, 2004).

Generally, there is a difference between the fibrous white matter astrocytes that express high levels of glial fibrillary acidic protein (GFAP) and the protoplasmic astrocytes found in the gray matter that express low levels of GFAP (Hewett, 2009). The cause of this differential GFAP expression, and other molecular differences between the two subclasses, has yet to be determined. Additional work has shown that p1, p2, and p3 domains give rise to VA1, VA2, and VA3 fibrous astrocytes, respectively (Hochstim et al., 2008). These astrocytes occupy discrete, adjacent domains corresponding to the dorsoventral positioning of their respective progenitor domains and express unique combinations of Slit and Reelin. Thus, it appears at these early stages of research that there are parallels between neural and astrocyte patterning in the spinal cord.

It is interesting to note that there is evidence for functional coupling of astrocytes in discrete neural networks. For example, neurons within the rat somatosensory cortex form discrete network units called barrels (Hewett, 2009). Excitatory neurons within these barrels are highly connected with one another, and the astrocytes within each barrel are much more frequently connected via gap junctions to each other than to astrocytes in adjacent barrels (Houades et al., 2008). It will be interesting to see if astrocytes in individual motor pools display a similar functional

organization and whether there is, at its root, a developmental patterning mechanism that explains this organization.

7.7.2 Oligodendrocytes

Oligodendrocytes are found throughout the CNS. *In vivo* studies in spinal cord have identified at least two distinct progenitor domains that generate oligodendrocyte precursors (OLPs), including the pMN domain and at least one *Dbx+* domain (Fogarty et al., 2005; Richardson et al., 2006; Rowitch, 2004). The pMN domain expresses *Nkx6.1* and *Nkx6.2*, which are necessary for the expression of *Olig2*, a bHLH transcription factor required for OLP and MN generation (Lu et al., 2000; Novitch et al., 2001; Rowitch, 2004).

Though oligodendrocytes and MNs share the same progenitor domain in the ventral spinal cord, they are generated at different time points, with neurogenesis preceding gliogenesis (Guillemot, 2007). Transcription factors play a role in this temporal switch. Studies by Zhou and colleagues showed that transient *Ngn1* and *Ngn2* expression in the pMN domain promotes neurogenesis, but when downregulated, gliogenesis is initiated (Zhou and Anderson, 2002). However, results from experiments performed by Sugimori and colleagues suggest a more complex mechanism involving combinatorial expression of transcription factors. In their model, coexpression of *Olig2* and *Ngn2* promotes the generation of MNs, while coexpression of *Mash1* and *Olig2* promotes the generation of oligodendrocytes, and the downregulation of *Ngn2* is only coincidental (Sugimori et al., 2007).

As mentioned earlier, while many of the OLPs generated in the spinal cord are from the pMN domain, there is at least one additional progenitor pool in the spinal cord. The idea that a separate, non-pMN-origin domain for OLPs existed was initially supported by the finding that OLPs could be generated *in vitro* from any dissected area of the spinal cord, though it was uncertain as to whether this was a phenomenon unique to *in vitro* conditions (Richardson et al., 2006). Another study then used a double knockout of *Nkx6.1* and *Nkx6.2* or separately a knockout of *Smo*, the mediator of Shh signaling. Either of these manipulations is sufficient to prevent MN and oligodendrocyte formation from the pMN domain; however, oligodendrocytes were still generated in the spinal cords of both of these mutants, indicating the presence of other OLP domains within the spinal cord (Cai et al., 2005). In a different series of experiments, mice expressing Cre recombinase under the control of *Dbx1*, a transcription factor expressed in the p0 and pd6 progenitor domains, were crossed to a Cre-dependent GFP reporter line. Cells expressing both GFP and *Olig2* were observed, indicating that a Dbx+ progenitor domain for *Olig2*-expressing cells was present (Fogarty et al., 2005).

Interestingly, oligodendrocytes from the dorsal and ventral domains are thought to compete for survival (Richardson et al., 2006). Because ventral oligodendrocytes form and migrate to their final destination first, it is possible that they outcompete the dorsally generated oligodendrocytes for trophic factors in the environment. It is also possible that the ventral OLPs actively repress the dorsally derived OLPs as they migrate throughout the spinal cord. This competition hypothesis is supported by the fact that more oligodendrocytes are generated from dorsal progenitor regions when ventral OLPs are eliminated in the double knockout of *Nkx6.1* and *Nkx6.2* (Cai et al., 2005).

Despite the existence of distinct progenitor domains and molecular pathways regulating the formation of astrocytes and oligodendrocytes, there appear to be some similarities that are common to both types of glia. For example, the transcription factors *Sox9* and *NFIA* are necessary for both oligodendrocyte and astrocyte precursor generation (Stolt et al., 2003). These common transcription factors suggest there are parallels in the differentiation pathways of these two cell types. Of additional interest, a recent paper by Rompani and colleagues has provided evidence of a common progenitor for oligodendrocytes and astrocytes in the chick retina (Rompani and Cepko, 2010). While such a common progenitor has not yet been found in the spinal cord, its existence cannot be ruled out at this time.

7.8 HUMAN DISEASES OF SPINAL CORD PATTERNING

The number of genes and developmental processes that cumulatively serve to pattern the spinal cord is extensive and this number continues to grow. This begs the question: are there human developmental or genetic diseases that are associated with dysfunctional spinal cord patterning? Surprisingly, there is not a definitive answer to this question, but future research will almost certainly serve to better define diseases and syndromes with specific spinal cord patterning defects.

The lack of clarity on this issue can be explained by several factors. First, studies focused on cell-type identification in human spinal cords are rare, especially during embryonic stages when the transcription factors used to define cell types in mouse molecular genetic studies are expressed. The cell types and their unique sets of transcription factors shown in Figures 7.6, 7.7, and 7.9 can now be used to guide scientists studying human spinal cords in both health and disease. Second, every gene known to be important for spinal cord patterning is also expressed in non-spinal cord tissues. This accounts for the pleiotropic effects and/or embryonic lethality of mutations in these genes. Thus, many candidate diseases of spinal cord patterning may go unnoticed because dysfunctional gene products may result in spontaneous abortion or are

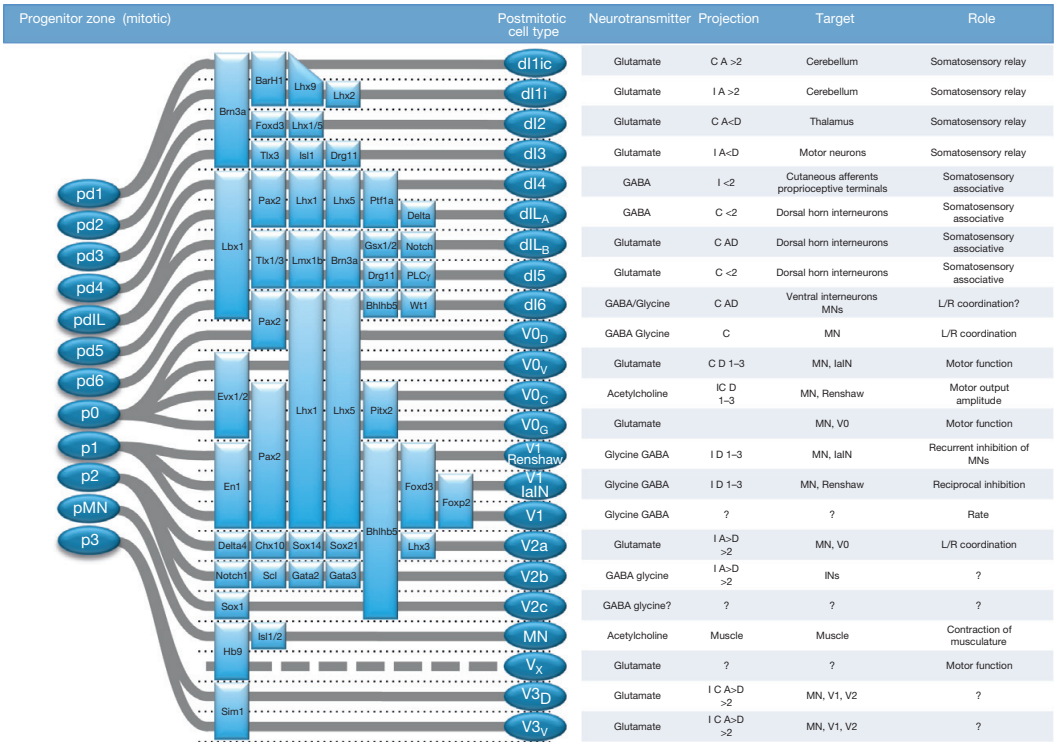

FIGURE 7.9 Diverse neuronal identities are specified by combinatorial transcription factor codes. Cells from the 12 spinal progenitor domains differentiate and migrate to their mature spinal positions. This process involves the expression of additional transcription factors as these cells become postmitotic. This figure depicts the combination of transcription factors that mark these cell types in an idealized spinal cored section. Projection code: I, ipsilateral; C, contralateral; A, ascending; D, descending; #, number of segments; V1-R, V1 Renshaw. *Adapted with permission from Elsevier from Alaynick WA, Jessell TM, and Pfaff S (2011) SnapShot: Spinal cord development.* Cell *146: 178-178.e1.*

masked by greater defects in other tissues. For example, *Isl1* knockout mice exhibit a striking defect in MN generation, arrest in development at E9.5, and die by E11.5, but the latter two phenotypes are better explained by a dorsal aorta defect than a lack of MNs because *choline acetyltransferase* knockout mice, which lack MN activity, survive until birth (Pfaff et al., 1996) . Hence, an opportunity to study the spinal cord patterning phenotype in the absence of other defects is limited. As a second example, mice and humans homozygous for mutations in *Chx10/Vsx2* (*Chx10*) share ocular developmental abnormalities typified by small eyes, retinal neuron differentiation defects, and congenital blindness. *Chx10* is expressed in multiple cell types in the developing eye, in addition to V2a interneurons in the ventral spinal cord (Burmeister et al., 1996; Ferda Percin et al., 2000). No obvious spinal cord phenotype, however, has been noted in either mice or humans. This may reflect any of several possibilities: (1) *Chx10* may be functionally redundant with another gene in the spinal cord and not in the eye; (2) the clinical issues related to blindness subvert the attention of both affected patients and clinicians away from subtler locomotor defects; or (3) there is sufficient plasticity or compensation in the locomotor circuitry to mask a potential spinal cord patterning phenotype. Neural plasticity is another major issue that may have hindered identification of spinal cord patterning defects, in general.

The best example of a human disease that very likely harbors a spinal cord patterning defect, at least in some patients, is holoprosencephaly (HPE). HPE is characterized by abnormal formation and segmentation of midline structures in the CNS (Ming and Muenke, 1998). In the most extreme 'alobar' cases, no separation of the hemispheres and ventricles is seen. Surprisingly, 20% of these infants survive over 12 months. One in 250 conceptions and 1 in 8000 live births are affected, making it an extremely common CNS disorder, but the etiology is highly heterogeneous (Raam et al., 2011). About half of all HPE cases are associated with either a monogenic syndrome or chromosomal defect while 10% are caused by a mutation in one of four genes: *SHH*, *ZIC2*, *SIX3*, or *TGIF*. Specific causes of the remaining 40% of cases, apart

from risk factors, have not been defined. Autosomal-recessive, autosomal-dominant, and X-linked-recessive pedigrees have all been identified.

The simplest model of HPE is illustrated by mutations in *Shh*. In *Shh* knockout mice the dorsal spinal cord pattern is largely maintained but expanded at the expense of the most ventral cell types. Specifically, Isl1+ MNs are absent at all spinal cord levels and there is no morphologically distinct floor plate. V3 interneurons were not studied, but it is assumed that they were also absent. Furthermore, the optic vesicles are fused at the midline, modeling human HPE. A human–mouse difference, however, lies in the fact that the *Shh* heterozygous mutant mice have no phenotype (Chiang et al., 1996), while, as mentioned earlier, certain human pedigrees do show dominant inheritance of HPE (with variable penetrance and expressivity). Thus, ventral spinal cord defects are expected in severe postnatal cases of HPE.

Other diseases with a potential for concomitant but, as yet, undefined spinal patterning defects would include Currarino syndrome (caused by mutations in *Mnx1/Hlxb9*); Greig cephalopolysyndactyly syndrome and Pallister–Hall syndrome (*Gli3*); lambdoid synostosis, aniridia with or without cerebellar ataxia and mental retardation (*Pax6*); Wilms' tumor (*Wt1*); basal cell nevus syndrome (*Ptch1*); and medulloblastoma (*Ptch2*), because each of these genes have known roles in spinal cord patterning. Despite the challenges to clearly identifying patterning defects in humans, a number of other poorly defined congenital and developmental disorders associated with motor or sensory–motor processing defects may be associated with spinal cord patterning defects. These could, speculatively, include monogenic syndromes, chromosomal defects, autism spectrum disorders, and 'cerebral' palsies. Particular attention to polymorphisms in both coding and noncoding regulatory regions of the genome, gene dosage, and epigenetic alterations are warranted as part of future research efforts.

7.9 LESSONS FROM SPINAL CORD PATTERNING FOR DISEASE MODELING AND REGENERATIVE MEDICINE

While the role that spinal cord patterning defects play in human disease is incompletely defined at present, our understanding of the inductive signals that regulate cell fate within the spinal cord is actively being applied to the study of human disease through the directed differentiation of ESCs. ESCs represent the *in vitro* counterpart of the inner cell mass or primitive epiblast of the preimplantation blastocyst. These cells were first isolated from mouse embryos in 1981 and are regularly used in gene targeting studies to generate both knock-in and knockout animals by placing genetically altered ESCs in wild-type host blastocysts and then deriving engineered mouse lines from the modified ESCs. In fact, this mouse genetic technology has been instrumental in uncovering many of the mechanisms by which the spinal cord is patterned as discussed in this chapter. The property of ESCs that is important for the present discussion is that they are pluripotent, possessing the ability to differentiate into tissues from each of the three germ layers of the embryo, including ectoderm and its derivative neural tissues.

In 2002, Wichterle and colleagues first reported that mouse ESCs can be efficiently differentiated into spinal MNs (Wichterle et al., 2002). The method is to first direct ESCs toward neural progenitors by removing the signals that maintain ESCs in the pluripotent state, for example, leukemia inhibitor factor. These neural progenitors, without any further exogenous signals, differentiate into a variety of neural cell types that correspond to cells from a range of neuroanatomic locations. By recapitulating the inductive signals present *in vivo*, the neural progenitors can be directed to a number of fates *in vitro*. To generate MNs, RA is supplied to specify rostral spinal cord or hindbrain fate at the expense of more rostral brain tissue, and Shh is added to bias the progenitors to more ventralized lineages, including MNs. MNs generated using this method coexpress the MN markers *Hb9* and *Isl1*, the MMC marker *Lhx3*, and the cervical spinal markers *Hoxc5* and *Hoxc6*, but generally lack expression of the LMC marker *Lhx1* and the thoracic spinal cord marker *Hoxc8*. This combination of marker expression indicates that the majority of the ESC-derived motor neurons (ESC-MNs) generated by the Wichterle protocol are of a rostral cervical, MMC-like identity. These ESC-MNs were shown to be capable of engrafting into the spinal cord and growing axons with appropriate projection patterns and target innervation given their MMC-like identity. This work was later extended to human ESCs (Li et al., 2005), which are now regularly generated by many labs.

More recently, two groups developed protocols to generate additional subtypes of mouse and human ESC-MNs in RA-free conditions (Patani et al., 2011; Peljto and Wichterle, 2011). The rationale for eliminating RA from the differentiation protocol was yet again taken from lessons learned from the basic neurobiology of spinal cord patterning, which was that RA promotes a rostral spinal cord identity and precludes the generation of more caudal MN subtypes that are specified by members of the FGF family and Gdf11 discussed earlier (Dasen and Jessell, 2009; Figure 7.5). While these are still early days for *in vitro* MN subtype specification, one can now envision generating specific MN subpopulations to address particular experimental questions, such as differing susceptibility of MMC and LMC MNs to death in spinal muscular atrophy (SMA).

In this section, the generation of ESC-MNs is highlighted because these particular cells have been a major focus of research in the stem cell and spinal cord research communities. The choice of generating ESC-MNs, in particular, comes from the fact that they are essential for movement and survival and are selectively vulnerable in at least two devastating neurologic diseases, amyotrophic lateral sclerosis (ALS) and SMA. It should be noted that these differentiation protocols can be adapted to generate other spinal neuron classes. For instance, ventral interneuron classes such as Chx10+ V2a interneurons are generated as 'contaminant' cells while following the ESC-MN differentiation protocol (Wichterle et al., 2002). In theory, the investigator can titrate Shh to enrich the culture for the desired class of neuron, or even eliminate the use of Shh entirely to selectively differentiate dorsal spinal cord interneuron classes. The addition of other morphogens at specific concentrations could also be useful. The current lack of focus on ESC-derived spinal cord cell types apart from ESC-MNs is that their functions are largely undefined in the context of both locomotor circuitry and human disease, but recent work has started to uncover important functions for several of these cell types (Alaynick et al., 2011; Goulding, 2009).

There are three reasons for pursuing this research. First, certain assays require large quantities of cells. In a 1-week differentiation, mouse ESCs can routinely generate tens of millions of purified MNs following fluorescent activated cell sorting. In contrast, a mouse spinal cord contains <50 000 MNs. Thus, ESC-derived cell types can be used in experiments that require large quantities of cells, including chromatin immunoprecipitation followed by massively parallel sequencing (ChIP-Seq) for the study of histone modifications or DNA:protein interactions, and cross-linking immunoprecipitation followed by massively parallel sequencing (CLIP-Seq) for the study of RNA:protein interactions. These facilitate the genome-wide interrogation of both pre- and posttranscriptional gene regulation, respectively. Second, a long-term goal is to develop cellular therapies in the setting of spinal cord disease, which may be treated by allogeneic stem cell transplants – a possibility which many scientific teams are now exploring. A final common motivation for using ESC-derived cell types is to model diseases by deriving 'designer' ESC lines harboring disease-associated alleles followed by their directed differentiation into the cell type of interest. In the event that these cells show a phenotype, this 'disease in a dish' can be probed for the root cause of disease or used to screen libraries for drugs that attenuate the phenotype. The field has been helped by the recent advent of induced pluripotent stem cells (iPS cells) (Takahashi and Yamanaka, 2006; Takahashi et al., 2007; Yu et al., 2007). These are generated when somatic cells are reprogrammed to pluripotency by one of several methods, most commonly lentiviral transduction of fibroblasts with a panel of transcription factors known to regulate the pluripotent state, namely *Pou5f1*, *Sox2*, *Klf4*, and *c-Myc*. This strategy circumvents two difficulties when trying to model disease *in vitro* using hESCs. First, hESC genomes are difficult to manipulate and iPS cells already contain the relevant mutation without the need for gene targeting. Second, if iPS cells are derived from patients where a genetic etiology is not yet defined, as in the majority of cases of sporadic ALS, for example, the iPS cells will still contain the genetic makeup associated with that patient's disease and may still therefore yield a valuable model. Notably, human iPS-derived MNs have now been derived from fibroblasts of both SMA (Ebert et al., 2009) and ALS patients (Dimos et al., 2008).

As further progress is made in understanding how individual cell types participate in locomotor circuitry and succumb to disease-related death, the stem cell and regenerative medicine communities will continue to draw on the principles in spinal cord patterning laid out in this chapter for insight into which cell types to generate and how to accomplish the task.

7.10 SUMMARY AND UNANSWERED QUESTIONS

The embryonic spinal cord forms a cylindrical structure that is exposed to an array of signals that specify the cell fate of uncommitted precursors. Many of the major signals are secreted factors that can be found in spatial gradients along the dorsoventral, rostrocaudal, and mediolateral axes. Together, these signals form a coarse three-dimensional grid, such that cells in the midst of this field will each be exposed to a unique combination of signals that direct cell fate. A mechanism of transcriptional cross-repression serves to sharpen the boundaries between each grid space and minimize hybrid cell identities, ultimately resulting in numerous neuronal subtypes, of which a large number have already been defined based on the unique combination of marker genes they express and their cell body position, morphology, pattern of connectivity, electrophysiological properties, and function. The outcome of this process is reflected in an elegant pattern of cell specification that underlies spinal circuit formation.

The amount of progress made in uncovering the basic biology behind spinal cord patterning is remarkable, but a great number of important questions remain. We leave the interested reader with this short list of some major questions and look forward to the answers in the future: (1) Beyond the dorsoventral patterning of the progenitor domains, is there further specification of postmitotic cells along this axis? (2) How does the spinal circuitry

change along the rostrocaudal axis? (3) What is the function of each neuronal subtype? (4) How is each subtype of cell interconnected with other subtypes? (5) Where are the DNA-binding sites and what genetic targets for the transcription factors are important for specifying cell identity? (6) How does the overexpression or deletion of a single transcription factor cascade into an entire fate change? (7) Is every cell within a particular neuronal subtype unique, or is there some cellular redundancy? (8) What really defines a neuronal subtype? (9) What is the extent of glial subtypes? Are they patterned in the same way that neurons are patterned? (10) How does time alter patterning and how is the precise temporal transition from neurogenesis to gliogenesis achieved? (11) Does the process of patterning a particular subtype make it prone to certain disease?

Glossary

Basic helix-loop-helix (bHLH) transcription factors Family of DNA-binding proteins that are characterized by a structural motif containing two alpha helices, one of which contains basic amino acids that facilitates DNA binding.

Combinatorial code A pervasive biological strategy for generating molecular complexity with a limited repertoire of factors. For example, many transcription factors operate as members of combinatorial codes that function coordinately to establish unique cellular identities.

Homeodomain A protein domain of approximately sixty amino acids that confers the ability to bind to specific DNA sequences; found in homeodomain transcription factors.

Interneuron Generic term for numerous classes of neurons whose cellular processes reside entirely within the central nervous system, unlike motor neurons.

LIM domain A protein domain important for mediating interactions with other LIM domain-containing proteins.

Motor column A collection of motor neurons found in roughly cylindrical structures that span many spinal segments and which innervate a group of muscles defined anatomically (e.g., the lateral motor column innervates limb muscles).

Motor neuron Special class of neuron that is defined by the presence of the cell soma within the central nervous system (brain or spinal cord) and an axon that targets muscle, gland, or postganglionic nervous tissue.

Motor neuron pool A cluster of motor neurons that collectively innervate a single muscle.

Patterning The process by which extrinsic and intrinsic signals regulate the development of unspecified precursor cells into an organized, functional structure replete with a myriad of diverse cell types.

References

Alaynick, W.A., Jessell, T.M., Pfaff, S.L., 2011. SnapShot: Spinal cord development. Cell 146 (1), 178 178.e1.

Alvarez-Medina, R., Cayuso, J., Okubo, T., Takada, S., Marti, E., 2008. Wnt canonical pathway restricts graded Shh/Gli patterning activity through the regulation of Gli3 expression. Development 135, 237–247.

Balaskas, N., Ribeiro, A., Panovska, J., et al., 2012. Gene regulatory logic for reading the Sonic Hedgehog signaling gradient in the vertebrate neural tube. Cell 148, 273–284.

Bel-Vialar, S., Itasaki, N., Krumlauf, R., 2002. Initiating Hox gene expression: In the early chick neural tube differential sensitivity to FGF and RA signaling subdivides the HoxB genes in two distinct groups. Development 129, 5103–5115.

Bertrand, N., Castro, D.S., Guillemot, F., 2002. Proneural genes and the specification of neural cell types. Nature Reviews Neuroscience 3, 517–530.

Briscoe, J., Novitch, B.G., 2008. Regulatory pathways linking progenitor patterning, cell fates and neurogenesis in the ventral neural tube. Philosophical Transactions of the Royal Society of London. Series B, Biological Sciences 363, 57–70.

Brown, T.G., 1911. The intrinsic factors in the act of progression in of the mammal. Proceedings of the Royal Society of London 84, 308–309.

Burmeister, M., Novak, J., Liang, M.Y., et al., 1996. Ocular retardation mouse caused by Chx10 homeobox null allele: Impaired retinal progenitor proliferation and bipolar cell differentiation. Nature Genetics 12, 376–384.

Cai, J., Qi, Y., Hu, X., et al., 2005. Generation of oligodendrocyte precursor cells from mouse dorsal spinal cord independent of Nkx6 regulation and Shh signaling. Neuron 45, 41–53.

Carpenter, E.M., 2002. Hox genes and spinal cord development. Developmental Neuroscience 24, 24–34.

Chiang, C., Litingtung, Y., Lee, E., et al., 1996. Cyclopia and defective axial patterning in mice lacking sonic hedgehog gene function. Nature 383, 407–413.

Choe, A., Phun, H.Q., Tieu, D.D., Hu, Y.H., Carpenter, E.M., 2006. Expression patterns of Hox10 paralogous genes during lumbar spinal cord development. Gene Expression Patterns 6, 730–737.

Corcoran, R.B., Scott, M.P., 2006. Oxysterols stimulate Sonic hedgehog signal transduction and proliferation of medulloblastoma cells. Proceedings of the National Academy of Sciences of the United States of America 103, 8408–8413.

Dasen, J.S., de Camilli, A., Wang, B., Tucker, P.W., Jessell, T.M., 2008. Hox repertoires for motor neuron diversity and connectivity gated by a single accessory factor, FoxP1. Cell 134, 304–316.

Dasen, J.S., Jessell, T.M., 2009. Hox networks and the origins of motor neuron diversity. Current Topics in Developmental Biology 88, 169–200.

Dasen, J.S., Liu, J.P., Jessell, T.M., 2003. Motor neuron columnar fate imposed by sequential phases of Hox-c activity. Nature 425, 926–933.

Dasen, J.S., Tice, B.C., Brenner-Morton, S., Jessell, T.M., 2005. A Hox regulatory network establishes motor neuron pool identity and target-muscle connectivity. Cell 123, 477–491.

del Barrio, M.G., Taveira-Marques, R., Muroyama, Y., et al., 2007. A regulatory network involving Foxn4, Mash1 and delta-like 4/Notch1 generates V2a and V2b spinal interneurons from a common progenitor pool. Development 134, 3427–3436.

Dessaud, E., Yang, L.L., Hill, K., et al., 2007. Interpretation of the sonic hedgehog morphogen gradient by a temporal adaptation mechanism. Nature 450, 717–720.

Dimos, J.T., Rodolfa, K.T., et al., 2008. Induced pluripotent stem cells generated from patients with ALS can be differentiated into motor neurons. Science 321, 1218–1221.

Dubrulle, J., Pourquie, O., 2004. fgf8 mRNA decay establishes a gradient that couples axial elongation to patterning in the vertebrate embryo. Nature 427, 419–422.

Duester, G., 2008. Retinoic acid synthesis and signaling during early organogenesis. Cell 134, 921–931.

Ebert, A.D., Yu, J., et al., 2009. Induced pluripotent stem cells from a spinal muscular atrophy patient. Nature 457, 277–280.

Ericson, J., Briscoe, J., Rashbass, P., van Heyningen, V., Jessell, T.M., 1997a. Graded sonic hedgehog signaling and the specification of cell fate in the ventral neural tube. Cold Spring Harbor Symposia on Quantitative Biology 62, 451–466.

Ericson, J., Rashbass, P., Schedl, A., et al., 1997b. Pax6 controls progenitor cell identity and neuronal fate in response to graded Shh signaling. Cell 90, 169–180.

Ferda Percin, E., Ploder, L.A., Yu, J.J., et al., 2000. Human microphthalmia associated with mutations in the retinal homeobox gene CHX10. Nature Genetics 25, 397–401.

Fogarty, M., Richardson, W.D., Kessaris, N., 2005. A subset of oligodendrocytes generated from radial glia in the dorsal spinal cord. Development 132, 1951–1959.

Fuccillo, M., Joyner, A.L., Fishell, G., 2006. Morphogen to mitogen: The multiple roles of hedgehog signalling in vertebrate neural development. Nature Reviews Neuroscience 7, 772–783.

Goulding, M., 2009. Circuits controlling vertebrate locomotion: Moving in a new direction. Nature Reviews Neuroscience 10, 507–518.

Greenwald, I., Rubin, G.M., 1992. Making a difference: The role of cell–cell interactions in establishing separate identities for equivalent cells. Cell 68, 271–281.

Grillner, S., Jessell, T., 2009. Measured motion: Searching for simplicity in spinal locomotor networks. Current Opinion in Neurobiology 19, 572–586.

Guillemot, F., 2007. Cell fate specification in the mammalian telencephalon. Progress in Neurobiology 83, 37–52.

Hewett, J.A., 2009. Determinants of regional and local diversity within the astroglial lineage of the normal central nervous system. Journal of Neurochemistry 110, 1717–1736.

Hochstim, C., Deneen, B., Lukaszewicz, A., Zhou, Q., Anderson, D.J., 2008. Identification of positionally distinct astrocyte subtypes whose identities are specified by a homeodomain code. Cell 133, 510–522.

Houades, V., Koulakoff, A., Ezan, P., Seif, I., Giaume, C., 2008. Gap junction-mediated astrocytic networks in the mouse barrel cortex. Journal of Neuroscience 28, 5207–5217.

Hunter, C.S., Rhodes, S.J., 2005. LIM-homeodomain genes in mammalian development and human disease. Molecular Biology Reports 32, 67–77.

Jessell, T.M., 2000. Neuronal specification in the spinal cord: Inductive signals and transcriptional codes. Nature Reviews Genetics 1, 20–29.

Ji, S.J., Zhuang, B., Falco, C., et al., 2006. Mesodermal and neuronal retinoids regulate the induction and maintenance of limb innervating spinal motor neurons. Developmental Biology 297, 249–261.

Lance-Jones, C., Omelchenko, N., Bailis, A., Lynch, S., Sharma, K., 2001. Hoxd10 induction and regionalization in the developing lumbosacral spinal cord. Development 128, 2255–2268.

Lee, S., Lee, B., Joshi, K., Pfaff, S.L., Lee, J.W., Lee, S.K., 2008. A regulatory network to segregate the identity of neuronal subtypes. Developmental Cell 14, 877–889.

Lee, S.K., Pfaff, S.L., 2001. Transcriptional networks regulating neuronal identity in the developing spinal cord. Nature Neuroscience 4 (Suppl), 1183–1191.

Lee, S.K., Pfaff, S.L., 2003. Synchronization of neurogenesis and motor neuron specification by direct coupling of bHLH and homeodomain transcription factors. Neuron 38, 731–745.

Lemons, D., McGinnis, W., 2006. Genomic evolution of Hox gene clusters. Science 313, 1918–1922.

Lewis, K.E., 2006. How do genes regulate simple behaviours? Understanding how different neurons in the vertebrate spinal cord are genetically specified. Philosophical Transactions of the Royal Society of London. Series B, Biological Sciences 361, 45–66.

Li, X.J., Du, Z.W., Zarnowska, E.D., et al., 2005. Specification of motoneurons from human embryonic stem cells. Nature Biotechnology 23, 215–221.

Liem Jr., K.F., Jessell, T.M., Briscoe, J., 2000. Regulation of the neural patterning activity of sonic hedgehog by secreted BMP inhibitors expressed by notochord and somites. Development 127, 4855–4866.

Liem Jr., K.F., Tremml, G., Jessell, T.M., 1997. A role for the roof plate and its resident TGFbeta-related proteins in neuronal patterning in the dorsal spinal cord. Cell 91, 127–138.

Liu, J.P., Laufer, E., Jessell, T.M., 2001. Assigning the positional identity of spinal motor neurons: Rostrocaudal patterning of Hox-c expression by FGFs, Gdf11, and retinoids. Neuron 32, 997–1012.

Liu, A., Niswander, L.A., 2005. Bone morphogenetic protein signalling and vertebrate nervous system development. Nature Reviews Neuroscience 6, 945–954.

Lu, Q.R., Yuk, D., Alberta, J.A., et al., 2000. Sonic hedgehog-regulated oligodendrocyte lineage genes encoding bHLH proteins in the mammalian central nervous system. Neuron 25, 317–329.

Ma, Y.C., Song, M.R., Park, J.P., et al., 2008. Regulation of motor neuron specification by phosphorylation of neurogenin 2. Neuron 58, 65–77.

Ming, J.E., Muenke, M., 1998. Holoprosencephaly: From Homer to Hedgehog. Clinical Genetics 53, 155–163.

Mizuguchi, R., Kriks, S., Cordes, R., Gossler, A., Ma, Q., Goulding, M., 2006. Ascl1 and Gsh1/2 control inhibitory and excitatory cell fate in spinal sensory interneurons. Nature Neuroscience 9, 770–778.

Mizuguchi, R., Sugimori, M., Takebayashi, H., et al., 2001. Combinatorial roles of olig2 and neurogenin2 in the coordinated induction of pan-neuronal and subtype-specific properties of motoneurons. Neuron 31, 757–771.

Moran-Rivard, L., Kagawa, T., Saueressig, H., Gross, M.K., Burrill, J., Goulding, M., 2001. Evx1 is a postmitotic determinant of v0 interneuron identity in the spinal cord. Neuron 29, 385–399.

Muhr, J., Andersson, E., Persson, M., Jessell, T.M., Ericson, J., 2001. Groucho-mediated transcriptional repression establishes progenitor cell pattern and neuronal fate in the ventral neural tube. Cell 104, 861–873.

Muroyama, Y., Fujihara, M., Ikeya, M., Kondoh, H., Takada, S., 2002. Wnt signaling plays an essential role in neuronal specification of the dorsal spinal cord. Genes and Development 16, 548–553.

Nakada, Y., Hunsaker, T.L., Henke, R.M., Johnson, J.E., 2004. Distinct domains within Mash1 and Math1 are required for function in neuronal differentiation versus neuronal cell-type specification. Development 131, 1319–1330.

Novitch, B.G., Chen, A.I., Jessell, T.M., 2001. Coordinate regulation of motor neuron subtype identity and pan-neuronal properties by the bHLH repressor Olig2. Neuron 31, 773–789.

Otaegi, G., Pollock, A., Hong, J., Sun, T., 2011. MicroRNA miR-9 modifies motor neuron columns by a tuning regulation of FoxP1 levels in developing spinal cords. Journal of Neuroscience 31, 809–818.

Palmesino, E., Rousso, D.L., Kao, T.J., et al., 2010. Foxp1 and lhx1 coordinate motor neuron migration with axon trajectory choice by gating Reelin signalling. PLoS Biology 8, e1000446.

Parr, B.A., Shea, M.J., Vassileva, G., McMahon, A.P., 1993. Mouse Wnt genes exhibit discrete domains of expression in the early embryonic CNS and limb buds. Development 119, 247–261.

Parras, C.M., Schuurmans, C., Scardigli, R., Kim, J., Anderson, D.J., Guillemot, F., 2002. Divergent functions of the proneural genes Mash1 and Ngn2 in the specification of neuronal subtype identity. Genes and Development 16, 324–338.

Patani, R., Hollins, A.J., Wishart, T.M., et al., 2011. Retinoid-independent motor neurogenesis from human embryonic stem cells reveals a medial columnar ground state. Nature Communications 2, 214.

Peljto, M., Wichterle, H., 2011. Programming embryonic stem cells to neuronal subtypes. Current Opinion in Neurobiology 21, 43–51.

Peng, C.Y., Yajima, H., Burns, C.E., et al., 2007. Notch and MAML signaling drives Scl-dependent interneuron diversity in the spinal cord. Neuron 53, 813–827.

Pfaff, S.L., Mendelsohn, M., Stewart, C.L., Edlund, T., Jessell, T.M., 1996. Requirement for LIM homeobox gene Isl1 in motor neuron generation reveals a motor neuron-dependent step in interneuron differentiation. Cell 84, 309–320.

Pfaff, S.L., Zhou, R.P., Young, J.C., Hayflick, J., Duesberg, P.H., 1985. Defining the borders of the chicken proto-fps gene, a precursor of Fujinami sarcoma virus. Virology 146, 307–314.

Raam, M.S., Solomon, B.D., Muenke, M., 2011. Holoprosencephaly: A guide to diagnosis and clinical management. Indian Pediatrics 48, 457–466.

Rahnama, F., Shimokawa, T., Lauth, M., et al., 26.

Richardson, W.D., Kessaris, N., Pringle, N., 2006. Oligodendrocyte wars. Nature Reviews Neuroscience 7, 11–18.

Rompani, S.B., Cepko, C.L., 2010. A common progenitor for retinal astrocytes and oligodendrocytes. Journal of Neuroscience 30, 4970–4980.

Rousso, D.L., Gaber, Z.B., Wellik, D., Morrisey, E.E., Novitch, B.G., 2008. Coordinated actions of the forkhead protein Foxp1 and Hox proteins in the columnar organization of spinal motor neurons. Neuron 59, 226–240.

Rowitch, D.H., 2004. Glial specification in the vertebrate neural tube. Nature Reviews Neuroscience 5, 409–419.

Saueressig, H., Burrill, J., Goulding, M., 1999. Engrailed-1 and netrin-1 regulate axon pathfinding by association interneurons that project to motor neurons. Development 126, 4201–4212.

Shirasaki, R., Pfaff, S.L., 2002. Transcriptional codes and the control of neuronal identity. Annual Review of Neuroscience 25, 251–281.

Sockanathan, S., Jessell, T.M., 1998. Motor neuron-derived retinoid signaling specifies the subtype identity of spinal motor neurons. Cell 94, 503–514.

Sprinzak, D., Lakhanpal, A., Lebon, L., et al., 2010. Cis-interactions between Notch and Delta generate mutually exclusive signalling states. Nature 465, 86–90.

Stolt, C.C., Lommes, P., Sock, E., Chaboissier, M.C., Schedl, A., Wegner, M., 2003. The Sox9 transcription factor determines glial fate choice in the developing spinal cord. Genes and Development 17, 1677–1689.

Sugimori, M., Nagao, M., Bertrand, N., Parras, C.M., Guillemot, F., Nakafuku, M., 2007. Combinatorial actions of patterning and HLH transcription factors in the spatiotemporal control of neurogenesis and gliogenesis in the developing spinal cord. Development 134, 1617–1629.

Takahashi, K., Tanabe, K., Ohnuki, M., et al., 2007. Induction of pluripotent stem cells from adult human fibroblasts by defined factors. Cell 131, 861–872.

Takahashi, K., Yamanaka, S., 2006. Induction of pluripotent stem cells from mouse embryonic and adult fibroblast cultures by defined factors. Cell 126, 663–676.

Tanabe, Y., William, C., Jessell, T.M., 1998. Specification of motor neuron identity by the MNR2 homeodomain protein. Cell 95, 67–80.

Thaler, J.P., Lee, S.K., Jurata, L.W., Gill, G.N., Pfaff, S.L., 2002. LIM factor Lhx3 contributes to the specification of motor neuron and interneuron identity through cell-type-specific protein–protein interactions. Cell 110, 237–249.

Timmer, J.R., Wang, C., Niswander, L., 2002. BMP signaling patterns the dorsal and intermediate neural tube via regulation of homeobox and helix–loop–helix transcription factors. Development 129, 2459–2472.

Wichterle, H., Lieberam, I., Porter, J.A., Jessell, T.M., 2002. Directed differentiation of embryonic stem cells into motor neurons. Cell 110, 385–397.

Wine-Lee, L., Ahn, K.J., Richardson, R.D., Mishina, Y., Lyons, K.M., Crenshaw 3rd, E.B., 2004. Signaling through BMP type 1 receptors is required for development of interneuron cell types in the dorsal spinal cord. Development 131, 5393–5403.

Yoon, K., Gaiano, N., 2005. Notch signaling in the mammalian central nervous system: Insights from mouse mutants. Nature Neuroscience 8, 709–715.

Yu, J., Vodyanik, M.A., Smuga-Otto, K., et al., 2007. Induced pluripotent stem cell lines derived from human somatic cells. Science 318, 1917–1920.

Zhou, Q., Anderson, D.J., 2002. The bHLH transcription factors OLIG2 and OLIG1 couple neuronal and glial subtype specification. Cell 109, 61–73.

Chapter 1, in full, is a reprint of the material as it appears in Gifford, W. D., Hayashi, M., Sternfeld, M., Tsai, J., Alaynick, W. A., & Pfaff, S. L. (2013). Chapter 7 - Spinal Cord Patterning. Pattering and Cell Type Specification in the Developing CNS and PNS: Comprehensive Developmental Neuroscience (Vol. 1). Academic Press. http://doi.org/10.1016/B978-0-12-397265-1.00047-2. The thesis author was the third author of this paper.

Chapter 2

Differential roles for inhibitory neurons revealed through creation of cell-type specific *de novo* networks

Differential roles for inhibitory neurons revealed through creation of cell-type specific *de novo* networks

Abstract

Inhibition plays many important roles within the central nervous system and its precise balance with excitation is crucial not only for complex processes like cognition, but also for motor behaviors, such as locomotion. In studies of spinal locomotor networks the influence of defined spinal interneuron subtypes has been removed, resulting in alterations to the stereotypic rhythmic pattern. However, due to the complexity of the remaining locomotor network, it is difficult to determine whether the pattern alteration was due to the change in the excitatory-to-inhibitory ratio or the removal of the specific neuronal subtype being investigated. To answer this question, we first differentiated ventral spinal neurons from mouse embryonic stem cells and then used these neurons to successfully generate highly defined *de novo* networks through the use of fluorescent activated cell sorting. From this experimental design we determined that networks of pure excitatory interneuron subtypes were sufficient to generate robust rhythmic bursts of activity, while networks of inhibitory interneurons were not. Inhibitory interneurons did, however, modulate the activity of excitatory networks. In excitatory V3 interneuron networks, increasing the contribution of inhibitory V1 interneurons increased the frequency of network bursting activity. In excitatory motor neuron networks, however, V1 interneurons caused the network to become increasingly fragmented. These results suggest that the ratio of excitatory and inhibitory neurons tunes network activity, but that cell type specific excitatory-inhibitory interactions determine the network parameters that are altered, therefore revealing a robust cellular mechanism to support the independent control of network frequency and coordination.

Introduction

The central nervous system (CNS) is composed of an incredibly diverse set of neuronal subtypes, which can be divided into generalized inhibitory and excitatory classes. While excitatory neurons drive neuronal networks, inhibitory neurons are generally thought of as keeping the central nervous system activity in check. If the correct balance between excitatory

and inhibitory neurons in the CNS is lost, studies have suggested many disorders, such as epilepsy, Parkinson's disease, autism, schizophrenia, and others may develop (Cline, 2005). However, despite the importance of this balance, the question remains as to what occurs when the ratio of excitatory and inhibitory neurons within a defined, biologically functioning network is changed.

One system that has been used to begin to address this question is the spinal locomotor central pattern generator (CPG), so named because of its ability to generate an autonomous, rhythmically patterned output without influence from descending brain or peripheral sensory inputs (Kiehn, 2006; McCrea & Rybak, 2008). In the locomotor CPG, connections between diverse spinal interneuron populations compose a circuit that drives patterned bursts of rhythmic activity in motor neurons on the left and right sides of the spinal cord, leading to alternation of left and right limbs, while at the same time generating alternating rhythms in motor neurons that activate muscles controlling the flexion and extension of limbs. Excitatory neurons have been shown to be necessary for network output, as antagonists of glutamatergic transmission block coherent network bursting (Feldman & Smith, 1989; Nishimaru, Takizawa, & Kudo, 2000; Whelan, Bonnot, & O'Donovan, 2000). Inhibitory neurons, on the other hand, modulate network output, as the application of inhibitory antagonists synchronize antagonistic motor neurons and alter the network's rate of activity (Cowley & Schmidt, 1995; Grillner, 2006).

In addition to these gross pharmacological changes, specific neuronal subtype manipulations can also be conducted. The $V0_v$, $V0_d$, V1, V2a, V2b, V3, and dI6 interneurons that compose the locomotor CPG each express unique transcriptional profiles providing genetic access to the neuronal subtypes, such that their function can be altered (Alaynick, Jessell, & Pfaff, 2011; Garcia-Campmany, Stam, & Goulding, 2010; Goulding & Pfaff, 2005; Grillner & Jessell, 2009; Stepien & Arber, 2008). For example, silencing V3 excitatory interneurons abolishes the strong rhythmic output that is characteristic of the locomotor CPG (Y. Zhang et al., 2008). Separately, if the influence of V1 inhibitory interneurons is removed from the network there is a significant decrease in the frequency of network output (Gosgnach et al., 2006). By removing V2b inhibitory interneurons, in addition to the V1 interneurons, synchrony between motor neurons that are normally antagonistic is revealed (J. Zhang et al., 2014). Each of these neuronal

subtypes release either inhibitory or excitatory neurotransmitters, so the question remains, is the resulting phenotype seen after the manipulation due to the specific neuronal subtype alteration or the change in the excitatory-to-inhibitory (E/I) ratio of the network? The ablation or silencing experiments cannot separate these two options due to the complex remaining spinal network, thus making concrete conclusions difficult (Büschges, Scholz, & El Manira, 2011; McLean & Dougherty, 2015). For this reason, we set out to generate highly defined *de novo* networks that would allow us to answer this question. Here, with the use of an innovative protocol, we have an unprecedented ability to observe how network dynamics change as the ratio of excitatory and inhibitory neurons is altered in a highly controlled, cell-type specific manner.

To generate defined *de novo* networks, we differentiated mouse embryonic stem cells (mESCs) into neurons found in the locomotor CPG, allowing us to take advantage of the already prevalent genetic tools used to access the network (Brown, Butts, McCreedy, & Sakiyama-Elbert, 2014; Wichterle, Lieberam, Porter, & Jessell, 2002; Wichterle & Peljto, 2008; Xu & Sakiyama-Elbert, 2015). When differentiated, we find that networks have the capability to generate large, spontaneous, glutamatergic-dependent bursts of activity, which can be driven to produce rhythmic output, all of which parallels the locomotor CPG. Additionally, in these networks, if the excitatory V3 interneurons are removed, we see that the *de novo* networks are significantly less rhythmic, paralleling data found when studying the locomotor CPG in the spinal cord (Y. Zhang et al., 2008). We then devised a novel protocol allowing us to purify the locomotor CPG neurons and generate networks of pure neuronal subtypes. In doing so we found that networks of pure excitatory interneurons were sufficient to produce robust, rhythmic bursts of activity, which stood in stark contrast to the low amplitude, non-rhythmic activity in networks of pure inhibitory interneurons. And finally, with the power of this new purification and network formation protocol, we examined the influence of the E/I ratio in pure networks driven by either V3 interneurons or motor neurons. Strikingly, two different phenotypes emerged. We found that in networks driven by V3 interneurons, a higher contribution of V1 interneurons resulted in an increased rate of network activity. Separately, when contributing to networks driven by motor neurons, V1 interneurons instead altered the pattern, not the rate, of network activity. Together, these data suggest the layered presence of speed and pattern control within the locomotor CPG.

Results

De novo generation of spinal cord neurons

To initiate the studies set out above, we first needed to generate large numbers of ventral spinal neurons from mESCs. To do this we differentiated mESCs with retinoic acid and smoothened agonist (SAG), an activator of the sonic hedgehog pathway (Peljto, Dasen, Mazzoni, Jessell, & Wichterle, 2010; Wichterle et al., 2002; Wichterle & Peljto, 2008). Using this protocol, different ventral spinal progenitor domains and their resulting post-mitotic neurons can be generated based on the degree of sonic hedgehog pathway activation, similar to *in vivo* differentiation of these neurons (Brown et al., 2014; Wichterle et al., 2002; Xu & Sakiyama-Elbert, 2015). Despite the numerous studies using this protocol, investigating the generation of these neurons has been limited, due to needing to fix the samples in order to identify the neuronal subtypes with antibody staining or *in situ* hybridization. The only exception to this requirement, up until this point, has been the use of mESC lines that contain the motor neuron specific promoter, Hb9, driving the expression of the reporter gene for GFP. These mESC lines allow for real-time, live imaging of motor neurons, something we needed in order to record the network activity of the differentiated neurons.

With the success of fluorescent motor neuron lines we wanted to generate fluorescent reporter lines for other neuronal subtypes generated during these differentiations. Having a large knowledge base of the unique transcription factors expressed in post-mitotic ventral spinal neurons and the available mouse genetic tools, we obtained mouse lines that were genetically engineered to express Cre-recombinase under the endogenous promoters of these unique transcription factors. Crossing these mice with a reporter mouse line expressing the genetic fluorescent reporter, tomato, under a CAG promoter, in a Cre-dependent manner, we were able to generate 4 mESC reporter lines which would label V1 interneurons, 2 lines for V2a interneurons, and 7 lines for V3 interneurons, in addition to two non-Cre-dependent Hb9-GFP lines (Figure 2.1a).

Once the mESC lines were derived, differentiations were conducted by dissociating mESCs, which were then held in suspension in media lacking leukemia inhibitory factor (LIF) for

Figure 2.1 *de novo* spinal networks differentiated from mESCs
(A) Sonic hedgehog signaling specifies progenitor domains, which give rise to post-mitotic neurons within the ventral spinal cord. These neurons express unique transcription factors that were used to generate mESC reporter lines (GFP and Tomato) or lines that ablate specific neuronal subtypes (DTA). The number of mESC lines generated are shown in parentheses. (B) Depiction of mESC differentiation protocol. (C) Representative images of V3 interneuron and V1 interneuron mESC reporter line after being exposed to a low (5 nM) or high (1000 nM) concentration of SAG during differentiation. (D) Quantification of neuronal subtypes generated at low (5 nM), medium (50 nM), or high (1000 nM) SAG. At low SAG, V1 interneurons are found in much higher concentration than V2a and V3 interneurons and motor neurons. At medium SAG, motor neurons and V3 interneurons are found in higher concentration than V1 interneurons. At high SAG, V3 interneurons are found in higher concentration than motor neurons and V2a and V1 interneurons. Motor neurons are also found in higher concentration than V1 interneurons. Mean ± standard error of the mean (SEM), n differentiations: 5 nM, 8; 50 nM, 8; 1000 nM, 8; *$p < 0.05$; **$p < 0.01$; ***$p < 0.001$; ****$p < 0.0001$, unpaired t test. (E) Representative traces of network activity in neurospheres differentiated under high and low SAG conditions. En1;Cre;R26/C:LSL:Tomato neurospheres. (F) Networks differentiated under high SAG conditions had higher amplitude, lower frequency bursts compared to networks differentiated under low SAG conditions. Mean ± SEM, n neurospheres: 1000 nM, 21; 5 nM 19; ***$p < 0.001$; ^$p < 1x10^{-10}$, unpaired t test.

A

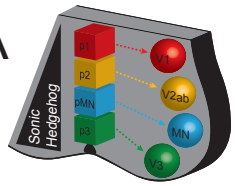

Postmitotic Type	Transmitter Class	Molecular Marker	Mouse embryonic stem cell lines
V1	GABA/Glycine	En1	En1:Cre;R26/C:LSL:Tomato (4)
V2a	Glutamate	Chx10	Chx10:Cre;R26/C:LSL:Tomato (2)
V2b	GABA/Glycine	Gata3	- - - - - - - - -
MN	Acetylcholine	Hb9	Hb9:GFP (2)
V3	Glutamate	Sim1	Sim1:Cre;R26/C:LSL:Tomato (7) Sim1:Cre;R26/C:LSL:DTA (2)

B

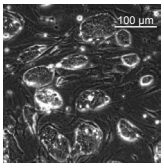

mES cells

6 day differentiation

Retinoic acid + SAG

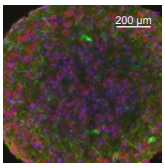

Neurospheres

Maturation

(1-28 days)

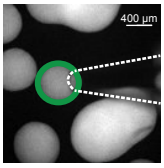

FACS or record activity

C

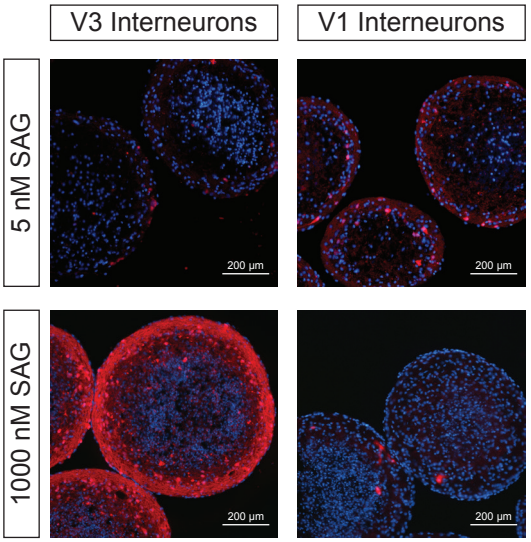

E

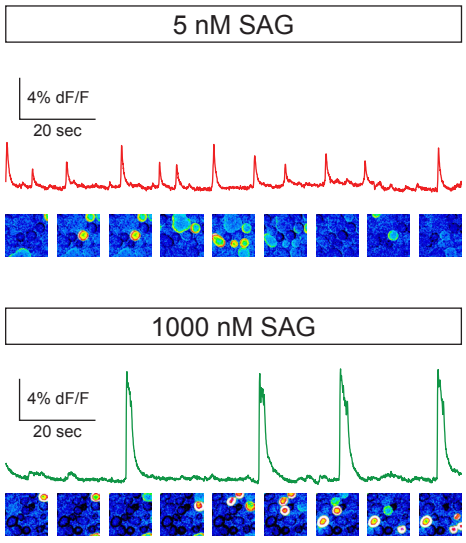

D

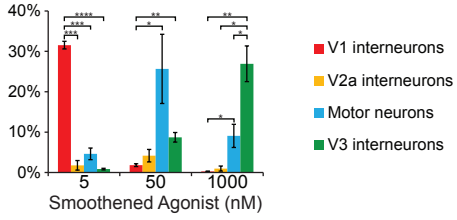

F

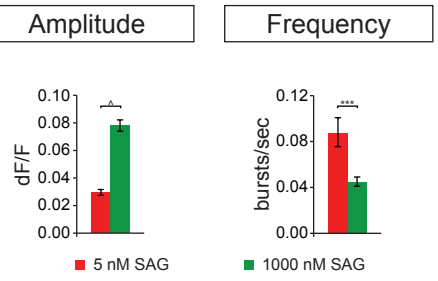

two days, resulting in the formation of embryoid bodies (EBs). At this point, the differentiation media was supplemented with 1000 nM retinoic acid (RA) to specify the EBs into a caudal spinal neuronal fate and with a low (5 nM), medium (50 nM), or high (1000 nM) concentration of SAG to ventralize the neuronal progenitors to varying degrees, thus producing different neuronal subtypes. After 4 days in this supplemented condition, hundreds of suspended spheres of neuronal progenitors and differentiated neurons existed, termed neurospheres (Figure 2.1b). To allow for increased proliferation of post-mitotic neurons, the neurospheres were kept in culture for 5 more days. Finally, for each mESC line differentiated under all three SAG concentrations, we dissociated the neurospheres into single cells, and used fluorescent activated cell sorting (FACS) to calculate the percentage of neurons that had been generated (Figure 2.2a and b).

During development, exposure to higher concentrations of sonic hedgehog increases the ventralization of progenitor domains. The same result holds true *in vitro.* When mESCs were differentiated using the lowest concentration of SAG the more dorsally located V1 interneurons were highly enriched in comparison to the V3 interneurons and motor neurons. This is in stark contrast to the high SAG condition, where the opposite was true. Here, both V3 interneurons and motor neurons were preferentially generated at the expense of the V1 interneurons, though there were significantly more V3 interneurons compared to motor neurons, as well. Motor neurons were most highly enriched at the middle SAG concentration (Figure 2.1c and d).

V2a interneurons were found in very low numbers, regardless of SAG concentration. While all other neuronal subtypes could be easily enriched to roughly 30%, the V2a interneurons averaged around 4% (Figure 2.1d). Noticing some variability in the two V2a mESC reporter lines used, a fine-tuned SAG analysis was conducted for each V2a mESC reporter line. Differentiating both mESCs lines in parallel, it appeared that one line differentiated more V2a interneurons at 15 nM SAG while the other peaked at 40 nM SAG. However, once again, this enrichment was only around 8% for both lines, lower than the other neuronal types we tested (Figure 2.2c). In previous studies, to increase V2a interneuron generation, DAPT, a gamma secretase inhibitor that blocks notch signaling, has been applied (Brown et al., 2014; Del Barrio et al., 2007). In our hands we found that the application of DAPT almost doubled the V2a population (Figure 2.2d). Moving forward, to obtain as many V2a neurons as possible, we continued to use DAPT in all

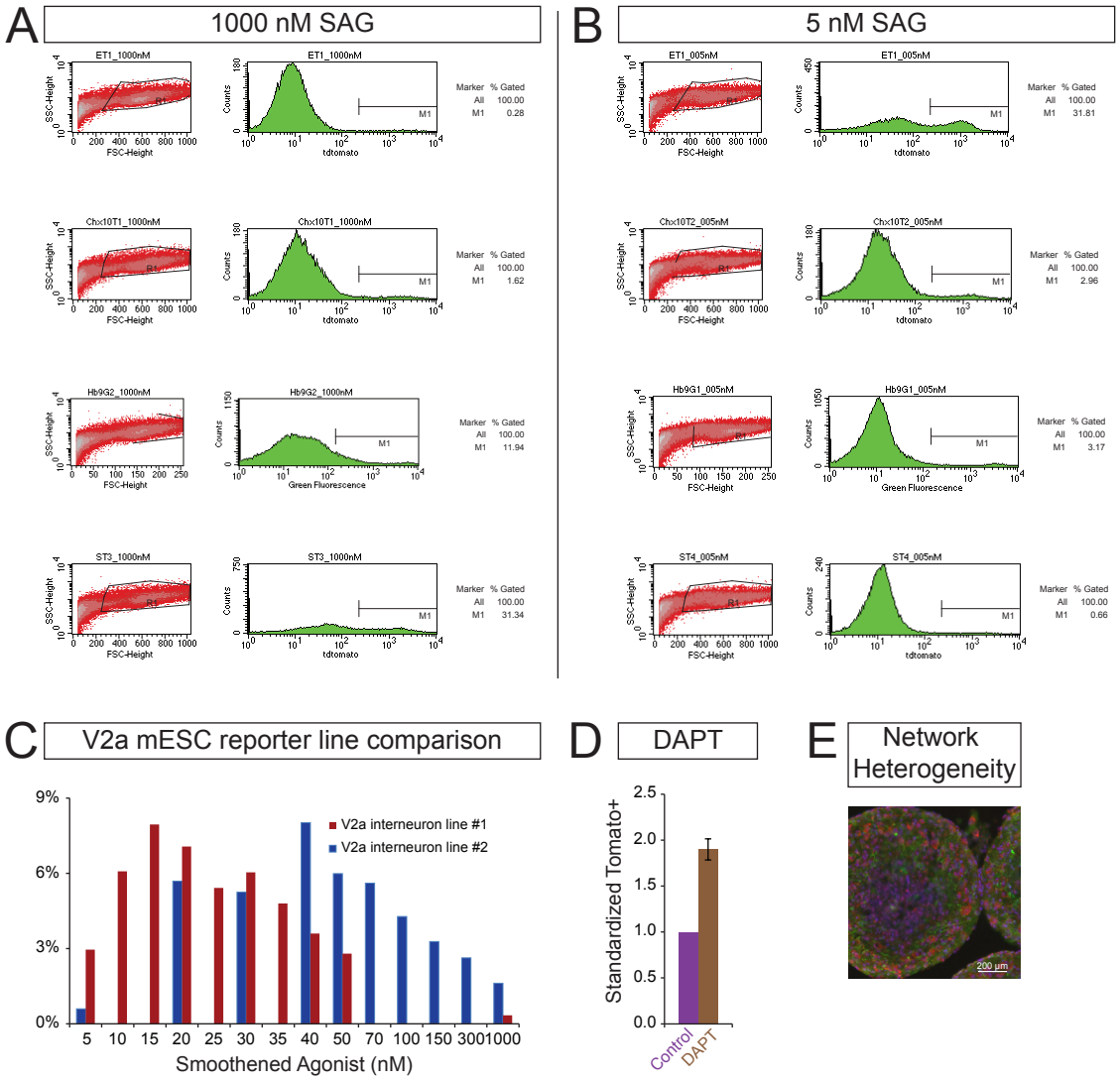

Figure 2.2 Neurosphere heterogeneity
(A,B) Example FACS quantification of neuronal populations found when different mESC reporter lines are differentiated under high (1000 nM) and low (5 nM) SAG. (C) Different SAG sensitivities in two different Chx:10:Cre;R26/C:LSL:Tomato mESC lines. (D) Use of the Notch inhibitor, DAPT, increases V2a differentiation almost two-fold. (E) Demonstration of neurosphere heterogeneity. Differentiated neurospheres contain differentiated neurons (red: neurotrace), but also astrocytes (green: GFAP staining). Blue: DAPI.

subsequent experiments.

The neuronal subtypes we investigated did not contribute to the entire cellular makeup of the neurospheres. This is most likely due to the extensive presence of neuronal progenitors. Furthermore, in addition to the degree of neuronal diversity within these neurospheres, this differentiation protocol also confers the proliferation of astrocytes (Figure 2.2e). Together, these data demonstrate that we have the capability to differentiate mESCs into heterogeneous neurospheres, biasing them toward different neuronal subtype compositions based on the applied concentration of SAG. And with the use of newly derived mESC fluorescent reporter lines, we can now identify neuronal subtypes in living samples.

Network properties of mESC-derived neurospheres

With a diverse set of neurons and astrocytes being generated, we began to wonder if a functional network was forming within these neurospheres. To investigate the formation of networks, we allowed the neurospheres to mature after their differentiation and then recorded their calcium activity in artificial cerebrospinal fluid (ACSF) by either using a mESC line that ubiquitously expressed GCaMP3 or loading them with Oregon Green BAPTA 488, a calcium indicator dye (Figure 2.1b). By drawing a region of interest around each neurosphere, the output investigated was the average neuronal activity throughout the entire network. We first set out to compare the activity of neurospheres that had been exposed to either high or low SAG concentrations during differentiation. Such a comparison revealed significantly different patterns of activity. Neurospheres differentiated under high SAG generated high amplitude, low frequency bursts compared to the low amplitude, high frequency activity seen in neurospheres differentiated with low SAG (Figure 2.1e and f and Video 2.1 and 2.2).

Due to the clean, large amplitude bursts seen in the high SAG neurospheres, we decided to continue with this differentiation protocol. Knowing that calcium imaging is an indirect measure of network activity, we first wanted to demonstrate that the calcium signal we were recording was indeed neuronal network activity. To check this we used a suction electrode to record the electrical activity of the neurospheres, while in parallel, measuring the calcium activity. These two signals highly correlate with each other, as would be expected (Figure 2.3a). To

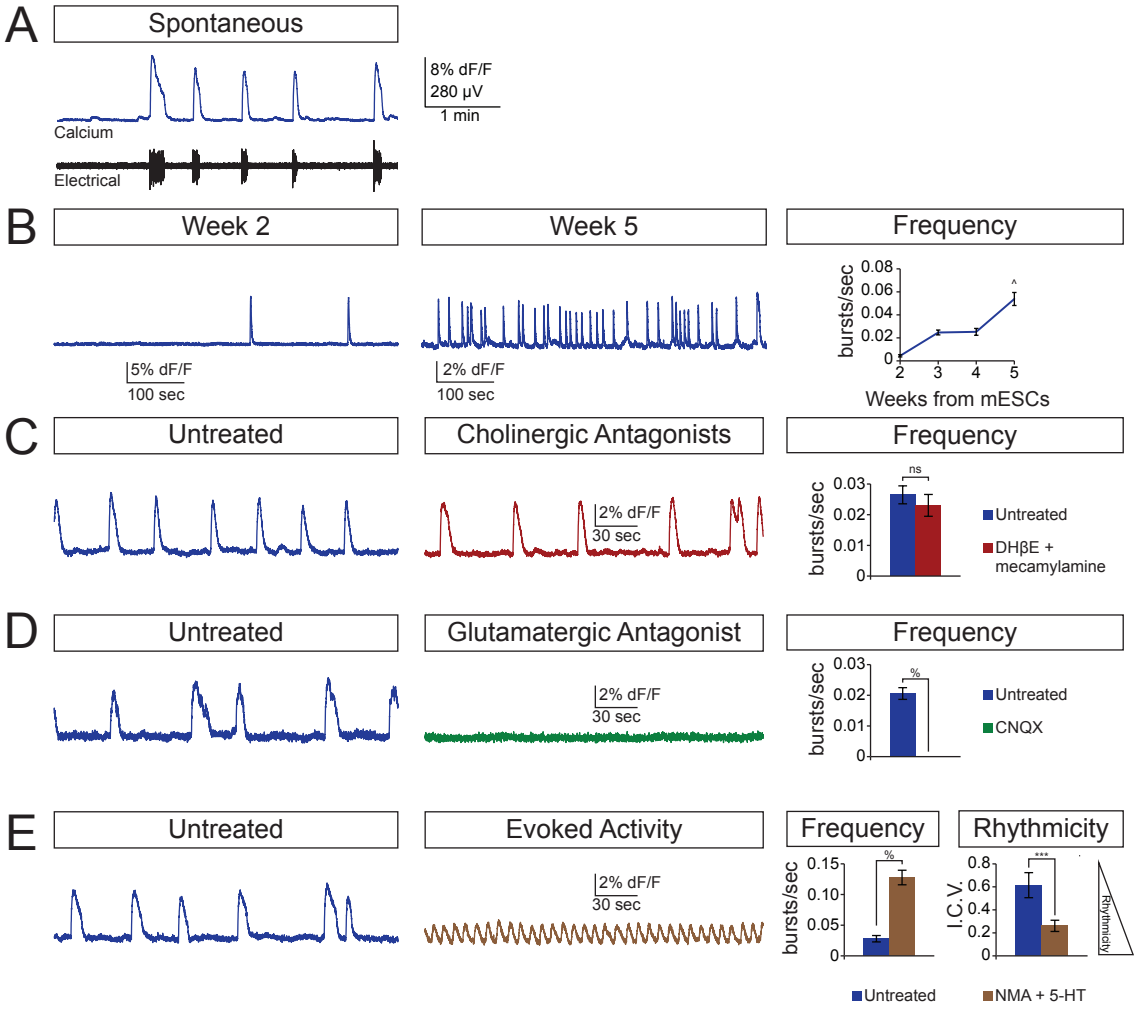

Figure 2.3 Basic network properties of neurospheres
(A) Comparison of calcium signal and electrical recording using a suction electrode of neurospheres differentiated from the CAG::GCaMP3 mESC line. (B) Increased activity of CAG::GCaMP3 neurospheres recorded over a 4 week period, starting after a week of differentiation. Neurosphere activity during week 5 was significantly faster than week 2. Mean ± SEM, n neurospheres: Week 2, 48; Week 5, 78; ^$p < 1x10^{-10}$, unpaired t test. (C) Cholinergic antagonists (DHβE and mecamylamine) lack significant effect on network activity rate. CAG::GCaMP3 neurospheres. Mean ± SEM, n neurospheres: 17; (ns) p=0.31, paired t test. (D) The application of CNQX, a glutamatergic antagonist blocks all activity in CAG::GCaMP3 neurospheres. Mean ± SEM, n neurospheres: 16; %$p < 1x10^{-5}$, paired t test. (D) Addition of evoking drugs (NMA and 5-HT) increases the frequency and rhythmicity of activity in CAG::GCaMP3 neurospheres. Rhythmicity is shown as a decrease in the interval coefficient of variation (I.C.V.). Mean ± SEM, n neurospheres: 18; frequency: %$p < 1x10^{-5}$; rhythmicity: **$p < 0.01$; paired t test.

determine how the spontaneous activity of the neurosphere networks changed over time, after the week of differentiation, we began recording the activity of the neurospheres multiple times a week for the next 4 weeks (2-5 weeks from mESCs). In doing so, we observed that spontaneous network activity increased in frequency over the course of the experiment (Figure 2.3b).

Realizing that these large bursts of activity had to be due to tightly coupled neuronal activity within the network, we asked what was connecting the neurons. Cholinergic antagonists, used to block motor neuron synaptic transmission had no significant effect on the burst frequency (Figure 2.3c). Next, to test the contribution of glutamatergic interneuron subtypes, we applied CNQX, an AMPA receptor, glutamatergic antagonist. This application abolished all network activity demonstrating that activity in these networks was driven by glutamatergic synapses (Figure 2.3d and Video 2.3).

Finally, knowing that the isolated ventral spinal cord is capable of generating rhythmic activity when evoked with NMA and 5-HT (Whelan et al., 2000), we were curious as to whether our *de novo* ventral spinal networks could also generate evoked rhythmic activity. Applying NMA and 5-HT (Evoked) to the networks not only induced a higher frequency of busting, but also induced a significantly increased regularity of the bursting pattern, as calculated by the peak-to-peak interval coefficient of variation (I.C.V.) (Figure 2.3e and Video 2.4 and 2.5). Taken together, our data demonstrates that *de novo* ventral spinal networks, derived from mESCs, form functional glutamatergic networks that are capable of generating a rhythmic bursting pattern of activity, suggesting that the core locomotor CPG elements are not only successfully being differentiated, but that they are also forming appropriate synaptic connections, resulting in coherent, locomotor CPG-like functional output.

Networks of pure excitatory V3 interneuron networks can generate rhythmic activity

The heterogeneous networks produced above are glutamatergic in nature, highly composed of V3 interneurons, and have the capacity to generate rhythmic patterns of activity when evoked. Knowing this and that V3 interneurons are necessary for robust rhythmic activity in the isolated spinal cord preparation (Y. Zhang et al., 2008), we asked whether these neurons, alone, were sufficient to drive rhythmic network activity. To be able to answer this question, we

needed to be able to generate networks of pure V3 interneurons. To this end, we differentiated our V3 interneuron reporter lines and dissociated the neurospheres into single cells, so that they could be run through FACS. After sorting the neurons from the heterogeneous cultures we were then able to reaggregate them into pure V3 interneuron networks (Figure 2.4a, 2.5a and b). We formed these new networks by sorting 50,000 V3 interneurons into wells of a non-adherent, u-bottomed 96-well dish. After sorting, the neurons were pelleted and the media was exchanged three times to remove the FACS sheath. Then, as this purification step removes the normally present astrocytes from the networks, we transferred the neurons to another u-bottomed well, which contained a sphere of 50,000 astrocytes, which had previously been dissected and purified from neonatal mouse pups (Ullian, Sapperstein, Christopherson, & Barres, 2001). The sorted neurons rapidly adhered to each other and to the pre-formed astrosphere, generating a new, highly purified V3 interneuron network, surrounding a layer of astrocytes (Figure 2.4a). Resorting samples demonstrated that we achieved greater than 98% purity from sorting (Figure 2.5c).

When it was time to image network activity, these reaggregated neurospheres were removed from their wells and loaded with calcium indicator dye to study their activity, as was done with the heterogeneous networks above. Similar to the heterogeneous networks, large spontaneous bursts of activity were observed in these designed networks. The purified V3 interneuron networks could also be induced into an increased rhythmic pattern of activity under evoked conditions (Figure 2.4b and d). The NMA and 5-HT application also increased network burst rate (Figure 2.4b and e). As further evidence of the purity of these glutamatergic, V3 interneuron networks, the application of the inhibitory antagonists strychnine and picrotoxin to the evoked condition (Evoked + Inhibitory Antagonists) showed no significant effect on burst amplitude (Figure 2.4c), network rhythmicity (Figure 2.4d), or rate of network activity (Figure 2.4e). This finding is in stark contrast to the dramatic decrease of network activity when CNQX was added to block glutamatergic signaling (Figure 2.4e). Therefore, networks of pure V3 interneuron networks are capable of generating an increased rhythmic pattern when evoked.

Curious as to how the activity of these purified networks might vary over time we observed them at weekly intervals for 5 weeks, starting at day 17, 1 week after reaggregating the networks. Over these five weeks, the frequency of network activity increased in both

Figure 2.4 Activity in pure excitatory networks differs greatly from inhibitory networks (A) Diagram of experimental design for purifying and reaggregating neurospheres. (B) Purified V3, V2a, and V1 interneuron and motor neuron networks exposed to different conditions. Representative traces are shown of network activity in spontaneous, evoked, evoked + inhibitory antagonists, and evoked + CNQX conditions. Tomato and GFP reporter lines shown in Figure 1a were used for the purification. (C) The spontaneous burst amplitude of purified V1 interneuron networks was significantly lower than V3 and V2a and motor neuron networks. There was no significant change in amplitude between the evoked and evoked + inhibitory antagonist conditions for V3 and V2a interneurons and motor neuron networks. There was a significant increase in amplitude when inhibitory antagonists were applied to V1 interneurons. Mean ± SEM, n differentiations (n neurospheres): V3, 22 (175); V2a, 5 (49); MN, 11 (49); V1, 12 (42); (ns) $p > 0.05$; **$p < 0.01$; %$p < 1x10^{-5}$; unpaired t test. (D) Rhythmicity increased (I.C.V. decreased) under the evoked condition in pure V3 and V2a interneuron networks, compared to their spontaneous activity. There was no significant increase in rhythm in pure motor neuron or V1 interneuron networks. The addition of inhibitory antagonists to the evoked condition did increase rhythmicity of V1 interneuron networks, but did not significantly alter rhythmicity for other networks. Mean ± SEM, n differentiations (n neurospheres): V3, 22 (175); V2a, 5 (49); MN, 11 (49); V1, 12 (42); (ns) $p > 0.05$; *$p < 0.05$; ***$p < 0.001$; %$p < 1x10^{-5}$; paired t test. (E) The evoked condition increased frequency in all networks with the application of inhibitory antagonists having no effect on any of the purified networks. Compared to the evoked condition, the application of CNQX significantly slows activity in networks of all purified subtypes. Mean ± SEM, n differentiations (n neurospheres): V3, 22 (175); V2a, 5 (49); MN, 11 (49); V1, 12 (42); (ns) $p > 0.05$; *$p < 0.05$; ***$p < 0.001$; %$p < 1x10^{-5}$; paired t test.

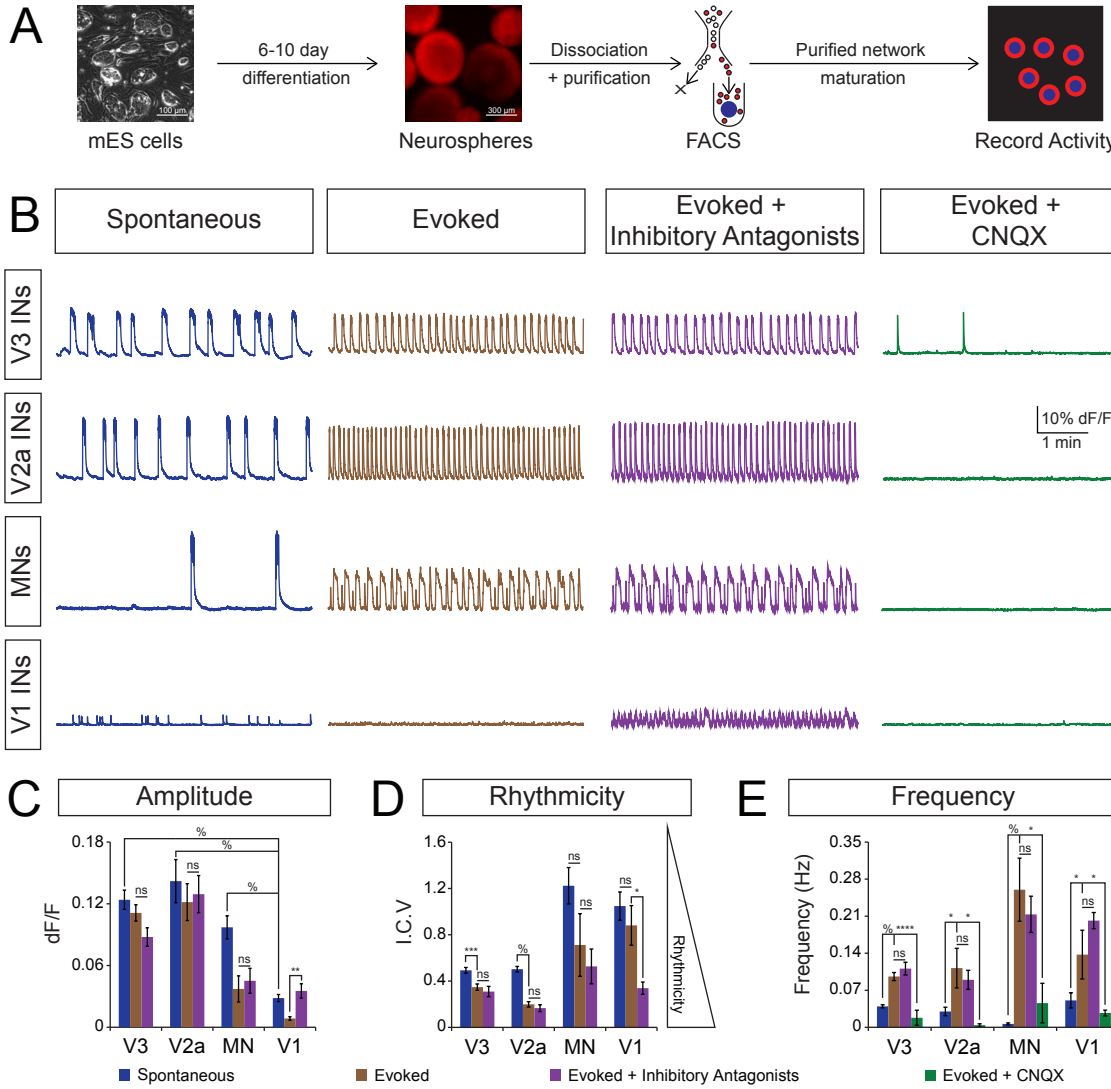
A
mES cells
6-10 day differentiation
Neurospheres
Dissociation + purification
FACS
Purified network maturation
Record Activity
B
Spontaneous
Evoked
Evoked + Inhibitory Antagonists
Evoked + CNQX
V3 INs
V2a INs
MNs
V1 INs
10% dF/F
1 min
C
Amplitude
dF/F
V3
V2a
MN
V1
Spontaneous
D
Rhythmicity
I.C.V
Rhythmicity
Evoked
Evoked + Inhibitory Antagonists
E
Frequency
Frequency (Hz)
Evoked + CNQX

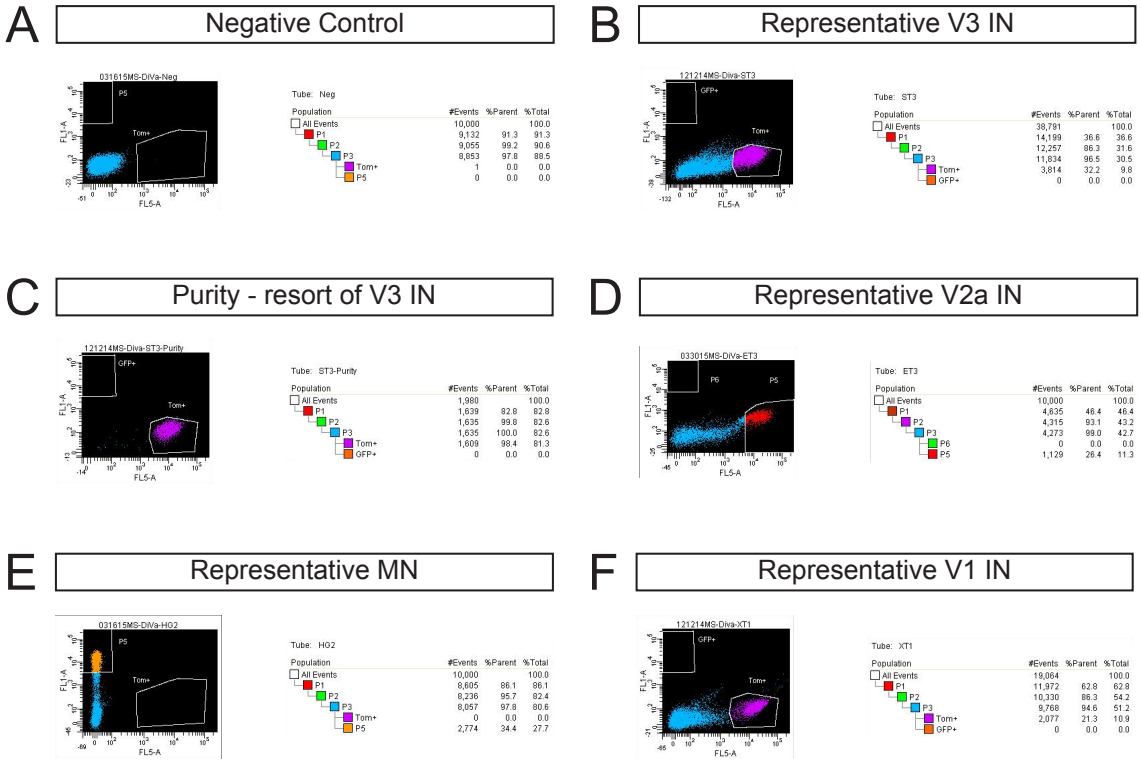

Figure 2.5 Representative FACS plots for generating designed neural networks
(A) Negative control sort of non-fluorescent mESC line. (B) Representative V3 interneuron (Sim1:Cre;R26/C:LSL:Tomato) sort. (C) Resorting of a V3 interneuron (Sim1:Cre;R26/C:LSL:Tomato) sort demonstrates achievement of high purity sort (98.4%). (D) Representative motor neuron (Hb9:GFP) sort. (E) Representative V2a interneuron (Chx10:Cre;R26/C:LSL:Tomato) sort. (F) Representative V1 interneuron (En1:Cre;R26/C:LSL:Tomato) sort.

spontaneous and evoked conditions (Figure 2.6a). The rhythmicity of the networks changed over time, as well. There was a significant decrease in rhythmicity from day 17 to day 24 in both the spontaneous and evoked conditions, but no change over the next four weeks (Figure 2.6a). In addition to demonstrating how network activity changes over time, these data also reveal that frequency and rhythmicity are biologically separable read-outs of network activity, as they change independently from each other, over time.

Another parameter this experimental design allows us to approach is whether network size alters network activity. Networks were reaggregated with 5-, 10-, 25-, 50-, and 100-thousand V3 interneurons and then activity was recorded 31 days from mESCs, 3 weeks after network reaggregation. Interestingly, while the spontaneous activity showed no difference in frequency over this large size range, evoked activity did show a significant decrease in network burst rate as network size increased (Figure 2.6b). Separately, the spontaneous network activity showed an increase in rhythmic pattern as network size increased, while there was no obvious change in the rhythmic pattern of activity in the evoked condition (Figure 2.6b).

Properties of pure networks of other excitatory neurons: V2a interneurons and motor neurons

After demonstrating that networks of pure V3 interneurons were sufficient to drive rhythmic network activity, we next asked whether the same was found in networks of other pure excitatory neuronal subtypes, so we generated networks composed of 50,000 V2a interneurons or motor neurons (Figure 2.5d and e). Compared to each other and to pure V3 interneuron networks, there was no significant difference in the amplitude of the spontaneous network activity (Figure 2.4b and c). Additionally, paralleling the data from the pure V3 interneuron networks, the amplitude, rhythmicity, and frequency of the V2a interneuron networks and motor neuron networks are unchanged between the evoked and evoked + inhibitory antagonist conditions, confirming the purity of these excitatory networks (Figure 2.4b, c, d, and e). Similarly, their evoked activity is dramatically reduced with the application of CNQX. This finding is expected for networks composed of glutamate releasing V2a interneurons, but motor neurons are typically known to release acetylcholine, but interestingly, cholinergic antagonists lacked any significant effect on motor neuron networks (Figure 2.7). While these findings may initially appear at odds

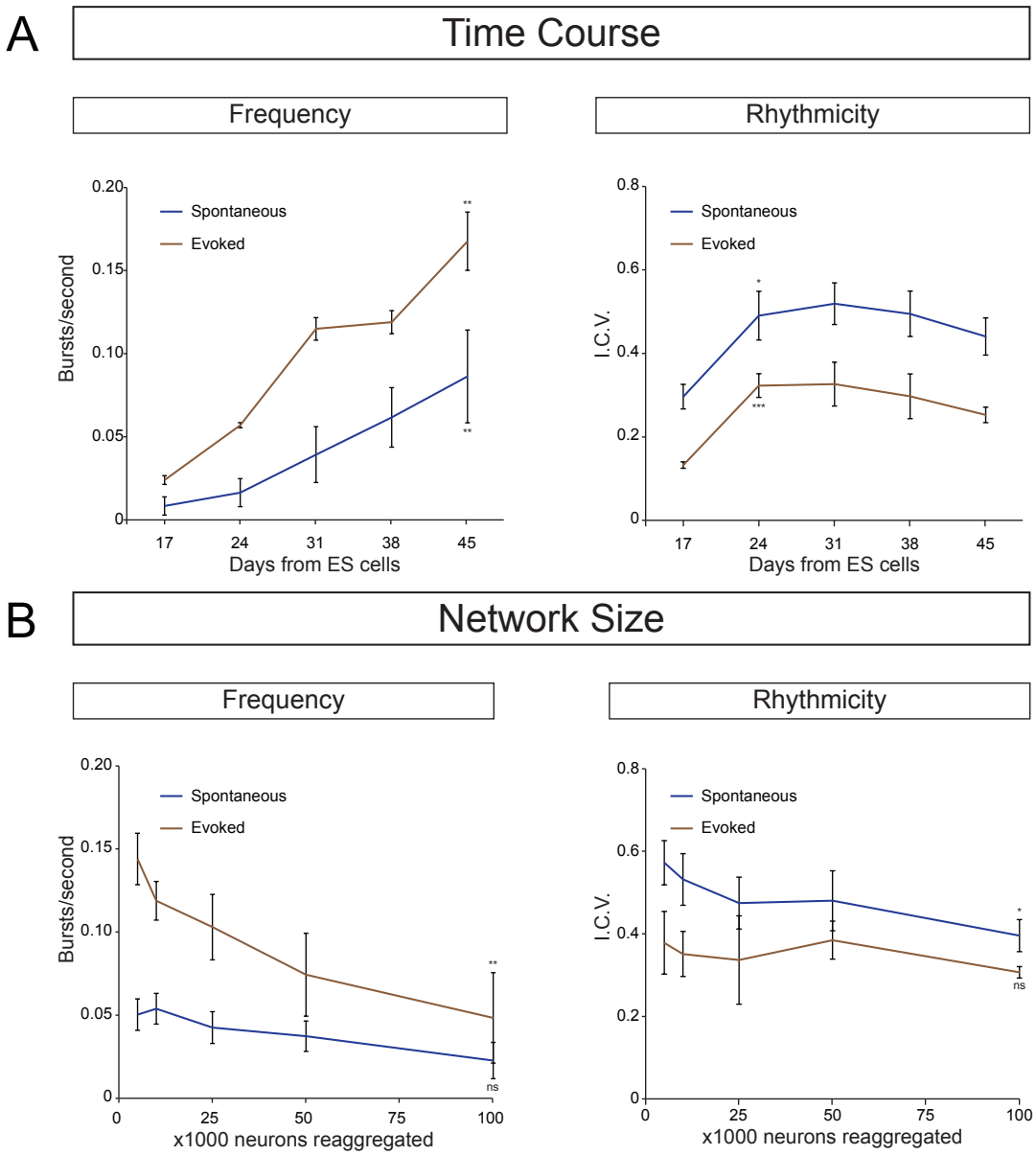

Figure 2.6 Alterations in frequency and rhythmicity as pure V3 interneuron networks mature or increase in size

(A) As pure V3 interneurons mature, the rate of spontaneous activity and evoked activity increases. Mean ± SEM, n networks-n neurospheres of (spontaneous) and [evoked]: D17 (4-19)/[4-19]; D45 (4-21)/[4-21]; **$p < 0.01$; unpaired t test. The rhythmicity of networks is also affected as pure V3 interneurons mature, though only between days 17 and 24, after that there is no significant change. Mean ± SEM, n networks-n neurospheres of (spontaneous) and [evoked]: D17 (4-19)/[4-19]; D45 (4-21)/[4-21]; *$p < 0.05$; ***$p < 0.001$; unpaired t test. (B) As more V3 interneurons are added to a network, there is no obvious change to the rate of spontaneous activity, but the rate of evoked activity significantly decreases. Mean ± SEM, n networks-n neurospheres of (spontaneous) and [evoked]: 5,000 (4-24)/[4-24]; 100,000 (4-24)/[4-23]; (ns) $p > 0.05$; *$p < 0.05$; unpaired t test. The rhythmicity of larger V3 interneuron networks is only increased in the spontaneous condition, not in the evoked. Mean ± SEM, n networks-n neurospheres of (spontaneous) and [evoked]: 5,000 (4-24)/[4-24]; 100,000 (4-24)/[4-23]; (ns) $p > 0.05$; *$p < 0.05$; unpaired t test.

with conventional knowledge, glutamatergic release of motor neurons has been, in fact, well documented (Herzog et al., 2004; Meister et al., 1993; Nishimaru, Restrepo, Ryge, Yanagawa, & Kiehn, 2005). Finally, one difference between these pure excitatory networks was found when studying their rhythmicity. Evoked pure V3 and V2a interneuron networks become significantly more rhythmic in comparison to their spontaneous network activity, but motor neuron networks, do not become more rhythmic (Figure 2.4d). This finding suggests that motor neurons have weaker synaptic coupling than the two excitatory interneuron subtypes tested. And furthermore, this finding suggests that in order to generate robust rhythmic motor output, the excitatory interneurons that compose the locomotor CPG are required.

Networks of pure inhibitory neurons lack rhythmicity

To test whether the activity described above for pure excitatory networks differs from networks composed of pure inhibitory neurons, we generated networks of 50,000 V1 interneurons (Figure 2.5f). While spontaneous activity can be observed in these V1 networks, the amplitudes are significantly lower than any of the pure excitatory networks (Figure 2.4c). Additionally, increased rhythmic activity is not evoked in these networks (Figure 2.4d). And while this lack of rhythmic activity is statistically similar to that of motor neuron networks, a large difference remains. Motor neuron network rhythmicity cannot be rescued with the application of inhibitory antagonists, while V1 inhibitory interneuron networks do respond with an increase in amplitude and rhythmicity (Figure 2.4c and d). Interestingly, similarly to the excitatory networks, the activity of the V1 interneuron networks can be significantly inhibited by CNQX (Figure 2.4e). And although we cannot exclude the presence of a small fraction of incorrectly sorted excitatory neurons or neurotransmitter fate switching (Dulcis, Jamshidi, Leutgeb, & Spitzer, 2013; Spitzer, 2012), our data has revealed strikingly different network activity between excitatory and inhibitory networks.

Shifting E/I neuronal balance in heterogeneous networks alters network output

Networks of pure inhibitory and excitatory neurons behave quite differently from each other, but what happens in mixed cultures? Knowing that differentiated neurospheres are

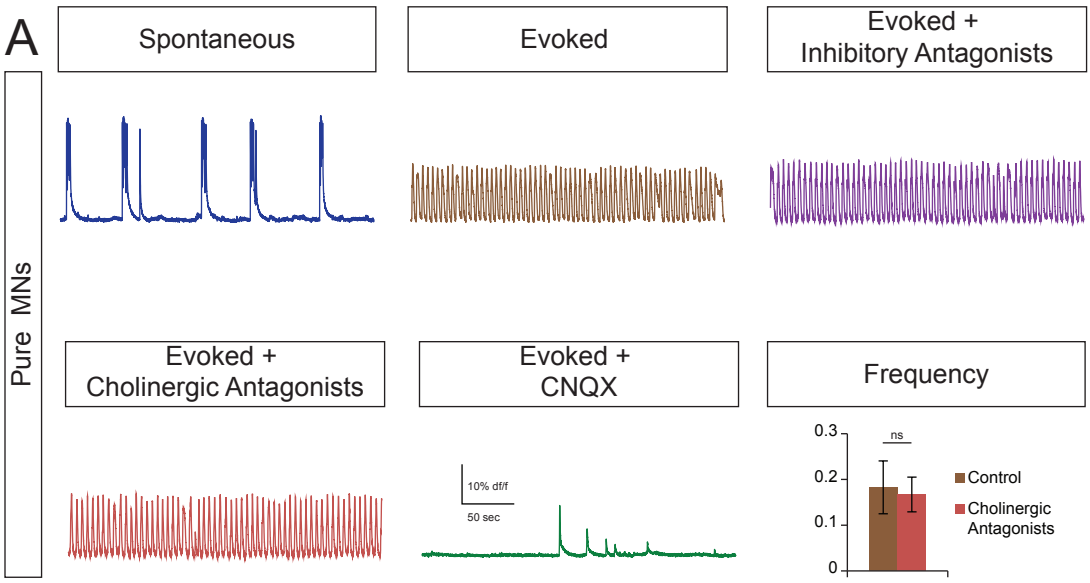

Figure 2.7 Cholinergic antagonists do not alter pure motor neuron network activity
(A) In pure motor neuron networks, the application of cholinergic antagonists lacks any significant change to the frequency of network activity compared to the control condition. Mean ± SEM, n differentiations (neurospheres): 4 (47); (ns) p = 0.52, paired t test.

composed of heterogeneous neuronal populations, we took these networks and studied their activity in the evoked and evoked + inhibitory antagonists conditions and noticed significant changes. When the activity of multiple neurospheres is averaged together for an experiment, the evoked condition shows a significantly increased rhythmic network output compared to the spontaneous condition (Figure 2.3e). However, individually, not all neurospheres increase their rhythmicity. We hypothesized that the rhythmic activity in these neurospheres was disrupted due to the presence and action of inhibitory interneurons. This hypothesis was confirmed by exposing these non-rhythmic neurospheres (I.C.V. > 0.2) to the evoked + inhibitory antagonists condition, which demonstrated that their rhythmic output could be significantly increased (Figure 2.8a). Separately, those networks that did respond rhythmically (I.C.V < 0.2) to the evoked condition slowed their rate of bursting with the application of inhibitory antagonists (Figure 2.8b). Put together, these data suggest that inhibitory neurons disrupt rhythmic activity and increase rhythmic network bursting frequency.

Since increasing the E/I ratio with inhibitory antagonists slows the rate of network activity and promotes rhythmic bursting, we were curious if we could reverse the results by decreasing the E/I ratio. To do this, we decided to genetically ablate an excitatory neuronal subtype from the heterogeneous networks. Based on the robust rhythmic activity of pure V3 networks, we hypothesized that removing V3 interneurons from the heterogeneous networks could adversely affect the rhythmic capability of the networks. To test this hypothesis, we first crossed mice that contained a transgene for the diphtheria toxin subunit-A (DTA), expressed in a Cre-dependent manner, to mice expressing Cre-recombinase under the Sim1 promotor, such that V3 interneurons would be killed upon differentiation (Figure 2.1a) (Y. Zhang et al., 2008). From this cross we derived mESCs that contained both transgenes and differentiated the V3 deleted ($V3^{-/-}$) and control lines in parallel under high SAG conditions.

When evoked, control lines showed a rhythmic pattern of activity while $V3^{-/-}$ lines showed a significantly reduced ability to generate robust rhythm. The frequency of activity is greater in $V3^{-/-}$ networks, as well (Figure 2.8c). Therefore, we have shown that decreasing the E/I ratio, through the removal of excitatory V3 interneurons, results in the opposite phenotypic response that occurred when we pharmacologically increased the E/I ratio (Figure 2.8a and b).

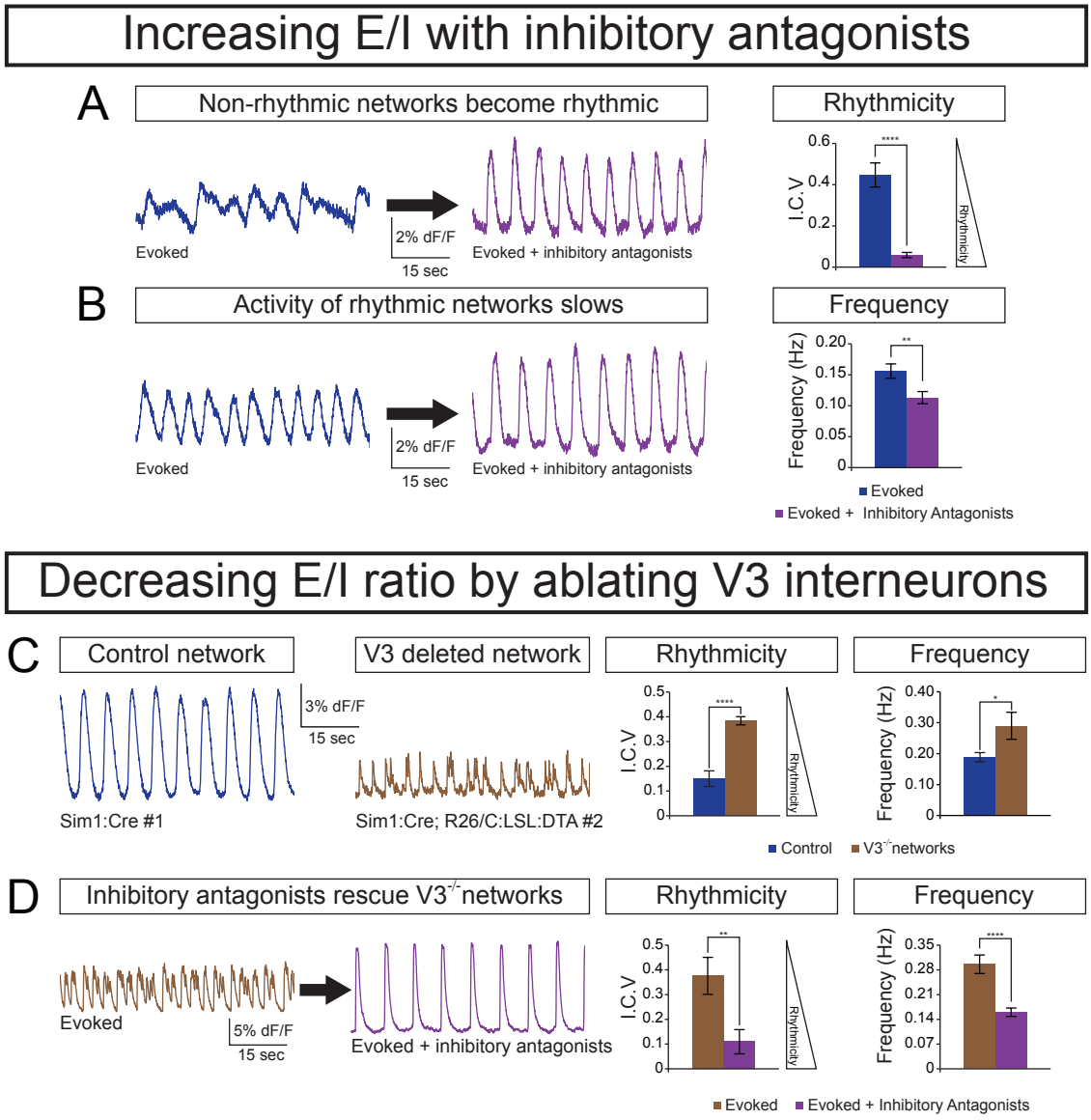

Figure 2.8 E/I ratio controls speed and rhythmicity in heterogeneous networks
(A) Wildtype, heterogeneous CAG::GCaMP3 networks that exhibit less rhythmic activity (I.C.V. >0.2) increase their rhythmicity after the application of inhibitory antagonists. Mean ± SEM, n neurospheres: 14; ****$p < 0.0001$, paired t test. (B) Highly rhythmic networks (I.C.V. <0.2) show a decrease in frequency with the application of inhibitory antagonists. Mean ± SEM, n neurospheres: 9; **$p < 0.01$, paired t test. (C) Ablating V3 interneurons from heterogeneous networks decreases rhythmicity and increases frequency. Control genotype: Sim1:Cre; $V3^{-/-}$ genotype: Sim1:Cre;R26/C:LSL:DTA. Mean ± SEM, n differentiations (n neurospheres): control, 5 (69); $V3^{-/-}$, 5 (85); *$p < 0.05$; ****$p < 0.0001$; unpaired t test. (D) $V3^{-/-}$ networks can be rescued with the application of inhibitory antagonists, increasing rhythmicity and decreasing frequency. $V3^{-/-}$ genotype: Sim1:Cre;R26/C:LSL:DTA. Mean ± SEM, n neurospheres: 18; ***$p < 0.001$; ****$p < 0.0001$; paired t test.

To build on this E/I concept even more, in one experiment we added inhibitory antagonists to the $V3^{-/-}$ neurospheres. This application demonstrated that the $V3^{-/-}$ networks are capable of robust rhythmic activity once inhibition is removed. Furthermore, we also observed a decrease in the frequency of these networks with the addition of inhibitory antagonists (Figure 2.8d). Together, all of these data demonstrate that the E/I ratio is crucial to generating network rhythmicity and controlling the rate of activity.

V1 interneurons increase the speed of V3 interneuron networks, not motor neuron networks

The neuronal subtype ablation and pharmacological studies in the heterogeneous neurospheres is informative, but has the same failings as those conducted in the spinal cord - multiple neuronal subtypes in uncontrollable numbers. To truly look at how neuronal subtypes and the E/I ratio influences network activity, we needed to create highly defined networks composed of known numbers of inhibitory and excitatory neurons. To do this, we followed the same protocol we used to generate pure neuronal networks, except in how the network was reaggregated. While the neurosphere assay was high throughput, allowing for multiple networks to be imaged at one time, this design only allowed for the full network output to be observed. For this reason, we chose to seed the neuronal networks for these experiments on a plate of astrocytes, instead (Figure 2.9a). With this design, we were able to image a large field of view, almost 15% of the network, with a low power objective, but we also gained the ability to sample sub-regions within that field of view, obtaining cellular resolution, with a higher power objective. For all networks in this set of experiments, we compared base networks composed of either 100,000 V3 interneurons or 100,000 motor neurons to which we added V1 interneurons (Figure 2.9a). By imaging the tomato fluorescence of V1 interneurons and averaging the intensity of the entire field of view, we can see a linear increase in tomato expression as the number of V1 interneurons increases (Figure 2.10).

Having demonstrated that we have tight control over the number of neurons we use to form networks, we mixed V1 interneurons into V3 interneuron and motor neuron base networks at varying concentrations. When testing V3+V1 networks, we found that V3 networks containing 40,000 V1 interneurons had almost double the rate of network activity when compared to pure

Figure 2.9 V1 interneurons alter activity rate of V3 interneuron networks
(A) Diagram of experimental design for plated *de novo* networks. (B) Representative traces of networks composed of 100,000 V3 interneurons mixed with 0, 20,000, or 40,000 V1 interneurons. Spontaneous activity and activity in inhibitory antagonists for the same networks are shown. (C) Representative traces of networks composed of 100,000 motor neurons mixed with 0, 20,000, or 40,000 V1 interneurons. Spontaneous activity and activity in inhibitory antagonists for the same networks are shown. (D) As V1 interneurons are added to V3 interneuron networks, the relative speed of the network increases. For each trial, the frequency of each network was standardized to the burst rate of the control network (0 V1 interneurons). Networks of 100,000 V3 interneurons + 40,000 V1 interneurons show significantly faster rate of activity than networks with 100,000 V3 interneurons + 5,000 V1 interneurons. Mean ± SEM, n networks: 5,000 V1 interneurons, 8; 40,000 V1 interneurons, 8; *$p < 0.05$; unpaired t test. (E) The rate of activity of motor neuron networks is not altered by V1 interneurons. A standardized rate of activity was calculated from the ratio of a network's activity in the inhibitory antagonist condition to that in the spontaneous condition. Inhibitory antagonists slow the activity of V3 interneuron networks if V1 interneurons are present, but motor neuron networks show no significant difference. Motor neurons: mean ± SEM, n networks: 0 V1 interneurons, 6; 40,000 V1 interneurons, 6; (ns) $p=0.63$; unpaired t test. (F) V1 interneurons decrease the amplitude of both V3 interneuron and motor neuron networks, but effect the amplitude of motor neuron networks more significantly than V3 interneuron networks. Mean ± SEM, n networks of (V3 interneurons) and [motor neurons]: 0 V1 interneurons, (7)/[8]; 5,000 V1 interneurons, (7)/[8]; 10,000 V1 interneurons, (7)/[8]; 15,000 V1 interneurons, (7)/[8]; 20,000 V1 interneurons, (7)/[8]; 40,000 V1 interneurons, (7)/[8]; *$p < 0.05$; **$p < 0.01$; ****$p < 0.0001$; unpaired t test. Inhibitory antagonists rescue the decrease in amplitude. (G) The presence of V1 interneurons increases the burst-to-burst amplitude coefficient of variation more dramatically in motor neuron networks than in V3 interneuron networks. Mean ± SEM, n networks of (V3 interneurons) and [motor neurons]: 0 V1 interneurons, (8)/[8]; 5,000 V1 interneurons, (8)/[8]; 10,000 V1 interneurons, (8)/[8]; 15,000 V1 interneurons, (8)/[8]; 20,000 V1 interneurons, (8)/[8]; 40,000 V1 interneurons, (8)/[8]; (ns) $p > 0.05$; *$p < 0.05$; **$p < 0.01$; ***$p < 0.001$; %$p < 1x10^{-5}$; unpaired t test. Inhibitory antagonists decrease the amplitude coefficient of variation in the networks.

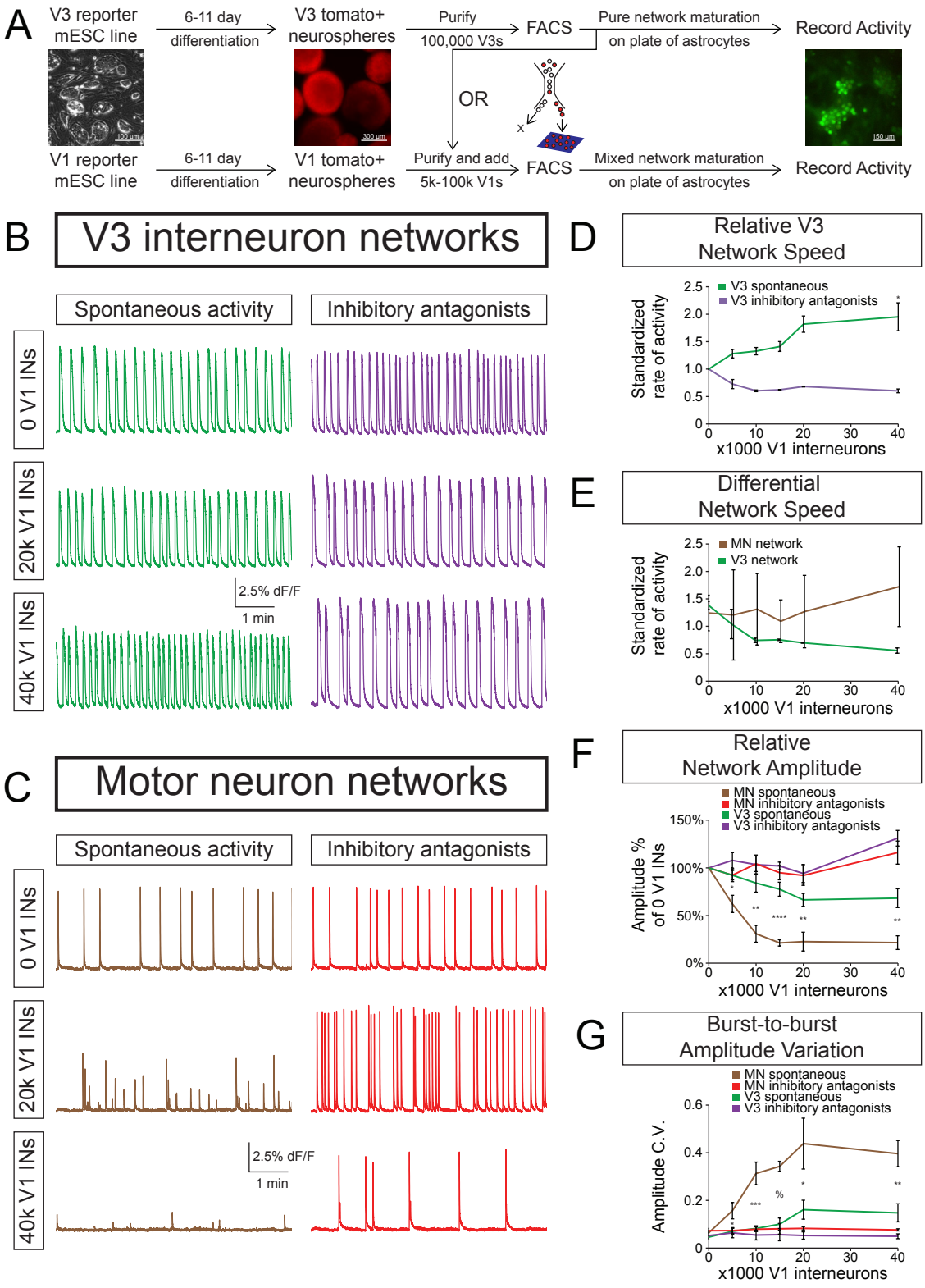
A
V3 reporter mESC line
6-11 day differentiation
V3 tomato+ neurospheres
Purify 100,000 V3s
FACS
Pure network maturation on plate of astrocytes
Record Activity
OR
V1 reporter mESC line
6-11 day differentiation
V1 tomato+ neurospheres
Purify and add 5k-100k V1s
FACS
Mixed network maturation on plate of astrocytes
Record Activity
B
V3 interneuron networks
Spontaneous activity
Inhibitory antagonists
0 V1 INs
20k V1 INs
40k V1 INs
2.5% dF/F
1 min
C
Motor neuron networks
Spontaneous activity
Inhibitory antagonists
0 V1 INs
20k V1 INs
40k V1 INs
2.5% dF/F
1 min
D
Relative V3 Network Speed
V3 spontaneous
V3 inhibitory antagonists
Standardized rate of activity
x1000 V1 interneurons
E
Differential Network Speed
MN network
V3 network
Standardized rate of activity
x1000 V1 interneurons
F
Relative Network Amplitude
MN spontaneous
MN inhibitory antagonists
V3 spontaneous
V3 inhibitory antagonists
Amplitude % of 0 V1 INs
x1000 V1 interneurons
G
Burst-to-burst Amplitude Variation
MN spontaneous
MN inhibitory antagonists
V3 spontaneous
V3 inhibitory antagonists
Amplitude C.V.
x1000 V1 interneurons

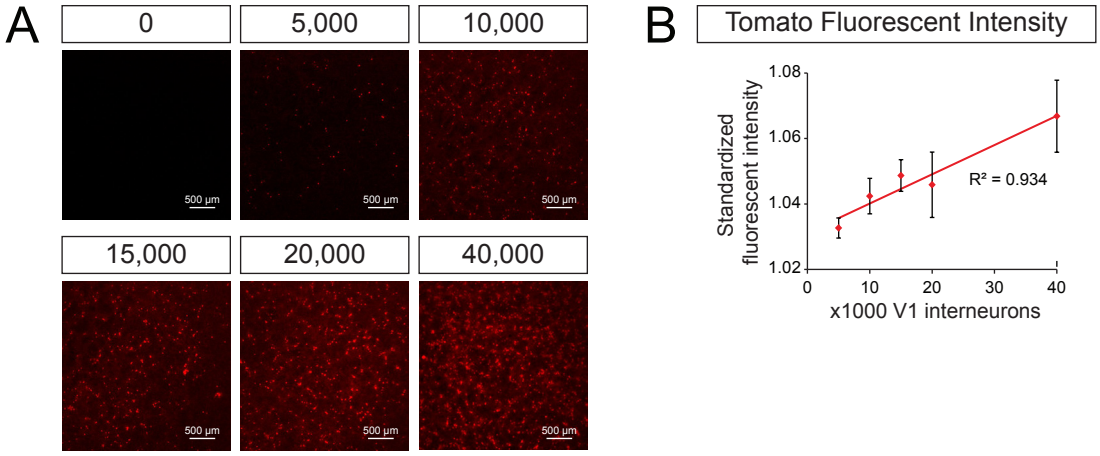

Figure 2.10 Tight control of neuronal contribution to de novo networks
(A) Tomato expression of plated V1 interneurons at different concentrations. (B) As the number of V1 interneurons is increased in networks of 100,000 motor neurons, there is a linear increase in tomato fluorescence intensity ($R^2 = 0.934$). Fluorescence for the entire field of view is averaged and then standardized to the auto-fluorescence of networks containing 0 V1 interneurons. Mean ± SEM, n = 7 networks per condition.

V3 networks and that the burst rate was significantly faster than when just 5,000 V1 interneurons were added and slowed by the application of inhibitory antagonists (Figure 2.9b and d and Video 2.6, 2.7, and 2.8). In addition to the alteration in network burst rate, the V1 interneurons also contributed to a decrease in burst amplitude (Figure 2.9b and f). When we tested these networks in the evoked condition we found that the rhythmic pattern of network activity was significantly hindered in networks that contained increased numbers of V1 interneurons (Figure 2.11). These changes to frequency, amplitude, and rhythmicity were negated with the addition of inhibitory antagonists, suggesting the influence of the V1 interneurons on the network was through their chemical synapses. We have now directly shown that decreasing the E/I ratio by increasing the number of inhibitory V1 interneurons in excitatory V3 interneuron networks increases the rate of network activity, decreases burst amplitude, and disrupts evoked rhythm.

With all of these changes observed in V3+V1 networks, we expected the same changes would be found when V1 interneurons were added to base networks of motor neurons, as V1 interneurons are well known to synapse onto motor neurons (Alvarez et al., 2005; Sapir et al., 2004; Saueressig, Burrill, & Goulding, 1999; Stam et al., 2012). To our surprise, we found results that were both similar and different from V3+V1 networks. As in V3+V1 networks, MN+V1 networks had lower burst amplitudes as V1 interneurons were increased (Figure 2.9c and f). While this change parallels what is seen in V3+V1 networks, the burst amplitude was much more affected in MN+V1 networks at every condition tested (Figure 2.9f). While V1 interneurons altered both V3+V1 and MN+V1 networks, the addition of inhibitory antagonists did not reveal any significant change to network frequency when applied to mixed MN+V1 networks (Figure 2.9e). Combined, we have now shown that V1 interneurons diminish network burst amplitude in both V3 interneuron and motor neuron networks, but that V1 interneurons selectively increase the rate of activity in V3 interneuron networks, lacking any significant effect on the standardized rate of motor neuron network activity.

V1 interneurons decouple motor neuron networks, not V3 interneuron networks

In addition to V1 interneurons decreasing the burst amplitude of MN+V1 networks more than V3+V1 networks, MN+V1 networks also showed significantly more burst-to-burst amplitude

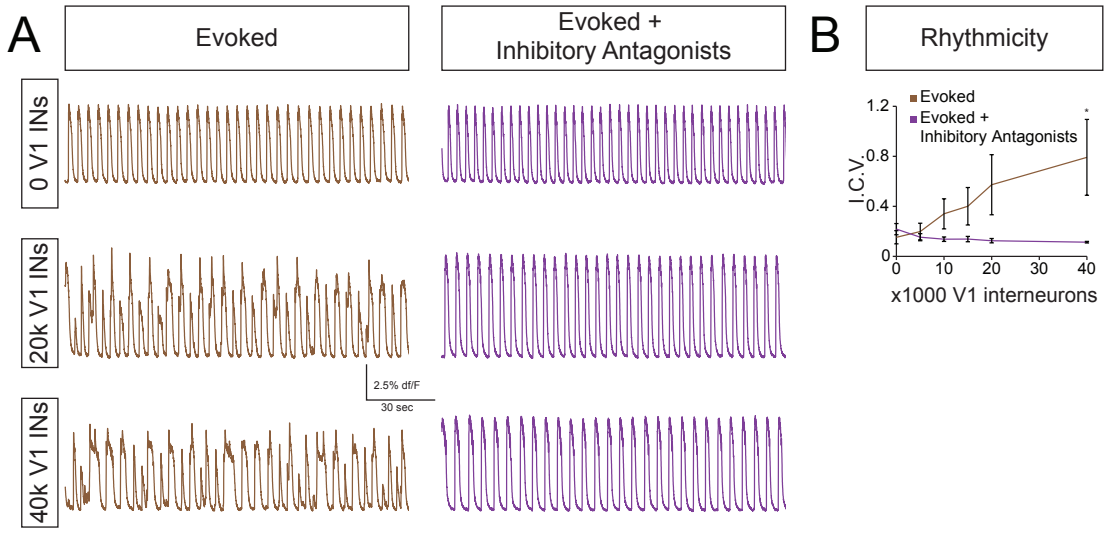

Figure 2.11 V1 interneurons disrupt rhythmic activity when added to V3 networks
(A) Representative traces of V3 interneuron networks mixed with different amounts of V1 interneurons in the evoked and evoked + inhibitory antagonists conditions. (B) Quantification of rhythmicity, demonstrating V1 interneurons disrupt V3 interneuron network rhythmicity. Mean ± SEM, n networks of (evoked): 0 (6); 40,000 (6); *$p < 0.05$; unpaired t test. The application of inhibitory antagonists rescues it.

Figure 2.12 V1 interneurons generate subnetworks within motor neuron networks
(A) V1 interneurons uncouple motor neuron networks. 10,000 V1 interneurons in a base network of 100,000 motor neurons reveals differentially active regions within a field of view during spontaneous activity, as demonstrated in Burst A and B. (B) When inhibitory antagonists are applied to mixed V1 interneuron and motor neuron networks, the neurons within the entire field of view are shown to burst together, as in Bursts C and D (same network as Figure 2.12a). **(**C) V1 interneurons increase the network complexity of motor neuron networks, but not V3 interneuron networks. Inhibitory antagonists are shown to decrease the complexity of MN+V1 networks. Median ± 95% CI, n networks of (V3 interneurons spontaneous), ((V3 interneurons inhibitory antagonists)), [motor neuron spontaneous], and [[motor neuron inhibitory antagonists]]: 0 V1 interneurons, (8)/((2))/[8]/[[5]]; 5,000 V1 interneurons, (8)/((2))/[8]/[[4]]; 10,000 V1 interneurons, (8)/((2))/[7]/[[6]]; 40,000 V1 interneurons, (8)/((2))/[7]/[[6]]; *$p < 0.05$; **$p < 0.01$; ***$p < 0.001$; %$p < 1x10^{-5}$; Kolmogorov–Smirnov test. (D) Imaging the calcium signal at the individual neuronal level reveals similar uncoupling at the cellular level in MN+V1 networks. 5 motor neuron traces from one representative 10:1 MN+V1 network under both the spontaneous and inhibitory antagonists conditions. While at first uncoupled, the same 5 neurons, once inhibitory antagonists are applied, burst in a correlated manner. (E) In a 1:1 V3:V1 mixed network, individual neuronal activity is tightly coupled. 5 traces from one representative network under both the spontaneous and inhibitory antagonists conditions. Application of inhibitory antagonists decreases the burst frequency of the same 5 neurons but they burst synchronously in both conditions. (F) At the cellular level, cross-correlation analysis shows that motor neurons, in an MN+V1 network are significantly less correlated than interneurons in a V3+V1 network. Even at 100,000 V1 interneurons, the V3+V1 networks are significantly more correlated than the MN+V1 networks containing 40,000 V1 interneurons. Mean ± SEM, n networks-neurons of (V3 interneurons spontaneous), ((V3 interneurons inhibitory antagonists)), [motor neuron spontaneous], and [[motor neuron inhibitory antagonists]]: 0 V1 interneurons, (8-160)/((2-40))/[8-160]/[[6-120]]; 5,000 V1 interneurons, (8-160)/((2-40))/[7-140]/[[6-120]]; 10,000 V1 interneurons, (8-160)/((2-40))/[7-140]/[[6-120]]; 40,000 V1 interneurons, (8-160)/((2-40))/[7-140]/[[6-120]]; 100,000 V1 interneurons, (4-80)/((2-40)); **$p < 0.01$; ***$p < 0.001$; ****$p < 0.0001$; unpaired t test . Inhibitory antagonists re-correlated networks containing V1 interneurons.

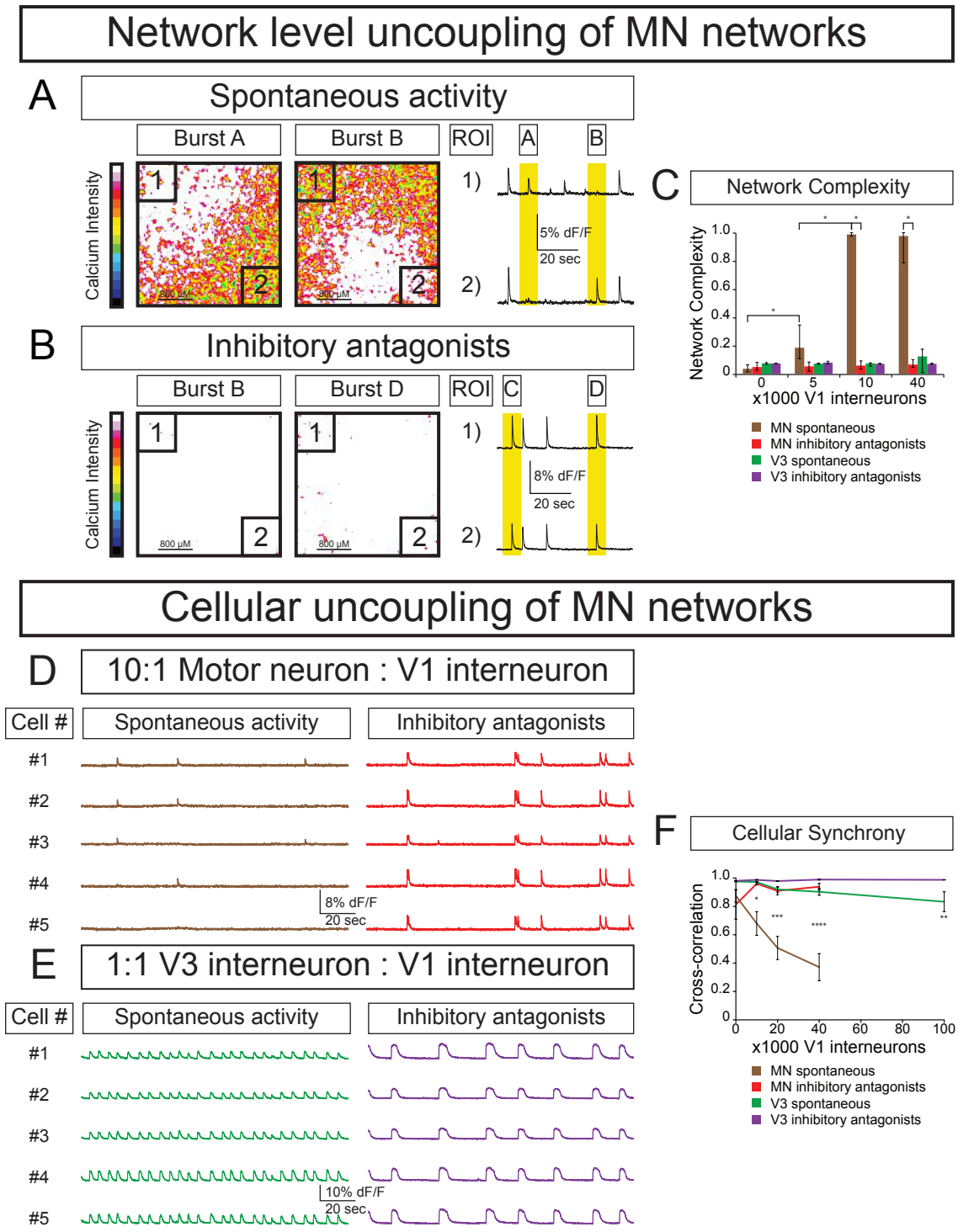
Network level uncoupling of MN networks
A
Spontaneous activity
Burst A
Burst B
ROI
A
B
Calcium Intensity
1
2
800 µM
1)
2)
5% dF/F
20 sec
B
Inhibitory antagonists
Burst B
Burst D
ROI
C
D
8% dF/F
20 sec
C
Network Complexity
Network Complexity
1.0
0.8
0.6
0.4
0.2
0
0
5
10
40
x1000 V1 interneurons
MN spontaneous
MN inhibitory antagonists
V3 spontaneous
V3 inhibitory antagonists
Cellular uncoupling of MN networks
D
10:1 Motor neuron : V1 interneuron
Cell #
Spontaneous activity
Inhibitory antagonists
#1
#2
#3
#4
#5
8% dF/F
20 sec
E
1:1 V3 interneuron : V1 interneuron
Cell #
Spontaneous activity
Inhibitory antagonists
#1
#2
#3
#4
#5
10% dF/F
20 sec
F
Cellular Synchrony
Cross-correlation
1.0
0.8
0.6
0.4
0.2
0
0
20
40
60
80
100
x1000 V1 interneurons
MN spontaneous
MN inhibitory antagonists
V3 spontaneous
V3 inhibitory antagonists

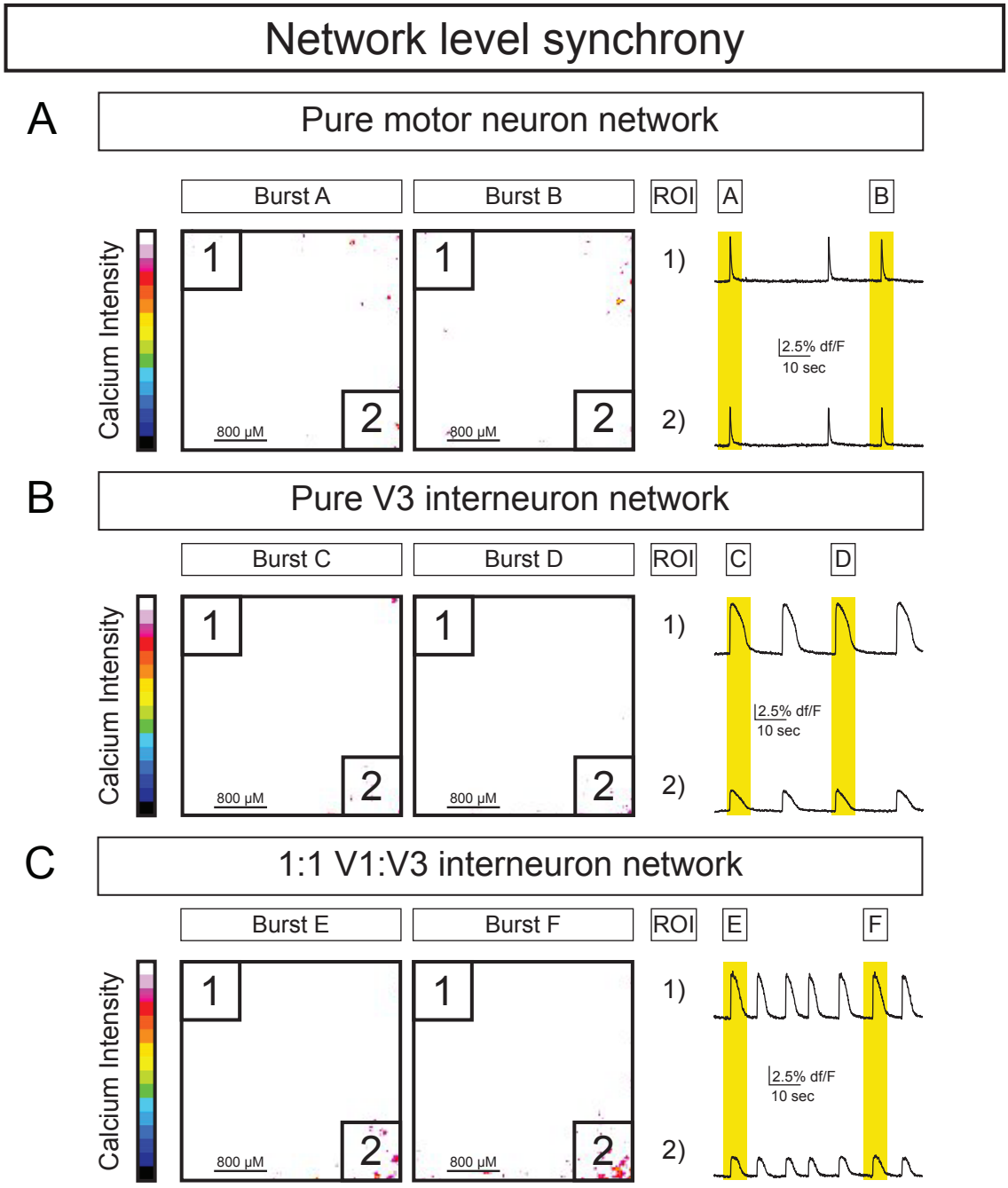

Figure 2.13 Synchronous activity observed in non-MN+V1 networks
(A) Representative pure motor neuron network demonstrating neuronal synchrony within a field of view for two different bursts (Bursts A and B). (B) Representative pure V3 interneuron network demonstrating neuronal synchrony within a field of view for two different bursts (Bursts C and D).(C) Representative 1:1 V3+V1 network demonstrating neuronal synchrony within a field of view for two different bursts (Bursts E and F).

variation than V3+V1 networks (Figure 2.9b, c, and g). We hypothesized that this variability was due to a desynchronization of the network. To test this assumption, instead of averaging the activity of the full field of view, in a 10:1 MN+V1 network, two regions of interest in opposite corners of the field of view were compared revealing distinct activity patterns (Figure 2.12a and Video 2.10). One could argue that this different activity pattern was a result of a physical separation in the network, however this was not the case, as when inhibitory antagonists were applied, the entire field of view burst synchronously (Figure 2.12b and Video 2.11). The network complexity observed in MN+V1 networks did not occur in pure motor neuron networks, pure V3 interneuron networks, or V3+V1 networks, suggesting a unique role of V1 influence on motor neuron networks (Figure 2.12a and c, 2.13 and Video 2.6, 2.7, and 2.9).

In addition to looking at the segregation of activity at a network level, with this plated network assay we are able to resolve the activity of individual neurons. As sub-networks are generated in MN+V1 networks, we knew that this had to be a result of differences at the individual neuron level. And though regionalization was not seen in V3+V1 networks, we were curious as to whether we could observe more subtle changes at the neuronal level. Here we show representative traces for 5 neurons within the same 10:1 MN+V1 network (Figure 2.12d). Some neurons burst together, while others do not. One neuron is even silent. However, upon application of inhibitory antagonists, the same 5 neurons from the same network are now active, and burst synchronously. This uncoupling of neurons within the motor neuron network is in stark contrast to what is found in pure MN networks, pure V3 interneuron networks, and even in 1:1 V3+V1 networks, as shown by 5 representative neurons bursting synchronously (Figure 2.12e). These differences can be quantified using a neuron-to-neuron cross-correlation analysis, demonstrating that motor neurons in MN+V1 networks are more likely to become unsynchronized than the interneurons in V3+V1 networks. Even 100,000 V1 interneurons do not desynchronize the V3+V1 networks to the same degree as the MN+V1 networks containing just 40,000 V1 interneurons (Figure 2.12f). All together, these results indicate that the E/I ratio within a network tunes a network's output in a context dependent manner, such that increasing numbers of V1 interneurons accelerate the rate of V3 interneuron network bursts, while they, instead, incrementally uncouple motor neuron networks (Figure 2.14).

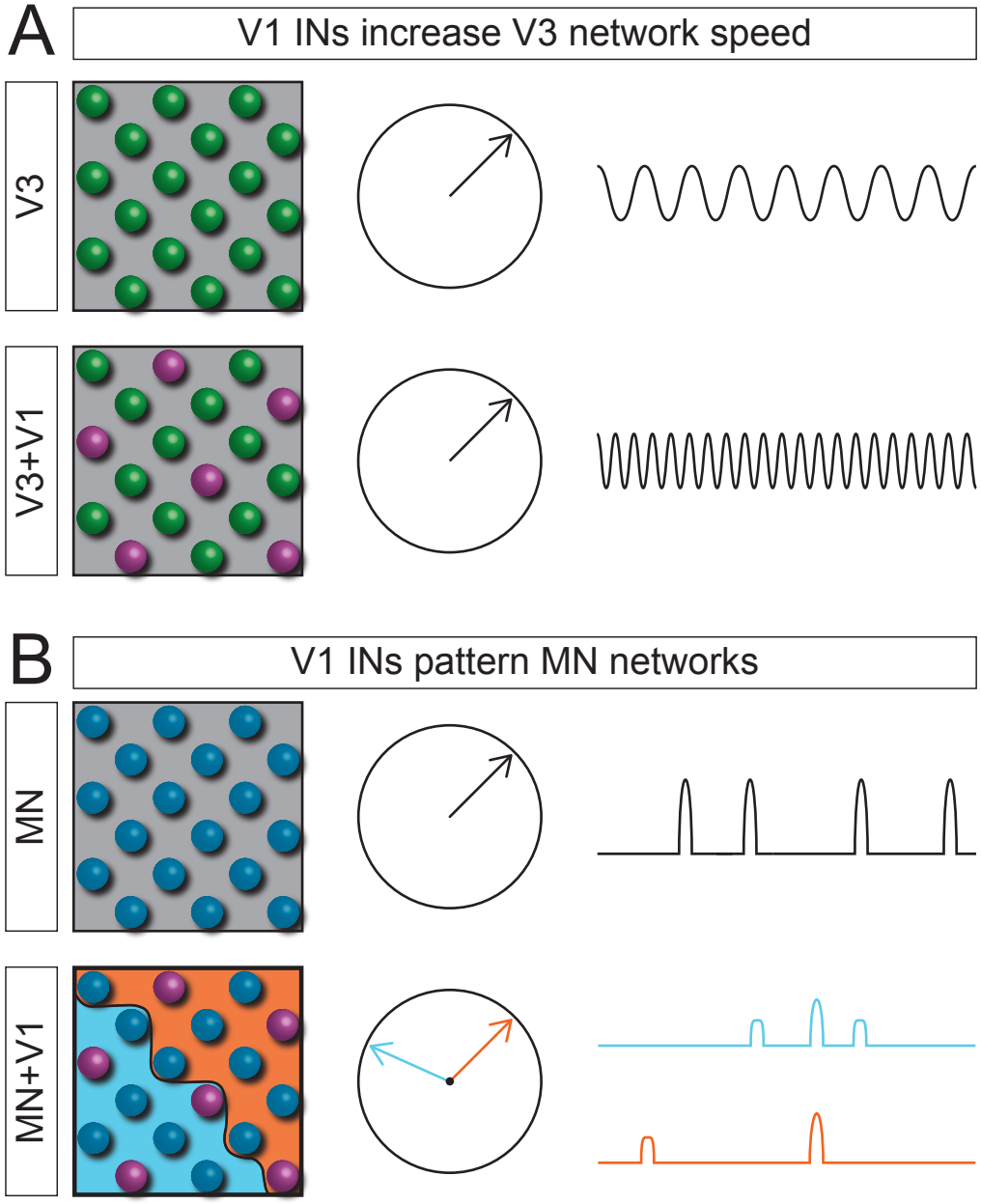

Figure 2.14 Recruitment of V1 interneurons alters network activity in a manner dependent upon cellular makeup of base network
(A) V1 interneurons increase the speed of V3 networks. Networks of V3 interneurons generate a coherent rhythmic output and as V1 interneurons are added, the network output increases speed. (B) V1 interneurons pattern motor neuron networks. Pure motor neuron networks fire in a coordinated manner, but V1 interneurons uncouple the larger network structure.

Discussion

The precise E/I balance in the nervous system is essential for its proper function (Cline, 2005). Here we use the locomotor CPG as an ideal model network to study this balance, as it is autonomous, has genetic tools that provide cellular access, and has a known output. Previously published studies have ablated or silenced different neuronal subtypes within the ventral spinal cord disrupting the locomotor CPG. But, due to the remaining complex network, it was impossible to know if this disruption was due to a change in the E/I balance of the network or the loss of the specific neuronal subtype. To circumvent this problem we sought to reduce the complexity of the locomotor CPG by generating simplified and highly defined *de novo* networks of ventral spinal neurons differentiated from mESCs. Using FACS, we created networks driven by V3 interneurons or motor neurons and recorded their activity using calcium imaging. Though these base networks behaved similarly, we found that inhibitory V1 interneurons, depending upon the network of excitatory neurons into which they were mixed, altered the network activity in differential ways. When mixed into a network of pure V3 interneurons, V1 interneurons increase the bursting rate of the network. In contrast, when part of a motor neuron network, V1 interneurons did not increase the rate of activity, but instead uncoupled the larger network into subnetworks. Therefore, we have concluded that the cellular E/I ratio plays a crucial role in tuning a network's activity, but also that the role of inhibition is context dependent, supporting the increasingly favored view that the locomotor CPG is layered into functional components for frequency and coordination (Garcia-Campmany et al., 2010; Grillner & Jessell, 2009; Hinckley et al., 2015; Kiehn, 2006; McCrea & Rybak, 2008).

De novo networks mimic the known properties of the locomotor CPG

Here we describe the first cell-type specific examination of highly defined *de novo* networks. Although studies have described how the output of the locomotor CPG changes when neuronal subtypes are ablated, the remaining network is still complex. By generating highly defined networks, composed of specific neuronal subtypes, we are able to dissect the role of neuronal subtypes in a manner not possible in more complex, *in vivo* assays.

And it should be noted, that the neurons we derived from the mESCs are very similar

to their *in vivo* counterparts. mESC derived motor neurons have been extensively studied and compared to their *in vivo* counterparts with data demonstrating that they migrate to the appropriate location within the spinal cord, form functional neuromuscular junctions, and have the appropriate electrophysiological properties (Miles et al., 2004; Soundararajan, Miles, Rubin, Brownstone, & Rafuse, 2006; Umbach, Adams, Gundersen, & Novitch, 2012; Wichterle et al., 2002). Furthermore, they, and the other interneurons generated here, are identified with the ubiquitously used, classical markers of the cardinal spinal neuronal subtypes (Figure 2.1a), and are generated in accordance with shifting levels of sonic hedgehog pathway activation (Figure 2.1d) (Alaynick et al., 2011). And finally, these mESC derived neurons appropriately express known marker genes for these cardinal neuronal subtypes (Figure 2.15), ultimately resulting in their appropriate neurotransmitter expression (Figure 2.4) (Al-Mosawie, Wilson, & Brownstone, 2007; Lundfald et al., 2007; Y. Zhang et al., 2008).

In addition to the similarities between *in vitro* and *in vivo* neuronal subtypes, many of the network properties of the locomotor CPG are also paralleled in our *de novo* networks. Spontaneous activity found in these neurospheres, both heterogeneous and purified, is also found in the isolated spinal cord preparation. And the rhythmic activity observed in the isolated spinal cord preparation is induced in our system using the same drugs (Whelan et al., 2000). Furthermore, the induced activity in both experimental paradigms is disrupted with the application of the glutamatergic, AMPA receptor antagonist CNQX (Feldman & Smith, 1989; Nishimaru et al., 2000; Whelan et al., 2000). Finally, both V3 interneurons and V1 interneurons are found to play similar roles *in vivo*. V3 interneuron ablation results in a disruption of rhythmic output (Figure 2.8b) (Y. Zhang et al., 2008) and the presence of V1 interneurons increases the rate of activity (Figure 2.9b and d) (Gosgnach et al., 2006). All of this data together provides us confidence in our system, allowing us to ask the questions in this paper that could not have been addressed *in vivo*.

Excitatory/inhibitory balance

Proper excitatory and inhibitory balance within the CNS is crucial to its function, and in the motor system the E/I ratio has been shown to alter the frequency and pattern of network

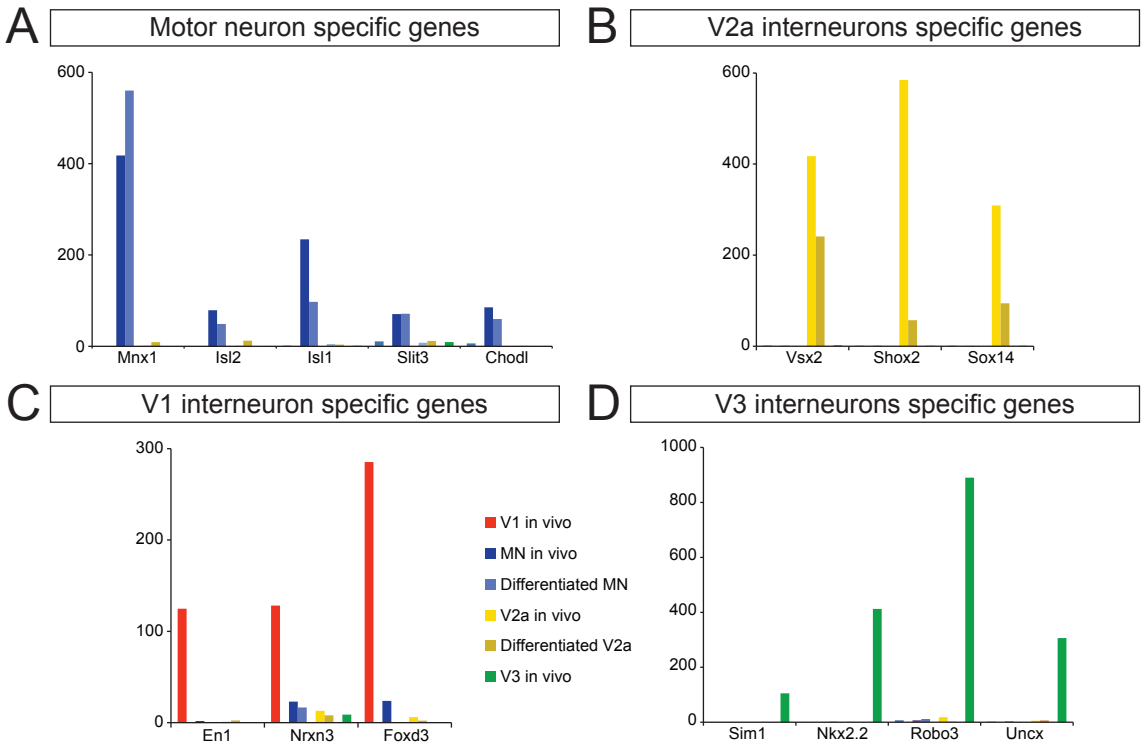

Figure 2.15 mESC derived neurons appropriately express known markers
(A) Known motor neuron genes are shown to be expressed in *in vivo* and mESC derived motor neurons. (B) Known V2a interneuron genes are shown to be expressed in *in vivo* and mESC derived V2a interneurons. (C) V1 interneurons genes are not misexpressed in mESC derived motor neurons or V2a interneurons. (D) V3 interneurons genes are not misexpressed in mESC derived motor neurons or V2a interneurons.

oscillations (Büschges et al., 2011; Gosgnach et al., 2006; Kiehn, 2011; Kishore, Bagnall, & McLean, 2014; McLean & Dougherty, 2015; McLean, Masino, Koh, Lindquist, & Fetcho, 2008; Y. Zhang et al., 2008). Here we have demonstrated that the E/I ratio does alter frequency and pattern but does so in a context dependent manner. By reducing the locomotor CPG into its component parts we have shown that the inhibitory V1 neurons increase the rate of V3 interneuron network activity, but segregate motor neuron driven networks into subunits.

The E/I ratio can be studied in synaptic contacts onto single cells or at the level of cellular composition in a network (Atallah & Scanziani, 2009; Berg, Alaburda, & Hounsgaard, 2007; Gosgnach et al., 2006; Kishore et al., 2014; Talpalar et al., 2013; Xue, Atallah, & Scanziani, 2014; J. Zhang et al., 2014; Y. Zhang et al., 2008). Numerous studies have investigated the recruitment of spinal neurons during locomotion and have demonstrated that different sets and numbers of neurons are recruited to achieve distinct motor outputs (Ampatzis, Song, Ausborn, & El Manira, 2014; Dougherty et al., 2013; Eklöf-Ljunggren et al., 2012; McLean, Fan, Higashijima, Hale, & Fetcho, 2007; McLean et al., 2008; Zhong, Sharma, & Harris-Warrick, 2011). Here we have created a novel assay to identify and purify neurons allowing us to generate a highly defined functional network. Using base excitatory networks of either V3 interneurons or motor neurons, we titrated V1 inhibitory neurons into the base excitatory networks, mimicking how these inhibitory neurons might be increasingly recruited during locomotion. Such tight control over network composition has only previously been possible in computational modeling.

From our *de novo* networks we found that simulating an increased recruitment of V1 interneurons change network output. Interestingly these inhibitory interneurons alter the network output differently depending upon the excitatory neuronal subtype composing the base network. We have shown that V1 interneurons increase the speed of V3 interneuron base networks, but not motor neuron base networks. Additionally, recruiting more V1 interneurons quickly uncouples networks of motor neurons, without any obvious effect on the synchrony of neurons within networks of V3 interneurons. As V3 interneurons have been found to be responsible for synchronizing motor output, the fact that networks of V3 interneurons cannot be uncoupled parallels the *in vivo* data (Bernhardt et al., 2012; Bernhardt, Gezelius, Vallstedt, Memic, & Kullander, 2009). We propose that weaker motor neuron-to-motor neuron connections allow the

V1 interneurons to more easily uncouple the MN+V1 networks, while strong excitatory synaptic connections between V3 interneurons allow V3+V1 networks to remain synchronous. The increased synaptic strength between V3 interneurons is supported by the finding that V3 networks are more rhythmic than motor neuron networks (Figure 2.4d). It should be noted, however, that other factors may also be contributing to this difference in network synchrony, such as stronger synaptic strength from V1 interneurons onto motor neurons than that from V1 interneurons onto V3 interneurons.

Many studies have shown that inhibition synchronizes neuronal firing and is responsible for coherent oscillations (Bartos, Vida, & Jonas, 2007; Cobb, Buhl, Halasy, Paulsen, & Somogyi, 1995; Lytton & Sejnowski, 1991; Van Vreeswijk, Abbott, & Ermentrout, 1994; Vida, Bartos, & Jonas, 2006; Wang & Buzsaki, 1996). Here we find that inhibition does the opposite - uncoupling motor neuron networks and disrupting the rhythmic activity of induced V3 interneuron networks. One reason for this discrepancy might be due to the fact that much of the work studying how inhibition alters network oscillations is done with the much faster, typically gamma, oscillations (Bartos et al., 2007). Perhaps slower network oscillations, such as those studied in this paper, require stronger excitatory drive, but faster network oscillations do require inhibition. Additionally, when synchrony is discussed in papers studying gamma oscillations, most often it is in terms of action potential timing, a timescale too fast for calcium imaging. So even though neurons within the networks we studied are becoming less correlated with the addition of V1 interneurons, as determined by calcium imaging, perhaps the inhibitory interneurons are increasing action potential synchronization in neurons that burst together. Further experiments should be conducted with paired cell recordings to determine if V1 interneurons are, in fact, increasing neuronal synchrony at the level of action potential timing.

Neuronal subtype specificity

Our results demonstrate that V1 interneurons increase the rate of V3 interneuron driven networks but not the rate of motor neuron driven networks. These results parallel and also provide greater clarity to a previous study that identified V1 interneurons having a role in locomotor speed regulation (Gosgnach et al., 2006). Our results suggest that the change in

locomotor speed, associated with the presence or absence of V1 interneurons in that study, is linked to the upstream network of interneurons in the locomotor CPG, not at the level of the motor neurons. However, our results do suggest that the V1 interneurons are, at a motor neuron level, responsible for the formation of motor units. Knowing that V1 interneurons are divided into Renshaw cells, Ia inhibitory interneurons, and other, unknown sub-populations begs the question of whether there are specific subtypes of V1 interneurons that differentially synapse onto V3 interneurons or motor neurons (Alvarez et al., 2005; Goulding, 2009; Sapir et al., 2004; Stam et al., 2012). Through the use of patch clamping and immunocytochemistry, future work should be able to successfully determine if differential synaptic connections are occurring.

Author Contributions

M.J.S and S.L.P. designed the study. M.J.S. generated mESC lines and conducted cell culture and calcium-imaging experiments. C.A.H. recorded electrophysiological activity. K.L.H. generated the CAG::GCaMP3 mouse line. M.T.P. generated an Hb9::GFP mESC line and provided cell culture support. S.P.D. designed and wrote analysis algorithms. M.J.S. and S.P.D. analyzed the data. M.J.S. and S.L.P. wrote the paper.

Acknowledgements

M.J.S was supported by the Rose Hills Foundation, the H.A. and Mary K. Chapman Charitable Trust, and the UCSD Neurosciences Graduate Program Training Grant. S.L.P. is an HHMI investigator and Benjamin H. Lewis chair in neuroscience. This research was supported by funding from the Howard Hughes Medical Institute, the Christopher and Dana Reeve Foundation, and the Marshall Foundation. We thank K. Sharma and M. Goulding for sharing mouse lines with us. K. Lettieri provided much appreciated mouse colony support.

References

Alaynick, W. A., Jessell, T. M., & Pfaff, S. L. (2011). SnapShot: spinal cord development. *Cell*, *146*(1), 178–178.e1. http://doi.org/10.1016/j.cell.2011.06.038

Al-Mosawie, A., Wilson, J. M., & Brownstone, R. M. (2007). Heterogeneity of V2-derived interneurons in the adult mouse spinal cord. *The European Journal of Neuroscience*, *26*(11), 3003–15. http://doi.org/10.1111/j.1460-9568.2007.05907.x

Alvarez, F. J., Jonas, P. C., Sapir, T., Hartley, R., Berrocal, M. C., Geiman, E. J., Todd, A., & Goulding, M. (2005). Postnatal phenotype and localization of spinal cord V1 derived interneurons. The Journal of Comparative Neurology, 493(2), 177–192. http://doi.org/10.1002/cne.20711

Ampatzis, K., Song, J., Ausborn, J., & El Manira, A. (2014). Separate Microcircuit Modules of Distinct V2a Interneurons and Motoneurons Control the Speed of Locomotion. *Neuron*, *83*(4), 934–943. http://doi.org/10.1016/j.neuron.2014.07.018

Atallah, B. V., & Scanziani, M. (2009). Instantaneous Modulation of Gamma Oscillation Frequency by Balancing Excitation with Inhibition. *Neuron*, *62*(4), 566–577. http://doi.org/10.1016/j.neuron.2009.04.027

Azim, E., Jiang, J., Alstermark, B., & Jessell, T. M. (2014). Skilled reaching relies on a V2a propriospinal internal copy circuit. *Nature*, *508*(7496), 357–363. http://doi.org/10.1038/nature13021

Bartos, M., Vida, I., & Jonas, P. (2007). Synaptic mechanisms of synchronized gamma oscillations in inhibitory interneuron networks. *Nature Reviews. Neuroscience*, *8*(1), 45–56. http://doi.org/http://doi.org/10.1038/nrn2044

Berg, R. W., Alaburda, A., & Hounsgaard, J. (2007). Balanced Inhibition and Excitation Drive Spike Activity in Spinal Half-Centers. *Science*, *315*(5810), 390–393. http://doi.org/10.1126/science.1134960

Bernhardt, N. R., Gezelius, H., Vallstedt, A., Memic, F., & Kullander, K. (2009). Netrin-1-dependent spinal interneuron subtypes are required for the formation of left-right alternating locomotor circuitry. *The Journal of Neuroscience*, *29*(50), 15642–15649. http://doi.org/10.1523/jneurosci.5096-09.2009

Bernhardt, N. R., Memic, F., Gezelius, H., Thiebes, A.-L., Vallstedt, A., & Kullander, K. (2012). DCC mediated axon guidance of spinal interneurons is essential for normal locomotor central pattern generator function. *Developmental Biology*, *366*(2), 279–289. http://doi.org/10.1016/j.ydbio.2012.03.017

Brown, C. R., Butts, J. C., McCreedy, D. A., & Sakiyama-Elbert, S. E. (2014). Generation of V2a interneurons from mouse embryonic stem cells. *Stem Cells and Development*, *23*(15), 1765–76. http://doi.org/10.1089/scd.2013.0628

Büschges, A., Scholz, H., & El Manira, A. (2011). New moves in motor control. *Current Biology : CB*, *21*(13), R513–R524. http://doi.org/10.1016/j.cub.2011.05.029

Cline, H. (2005). Synaptogenesis : A Balancing Act. *Current Biology*, *15*(6), R203–R205. http://doi.org/10.1016/j.cub.2005.03.010

Cobb, S. R., Buhl, E. H., Halasy, K., Paulsen, O., & Somogyi, P. (1995). Synchronization of neuronal activity in hippocampus by individual GABAergic interneurons. *Nature*, *378*(6552), 75–78. http://doi.org/10.1038/378075a0

Cowley, K. C., & Schmidt, B. J. (1995). Effects of inhibitory amino acid antagonists on reciprocal inhibitory interactions during rhythmic motor activity in the in vitro neonatal rat spinal cord. *Journal of Neurophysiology*, *74*(3), 1109–1117.

Del Barrio, M. G., Taveira-Marques, R., Muroyama, Y., Yuk, D.-I., Li, S., Wines-Samuelson, M., Shen, J., Smith, H., Xiang, M., Rowitch, D., & Richardson, W. D. (2007). A regulatory network involving Foxn4, Mash1 and delta-like 4/Notch1 generates V2a and V2b spinal interneurons

from a common progenitor pool. Development, 134(19), 3427–3436. http://doi.org/10.1242/dev.005868

Dougherty, K. J., Zagoraiou, L., Satoh, D., Rozani, I., Doobar, S., Arber, S., Jessell, T., Kiehn, O. (2013). Locomotor rhythm generation linked to the output of spinal shox2 excitatory interneurons. Neuron, 80(4), 920–933. http://doi.org/10.1016/j.neuron.2013.08.015

Dulcis, D., Jamshidi, P., Leutgeb, S., & Spitzer, N. C. (2013). Neurotransmitter switching in the adult brain regulates behavior. *Science*, *340*(6131), 449–453. http://doi.org/10.1126/science.1234152

Eklöf-Ljunggren, E., Haupt, S., Ausborn, J., Dehnisch, I., Uhlén, P., Higashijima, S., & El Manira, A. (2012). Origin of excitation underlying locomotion in the spinal circuit of zebrafish. *Proceedings of the National Academy of Sciences of the United States of America*, *109*(14), 5511–5516. http://doi.org/10.1073/pnas.1115377109

Feldman, J. L., & Smith, J. C. (1989). Cellular Mechanisms Underlying Modulation. *Annals of the New York Academy of Sciences*, *563*, 114–130. http://doi.org/10.1111/j.1749-6632.1989.tb42194.x

Garcia-Campmany, L., Stam, F. J., & Goulding, M. (2010). From circuits to behaviour: motor networks in vertebrates. *Current Opinion in Neurobiology*, *20*(1), 116–125. http://doi.org/10.1016/j.conb.2010.01.002

Gosgnach, S., Lanuza, G. M., Butt, S. J. B., Saueressig, H., Zhang, Y., Velasquez, T., Riethmacher, D., Callaway, E., Kiehn, O., & Goulding, M. (2006). V1 spinal neurons regulate the speed of vertebrate locomotor outputs. Nature, 440(7081), 215–219. http://doi.org/10.1038/nature04545

Goulding, M. (2009). Circuits controlling vertebrate locomotion: moving in a new direction. *Nature Reviews. Neuroscience*, *10*(7), 507–518. http://doi.org/10.1038/nrn2608

Goulding, M., & Pfaff, S. L. (2005). Development of circuits that generate simple rhythmic behaviors in vertebrates. *Current Opinion in Neurobiology*, *15*(1), 14–20. http://doi.org/10.1016/j.conb.2005.01.017

Grillner, S. (2006). Biological pattern generation: the cellular and computational logic of networks in motion. *Neuron*, *52*(5), 751–766. http://doi.org/10.1016/j.neuron.2006.11.008

Grillner, S., & Jessell, T. M. (2009). Measured motion: searching for simplicity in spinal locomotor networks. *Current Opinion in Neurobiology*, *19*(6), 572–586. http://doi.org/10.1016/j.conb.2009.10.011

Herzog, E., Landry, M., Buhler, E., Bouali-Benazzouz, R., Legay, C., Henderson, C. E., Nagy, F., Dreyfus, P., Giros, B., & El Mestikawy, S. (2004). Expression of vesicular glutamate transporters, VGLUT1 and VGLUT2, in cholinergic spinal motoneurons. European Journal of Neuroscience, 20(7), 1752–1760. http://doi.org/10.1111/j.1460-9568.2004.03628.x

Hinckley, C. A., Alaynick, W. A., Gallarda, B. W., Hayashi, M., Hilde, K. L., Driscoll, S. P., Dekker, J., Tucker, H., Sharpee, T., & Pfaff, S. L. (2015). Spinal Locomotor Circuits Develop Using Hierarchical Rules Based on Motorneuron Position and Identity. Neuron, 87(5), 1008–1021. http://doi.org/10.1016/j.neuron.2015.08.005

Kiehn, O. (2006). Locomotor circuits in the mammalian spinal cord. *Annual Review of Neuroscience*, *29*, 279–306. http://doi.org/10.1146/annurev.neuro.29.051605.112910

Kiehn, O. (2011). Development and functional organization of spinal locomotor circuits. *Current*

Opinion in Neurobiology, *21*(1), 100–109. http://doi.org/10.1016/j.conb.2010.09.004

Kishore, S., Bagnall, M. W., & McLean, D. L. (2014). Systematic shifts in the balance of excitation and inhibition coordinate the activity of axial motor pools at different speeds of locomotion. *The Journal of Neuroscience*, *34*(42), 14046–14054. http://doi.org/10.1523/jneurosci.0514-14.2014

Lee, S.-K., Jurata, L. W., Funahashi, J., Ruiz, E. C., & Pfaff, S. L. (2004). Analysis of embryonic motoneuron gene regulation: derepression of general activators function in concert with enhancer factors. *Development*, *131*(14), 3295–3306. http://doi.org/10.1242/dev.01179

Lundfald, L., Restrepo, C. E., Butt, S. J. B., Peng, C.-Y., Droho, S., Endo, T., Zeilhofer, H., Sharma, K., Kiehn, O. (2007). Phenotype of V2-derived interneurons and their relationship to the axon guidance molecule EphA4 in the developing mouse spinal cord. European Journal of Neuroscience, 26(11), 2989–3002. http://doi.org/10.1111/j.1460-9568.2007.05906.x

Lytton, W. W., & Sejnowski, T. J. (1991). Simulations of cortical pyramidal neurons synchronized by inhibitory interneurons. *Journal of Neurophysiology*, *66*(3), 1059–1079.

McCrea, D. A., & Rybak, I. A. (2008). Organization of mammalian locomotor rhythm and pattern generation. *Brain Research Reviews*, *57*(1), 134–146. http://doi.org/10.1016/j.brainresrev.2007.08.006

McLean, D. L., & Dougherty, K. J. (2015). Peeling back the layers of locomotor control in the spinal cord. *Current Opinion in Neurobiology*, *33*, 63–70. http://doi.org/10.1016/j.conb.2015.03.001

McLean, D. L., Fan, J., Higashijima, S., Hale, M. E., & Fetcho, J. R. (2007). A topographic map of recruitment in spinal cord. *Nature*, *446*(7131), 71–75. http://doi.org/10.1038/nature05588

McLean, D. L., Masino, M. A., Koh, I. Y. Y., Lindquist, W. B., & Fetcho, J. R. (2008). Continuous shifts in the active set of spinal interneurons during changes in locomotor speed. *Nature Neuroscience*, *11*(12), 1419–1429. http://doi.org/10.1038/nn.2225

Meister, B., Arvidsson, U., Zhang, X., Jacobsson, G., Villar, M. J., & Hökfelt, T. (1993). Glutamate transporter mRNA and glutamate-like immunoreactivity in spinal motoneurones. *Neuroreport*, *5*(3), 337–340.

Miles, G. B., Yohn, D. C., Wichterle, H., Jessell, T. M., Rafuse, V. F., & Brownstone, R. M. (2004). Functional properties of motoneurons derived from mouse embryonic stem cells. *The Journal of Neuroscience*, *24*(36), 7848–7858. http://doi.org/10.1523/jneurosci.1972-04.2004

Nishimaru, H., Restrepo, C. E., Ryge, J., Yanagawa, Y., & Kiehn, O. (2005). Mammalian motor neurons corelease glutamate and acetylcholine at central synapses. *Proceedings of the National Academy of Sciences of the United States of America*, *102*(14), 5245–5249. http://doi.org/10.1073/pnas.0501331102

Nishimaru, H., Takizawa, H., & Kudo, N. (2000). 5-Hydroxytryptamine-induced locomotor rhythm in the neonatal mouse spinal cord in vitro. *Neuroscience Letters*, *280*(3), 187–190. http://doi.org/10.1016/S0304-3940(00)00805-3

Peljto, M., Dasen, J. S., Mazzoni, E. O., Jessell, T. M., & Wichterle, H. (2010). Functional Diversity of ESC-Derived Motor Neuron Subtypes Revealed through Intraspinal Transplantation. *Cell Stem Cell*, *7*(3), 355–366. http://doi.org/10.1016/j.stem.2010.07.013

Sapir, T., Geiman, E. J., Wang, Z., Velasquez, T., Mitsui, S., Yoshihara, Y., Frank, E., Alvarez, F., & Goulding, M. (2004). Pax6 and engrailed 1 regulate two distinct aspects of renshaw

cell development. The Journal of Neuroscience, 24(5), 1255–1264. http://doi.org/10.1523/jneurosci.3187-03.2004

Saueressig, H., Burrill, J., & Goulding, M. (1999). Engrailed-1 and netrin-1 regulate axon pathfinding by association interneurons that project to motor neurons. *Development*, *126*(19), 4201–4212.

Soundararajan, P., Miles, G. B., Rubin, L. L., Brownstone, R. M., & Rafuse, V. F. (2006). Motoneurons Derived from Embryonic Stem Cells Express Transcription Factors and Develop Phenotypes Characteristic of Medial Motor Column Neurons. *The Journal of Neuroscience*, *26*(12), 3256–3268. http://doi.org/10.1523/jneurosci.5537-05.2006

Spitzer, N. C. (2012). Activity-dependent neurotransmitter respecification. *Nature Reviews Neuroscience*, *13*(2), 94–106. http://doi.org/10.1038/nrn3154

Stam, F. J., Hendricks, T. J., Zhang, J., Geiman, E. J., Francius, C., Labosky, P. A., Clotman, F., & Goulding, M. (2012). Renshaw cell interneuron specialization is controlled by a temporally restricted transcription factor program. Development (Cambridge, England), 139(1), 179–190. http://doi.org/10.1242/dev.071134

Stepien, A. E., & Arber, S. (2008). Probing the locomotor conundrum: descending the "V" interneuron ladder. *Neuron*, *60*(1), 1–4. http://doi.org/10.1016/j.neuron.2008.09.030

Talpalar, A. E., Bouvier, J., Borgius, L., Fortin, G., Pierani, A., & Kiehn, O. (2013). Dual-mode operation of neuronal networks involved in left-right alternation. *Nature*, *500*(7460), 85–88. http://doi.org/10.1038/nature12286

Ullian, E. M., Sapperstein, S. K., Christopherson, K. S., & Barres, B. A. (2001). Control of synapse number by glia. *Science*, *291*(5504), 657–661. http://doi.org/10.1126/science.291.5504.657

Umbach, J. A., Adams, K. L., Gundersen, C. B., & Novitch, B. G. (2012). Functional Neuromuscular Junctions Formed by Embryonic Stem Cell-Derived Motor Neurons. *PLoS One*, *7*(5), e36049. http://doi.org/10.1371/journal.pone.0036049

Van Vreeswijk, C., Abbott, L. F., & Ermentrout, G. B. (1994). When inhibition not excitation synchronizes neural firing. *Journal of Computational Neuroscience*, *1*(4), 313–321.

Vida, I., Bartos, M., & Jonas, P. (2006). Shunting inhibition improves robustness of gamma oscillations in hippocampal interneuron networks by homogenizing firing rates. *Neuron*, *49*(1), 107–117. http://doi.org/10.1016/j.neuron.2005.11.036

Wang, X.-J., & Buzsaki, G. (1996). Gamma Oscillation by Synaptic Inhibition in a Hippocampal Interneuronal Network Model. *The Journal of Neuroscience*, *16*(20), 6402–6413.

Whelan, P., Bonnot, A., & O'Donovan, M. J. (2000). Properties of rhythmic activity generated by the isolated spinal cord of the neonatal mouse. *Journal of Neurophysiology*, *84*(6), 2821–2833.

Wichterle, H., Lieberam, I., Porter, J. A., & Jessell, T. M. (2002). Directed differentiation of embryonic stem cells into motor neurons. *Cell*, *110*(3), 385–397.

Wichterle, H., & Peljto, M. (2008). Differentiation of mouse embryonic stem cells to spinal motor neurons. *Current Protocols in Stem Cell Biology*, *Chapter 1*(May), Unit 1H.1.1–1H.1.9. http://doi.org/10.1002/9780470151808.sc01h01s5

Xu, H., & Sakiyama-Elbert, S. E. (2015). Directed Differentiation of V3 Interneurons from Mouse Embryonic Stem Cells. *Stem Cells and Development*, *24*(22), 2723–2732. http://doi.

org/10.1089/scd.2015.0122

Xue, M., Atallah, B. V., & Scanziani, M. (2014). Equalizing excitation–inhibition ratios across visual cortical neurons. *Nature*, *511*(7511), 596–600. http://doi.org/10.1038/nature13321

Zhang, J., Lanuza, G. M., Britz, O., Wang, Z., Siembab, V. C., Zhang, Y., Velasquez, T., Alvarez, F., Frank, E., & Goulding, M. (2014). V1 and V2b interneurons secure the alternating flexor-extensor motor activity mice require for limbed locomotion. Neuron, 82(1), 138–150. http://doi.org/10.1016/j.neuron.2014.02.013

Zhang, Y., Narayan, S., Geiman, E., Lanuza, G. M., Velasquez, T., Shanks, B., Akay, T., Dyck, J., Pearson, K., Gosgnach, S., Fan, C., & Goulding, M. (2008). V3 spinal neurons establish a robust and balanced locomotor rhythm during walking. Neuron, 60(1), 84–96. http://doi.org/10.1016/j.neuron.2008.09.027

Zhong, G., Sharma, K., & Harris-Warrick, R. M. (2011). Frequency-dependent recruitment of V2a interneurons during fictive locomotion in the mouse spinal cord. *Nature Communications*, *2*, 274. http://doi.org/10.1038/ncomms1276

Chapter 3

Future directions and conclusions

Future directions and conclusions

Introduction

Chapter 1 set up the introduction to the developmental patterning of the spinal cord. Chapter 2 demonstrated novel *in vitro* techniques used to investigate the locomotor CPG found within the ventral horn of the spinal cord. In this chapter, I will discuss the benefits of the new experimental designs described in Chapter 2, and how they can be used or manipulated to further investigate the development and function of neural networks. Some of the ideas set out below have been inspired by experiments conducted throughout the course of setting up this new experimental system, but due to timing have not been followed up. Others are put forth as exciting new directions for the current system, now that it is working robustly. All paths, however, expand upon the work described in Chapter 2 and delve into fundamental neurobiological questions.

Neuronal subtype mixing

As discussed in Chapter 2, V1 interneurons increase the speed of V3 networks, but uncouple motor neuron networks. The next obvious set of experiments would be to mix additional cell types. One future mix should be MN+V3 networks. As networks of motor neurons do not significantly increase in rhythmicity when evoked, might adding V3 interneurons to motor neuron networks allow these networks to become rhythmic? Is there a critical threshold of V3 interneurons needed to invoke rhythmic activity in the motor neuron networks? To answer these questions, different numbers of V3 interneurons should be added to networks composed of 100,000 motor neurons.

Furthermore, in V3+V1 networks, uncoupling of neurons was demonstrated to be very difficult, even at a 1:1 ratio. To investigate how few V3 interneurons are necessary to synchronize a network, V1+V3 networks should be tested. Here, 100,000 V1 interneurons would compose the base network to which different numbers of V3 interneurons would be added. Such a design would result in very low E/I ratios, from which, I hypothesize, would allow the network to become uncoupled similarly to what occurs at higher E/I ratios in MN+V1 networks.

Finally, MN+V3+V1 networks should be investigated. I would initially plan to use 50,000 of each motor neurons and V3 interneurons to have a base network of 100,000 excitatory neurons. To these networks I would add V1 interneurons in the same number used in Chapter 2. I believe two main outcomes could be hypothesized from this experiment, and it is not clear which would actually occur. One, the V3 interneurons would synchronize the entire network, such that the V1 interneuron addition would increase network speed, as if the network was composed of just V3 interneurons, instead of both V3 interneurons and motor neurons. Such a result would suggest that the influence of the V1 interneurons onto motor neurons is overridden by the excitatory drive motor neurons receive from V3 interneurons, thus maintaining motor neuron synchrony. Separately, it is entirely possible, and I think more interesting, that in an MN+V3+V1 network, different layering would exist, such that the addition of V1 interneurons would increase the rate of network activity, but at the same time segregate the activity of the motor neurons. This result would suggest that the interconnectivity of V3 interneurons is very strong, preventing their activity from being uncoupled by the V1 interneurons, as previously shown in V3+V1 networks. But, at the same time, such a result would suggest that the synaptic strength of V3 interneurons onto motor neurons is weaker than the influence of V1 interneurons onto motor neurons, such that the V1 interneurons would still uncouple the activity of motor neurons.

The three mixing experiments laid out here – MN+V3, V1+V3, and MN+V3+V1 – are those that I believe follow most logically from the work described in Chapter 2 and are the most compelling to investigate. However, I do acknowledge that this set of experiments it is far from an exhaustive list. Additional experiments would include mixing other spinal interneuron subtypes not discussed here, such as V2a and V2b interneurons. Furthermore, knowing that network activity differs dramatically in the spinal cord when compared to the hippocampus or cortex, it would also be interesting to design networks with hippocampal or cortical neurons.

Kebab

An experiment used to look at the propagation of activity through the network involved a different technique, which I called the kebab. Here, heterogeneous neurospheres, after their 6 day

differentiation, were threaded onto a thin wire such that they were in tight contact with each other. After culturing this kebab for ten days, the neurospheres fused together to form one coherent network. This kebab was then loaded with calcium dye, similarly to the individual neurospheres, and then imaged. Bursts of activity can be seen to travel down the network, taking about 1.6 sec from one end to the other, a distance of around 16 mm, suggesting an approximate 10 mm/sec propagation rate (Figure 3.1).

This experiment was conducted prior to the time I generated the designer network protocol. One interesting set of experiments would be to do this kebab assay with neurospheres of pure excitatory neuronal subtypes. The data collected thus far would suggest that motor neurons have weaker synaptic connections than the V3 interneurons. For this reason, one might hypothesize that kebabs formed with V3 interneurons would have an increased propagation rate compared to kebabs composed of motor neurons. However, it should be noted that motor neurons are known for their long projecting axons. Perhaps this would allow for fewer synaptic relays to be needed in order to propagate the burst from one end of the kebab to the other.

Following along with the idea that axon projection length determines the burst propagation rate of a network, Matthew Pankratz, a post-doc in our lab has shown that young neurospheres have robust neurite outgrowth, but that older ones do not (Figure 3.2). I would hypothesize that with this limited axonal outgrowth, much slower propagation rates would be seen in a kebab composed of older neurospheres than one composed of younger neurospheres due to the increased need of synaptic relays.

Finally, while testing propagation rate, myelination is obviously something to consider. In purified cultures, there should be no oligodendrocytes. If oligodendrocyte precursor cells (OPCs) were added to these cultures, would they differentiate? If they do, would the oligodendrocytes myelinate the axons in the kebab? To test if this myelination was functionally relevant in this system, propagation rates could be tested. If myelination does increase the propagation rate, one could see using this *in vitro* system to study many aspects of myelination.

Microislands

One fundamental question about how the locomotor CPG generates rhythmic output is

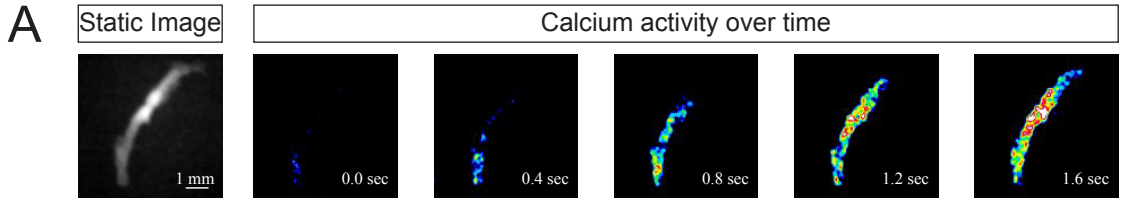

Figure 3.1 Kebabs demonstrate propagation of network activity
(A) Neurospheres were threaded onto a wire and fused into a coherent network, as seen in the static fluorescent image. After about 1.6 sec network activity is shown to propagate from one end of the network to the other.

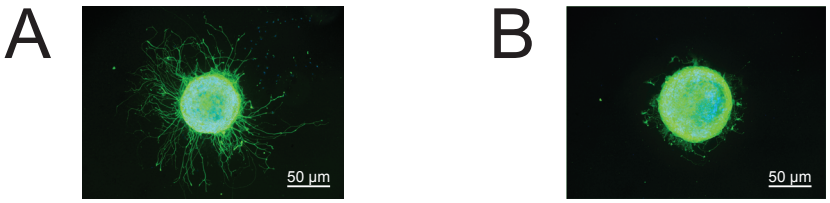

Figure 3.2 Younger neurospheres have higher outgrowth capability than older neurospheres
(A) Neurosphere plated on a coverslip shows a high degree of outgrowth when plated after 7 days of differentiation. (B) Dramatically less outgrowth is observed in the neurosphere plated after 21 days of differentiation. Both neurospheres were plated for one day prior to fixation and imaging. Green fluorescence is a tau:GFP transgene, labeling the axons of all neurons.

whether there is a pacemaker cell that drives the network. While the answer to this question has been long sought, the current consensus is that the rhythmicity is due to a converging network, not an individual neuron or neuronal subtype (Harris-Warrick, 2010). However, there has, to this point, been no way to prove this belief. But we could finally answer this question by using microislands (Allen, 2006; Furshpan, MacLeish, O'Lague, & Potter, 1976), a technique that allows for culturing networks composed of a small numbers of neurons. By plating purified neuronal subtypes on these microislands we would be able to determine if rhythmicity was possible in a network of a small number of neurons or even one neuron and whether neuronal subtype identity mattered.

We conducted this experiment once, using purified V3 interneurons, as we know that larger networks composed of V3 interneurons were capable of generating rhythmic activity. Unfortunately, only two microislands were successfully formed. One microisland had one neuron and another had two. Their activity differed greatly, though neither demonstrated rhythmic activity in the evoked condition (Figure 3.3). Many questions from this one experiment arose. Did the difference in these two microislands result from one or two neurons comprising the network? Or was the activity simply random variation? Or could it be, despite both microislands being composed of V3 interneurons, that the neurons were different subtypes of V3 interneurons – a possibility discussed in Chapter 2? We know large networks of V3 interneurons are capable of generating rhythmic activity, so does the fact that these two networks composed of one or two neurons suggest an answer? Certainly more experiments need to be conducted, but I believe these results are a strong indication that rhythmicity truly is an emergent network property, not capable of being consistently reproduced in these small networks. If this hypothesis is true, we are lead to ask how many V3 interneurons are sufficient for generating robust rhythmic activity. Data presented here combined with the findings in Chapter 2 (Figure 2.6b) suggest that number is between 2 neurons and 5,000 neurons.

Spinal Cord Injury

Spinal cord injury repair through stem cell or progenitor cell transplant has become a hotbed of research recently (Falnikar, Li, & Lepore, 2015; Tso & McKinnon, 2015). We

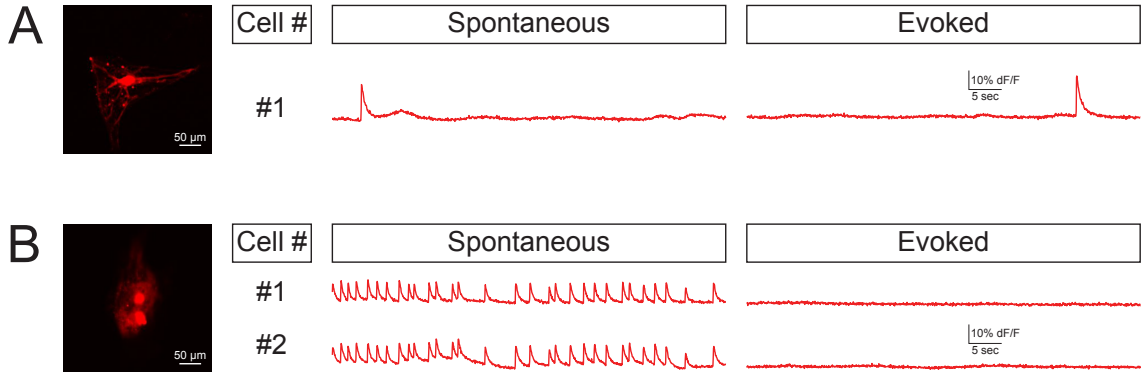

Figure 3.3 Microislands can be used to generate small neuronal networks
(A,B) Microislands with one or two neurons. The activity of all cells in the spontaneous and evoked condition is shown.

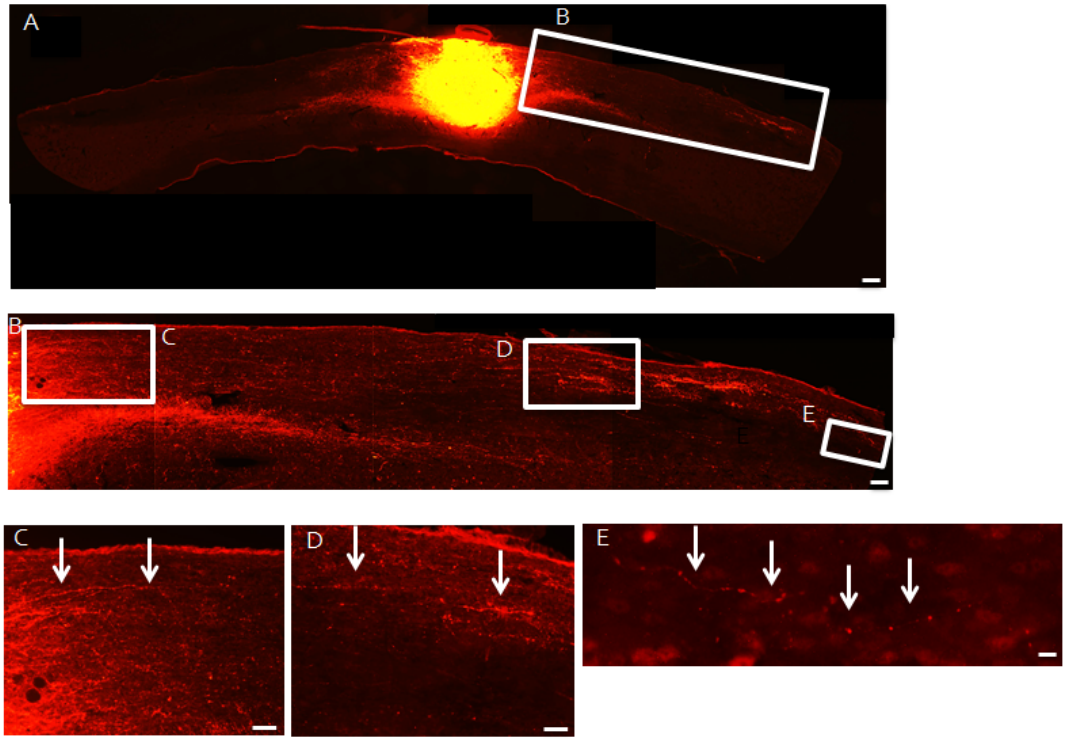

Figure 3.4 Cells derived from mESCs successfully fill lesion in SCI animal
(A) Longitudinal section of a spinal cord injury engraftment with cells differentiated from an Olig2:Cre;R26/C:LSL:Tomato mESC line. (B) Magnified region shown in A. (C-E) Magnified regions of interest shown in B. Scale bar: 250µm (A), 100µm (B), 50µm (C,D), 25µm (E).

conducted one experiment in which we, in collaboration with the Tuszynski lab, dissociated day 6 neurospheres of a Olig2:Cre;LSL:Tomato mESC line and injected the cells into a C4 dorsal column wire knife lesion. As Olig2:Cre labels almost the complete ventral horn of developing mouse embryos (Chen et al., 2011), this mESC line labels roughly 98% of the cells generated when differentiated with 1000 nM SAG (data not shown). As can be seen, the graft is brightly fluorescent, and axons extend outward from the graft (Figure 3.4). Unfortunately, one can also see that the cells that were injected into the spinal cord also enlarged the injury due their massive proliferation.

Our new experimental sorting paradigm will allow us to sort post-mitotic neurons into these injury models instead of injecting all of the cells present at day 6. This sorting will be incredibly useful in preventing over-expansion within the graft, as the neurons will no longer proliferate. Not only will the non-proliferation of these neurons prevent increased damage to the graft, but they will also dramatically decrease the risk of unwanted tumor formation (Lee, Tang, Rao, Weissman, & Wu, 2013). Furthermore, by injecting specific neuronal subtypes into experimental animals, it will be possible to determine if one specific neuronal subtype is better than another at promoting recovery from spinal cord injury. It may also demonstrate a need for a mixture of neuronal subtypes, not just one. This is a question that cannot be answered with the current protocols due to the fact that the injected stem cells and progenitor cells differentiate somewhat haphazardly.

CRISPR Screening

Finally, CRISPR, the recently discovered, powerful genetic manipulation technique, provides an easy and efficient way to screen for genes necessary for the network formation and function described in Chapter 2 (Gaj, Gersbach, & Barbas, 2013). For instance, are gap junctions important for these networks? Gap junction pharmacology is notoriously bad due to off-target effects (Juszczak & Swiergiel, 2009), but by using serial application of CRISPR, most, if not all, of the gap junction proteins found in neurons could be deleted in mESCs. Once generated, these mESC lines could be differentiated into neurons and formed into networks to assess the role of gap junctions in network function.

An additional question we had about our system, though never got around to answering, was what role synaptic recognition proteins played in the development of the network. Again, CRISPR could be used to mutate cell adhesion molecules after which network function could be assessed. Not only would this type of work be interesting in a network composed of pure neuronal subtypes, but I believe it has the potential to be even more intriguing in mixed cultures because it may be possible to find molecules that are necessary for V3-V1 connections but not V3-V3 connections. If such a molecule exists, one may find that a mixed V3+V1 network would behave similarly to a pure V3 network if that molecule was mutated, as the V1 interneurons would no longer be able to influence the base V3 networks. Obviously other possible combinations could be explored, as well. And while we have no preliminary data on using CRISPR in this system, CRISPR is incredibly robust, so it is highly expected that the combination of CRISPR with this newly described designer network protocol would provide great insight into the development and function of neuronal networks.

Conclusion

In this chapter I have set out numerous avenues that follow up experiments detailed in Chapter 2. Some are simply an added layer to the experiments conducted in that chapter, while others ask very different questions, though all still revolve around the core principle of the thesis: the development and function of the locomotor central pattern generator. It is my hope that others will use the novel experimental paradigms I have created during my graduate career to answer these questions and many others not addressed here.

References

Allen, T. G. J. (2006). Preparation and maintenance of single-cell micro-island cultures of basal forebrain neurons. *Nature Protocols*, *1*(6), 2543–50. http://doi.org/10.1038/nprot.2006.394

Chen, J.-A., Huang, Y.-P., Mazzoni, E. O., Tan, G. C., Zavadil, J., & Wichterle, H. (2011). Mir-17-3p controls spinal neural progenitor patterning by regulating olig2/irx3 cross-repressive loop. *Neuron*, *69*(4), 721–35. http://doi.org/10.1016/j.neuron.2011.01.014

Falnikar, A., Li, K., & Lepore, A. C. (2015). Therapeutically targeting astrocytes with stem and progenitor cell transplantation following traumatic spinal cord injury. *Brain Research*, *1619*, 91–103. http://doi.org/10.1016/j.brainres.2014.09.037

Furshpan, E. J., MacLeish, P. R., O'Lague, P. H., & Potter, D. D. (1976). Chemical transmission

between rat sympathetic neurons and cardiac myocytes developing in microcultures: evidence for cholinergic, adrenergic, and dual-function neurons. *Proceedings of the National Academy of Sciences of the United States of America*, *73*(11), 4225–4229. http://doi.org/10.1073/pnas.73.11.4225

Gaj, T., Gersbach, C. A., & Barbas, C. F. (2013). ZFN, TALEN, and CRISPR/Cas-based methods for genome engineering. *Trends in Biotechnology*, *31*(7), 397–405. http://doi.org/10.1016/j.tibtech.2013.04.004

Harris-Warrick, R. M. (2010). General principles of rhythmogenesis in central pattern generator networks. *Progress in Brain Research*, *187*, 213–22. http://doi.org/10.1016/B978-0-444-53613-6.00014-9

Juszczak, G. R., & Swiergiel, A. H. (2009). Properties of gap junction blockers and their behavioural, cognitive and electrophysiological effects: animal and human studies. *Progress in Neuro-Psychopharmacology & Biological Psychiatry*, *33*(2), 181–98. http://doi.org/10.1016/j.pnpbp.2008.12.014

Lee, A. S., Tang, C., Rao, M. S., Weissman, I. L., & Wu, J. C. (2013). Tumorigenicity as a clinical hurdle for pluripotent stem cell therapies. *Nature Medicine*, *19*(8), 998–1004. http://doi.org/10.1038/nm.3267

Tso, D., & McKinnon, R. D. (2015). Cell replacement therapy for central nervous system diseases. *Neural Regeneration Research*, *10*(9), 1356–1358. http://doi.org/10.4103/1673-5374.165209

Methods

Chapter 1 Methods

Chapter 1 does not contain experimental data.

Chapter 2 Methods

Mouse lines

The generation and genotyping of the En1::Cre, Chx10::Cre, Hb9::GFP, and Sim1::Cre alleles in mice has previously been described (Azim, Jiang, Alstermark, & Jessell, 2014; Gosgnach et al., 2006; Lee, Jurata, Funahashi, Ruiz, & Pfaff, 2004; Sapir et al., 2004; Zhang et al., 2008). The R26/C:LSL:Tomato and R26/C:LSL:DTA lines were obtained from Jackson Laboratory (007905 and 010527, respectively). Transgenic CAG::GCaMP3 mice were generated by using restriction enzymes to cleave the promoter+reporter fragments from the bacterial plasmid, and injecting the purified DNA into mouse oocyte pronuclei. After microinjection, founders were genotyped by PCR with the GFP primers and screened for ubiquitous presence of GCaMP3. All experiments were done in accordance with Institutional Animal Care and Use Committee animal protocols.

Deriving embryonic stem cells lines

Blastocysts flushed 3.5 days after fertilization using M2 media (MR-015-D, Millipore). Each individual blastocyst is placed in one well of a 96-well plate containing primary mouse embryonic fibroblasts (pMEF - GlobalStem) with 2i media (SF016-100, Millipore). After 5 days of incubation, the 2i media is aspirated and each hatched blastocyst is dissociated using accutase and passaged to one well of a 24-well plate with pMEF and 2i media. Colonies are visible after one or two days. Every second passage with accutase decreases the concentration of 2i media from 100% to 75%, 50%, 25% and finally to 0% with FCS media [Knockout DMEM (Life Technologies), 1X HEPES (Life Technologies), 1X non-essential amino acids (Life Technologies), 200 mM L-glutamine (Life Technologies), 10% ES-qualified fetal bovine serum (Millipore), 0.1 mM β-mercaptoethanol (Sigma), 1,000-2,000 units of leukemia inhibitory factor (LIF) (Calbiochem), 1X Antibiotic-Antimycotic (Life Technologies)] making up the other

fraction. After colonies have been established, mESCs are passaged as needed using 0.25% trypsin (Life Technologies) and plated into FCS media. At times, 2x the concentration of LIF was used to improve mESC colony morphology.

Differentiation of embryonic stem cells

mESCs are differentiated in suspension in 10 cm petri dishes. $1x10^6$ dissociated mESCs are resuspended in 10 ml ADFNK media [Advanced D-MEM/F-12 (Life Technologies): Neurobasal medium (Life Technologies) (1:1), 10% Knockout Serum Replacement (Life Technologies), 200 mM L-Glutamine (Life Technologies), and 0.1 mM β-mercaptoethanol (Sigma)]. Two days later, embryoid bodies (EBs) were allowed to settle to the bottom of a 15 mL conical tube. Media was aspirated, and a third to a tenth of the EBs were transferred to a new 10 cm plate with fresh ADFNK media that was supplemented with 1 μM all-trans retinoic acid (RA, Sigma) and 5 nM to 1000 nM smoothened agonist (SAG, Calbiochem). Two days later, freshly supplemented media was exchanged (Peljto, Dasen, Mazzoni, Jessell, & Wichterle, 2010; Wichterle, Lieberam, Porter, & Jessell, 2002; Wichterle & Peljto, 2008). On day 6, if to be used for sorting, heterogeneous neurospheres were maintained in non-supplemented ADFNK media. If used for imaging, heterogeneous neurospheres were switched to a neuronal media [Neurobasal medium (Life Technologies), 2% ES-qualified fetal bovine serum (Millipore), 200 mM L-Glutamine (Life Technologies), 1X B-27 supplement (Life Technologies), L-glutamic acid (Sigma), 1X Antibiotic-Antimycotic (Life Technologies), 10 ng/ml Human Brain Derived Neurotrophic Factor (BDNF, Peprotech 450-02) and 10 ng/ml Recombinant Murine Glial-Derived Neurotrophic Factor (GDNF, Peprotech 450-44)]. Half the media was exchanged 3 times a week until activity was recorded. Activity of these heterogeneous networks, unless otherwise noted, was recorded 15-17 days from mESC.

Fluorescent activated cell sorting

Neurospheres, 6-11 days from mESCs, were dissociated (Papain, Worthington), and then counted with a BD FACScan to determine the percentage of neurons composing neurospheres at different SAG concentrations. For sorting and generating purified networks, the BD FACSDIVA

and BD Influx were used to sort neurons into low-adherent, u-bottomed 96-well dishes (Corning 7007).

Astrocyte preparation

To derive cortical astrocytes for reaggregated *de novo* networks we used a similar protocol to McCarthy and DeVellis procedure described previously, adapted for mice (Ullian, Sapperstein, Christopherson, & Barres, 2001). P0-P3 mouse cortices were dissected and dissociated (Papain, Worthington). They were grown in a T-75 flask for 3-4 days with AGM media [DMEM + GlutaMAX (Life Technologies), 10% ES-qualified fetal bovine serum (Millipore), 1 mM Na-Pyruvate (Life Technology), 5 µg/ml insulin (Sigma – I1882), 5 µg/ml n-acetylcysteine, 1 µM hydrocortisone (Sigma – H0888), 1X Antibiotic-Antimycotic (Life Technologies)]. Following a 1X PBS wash, contaminating cells were shaken off and then the media was exchanged. 1-3 days later, once confluent, 10 µM AraC (Sigma – 1768) was added and subsequently removed two days later with three washes with 1x PBS. To use, cells were dissociated in 0.05% Trypsin (Life Technologies). For astrosphere formation 50,000 astrocytes were placed in each well of a 96-well ultra-low adherent u-bottomed plate (Corning – 7007) and spun at 300g to aggregate the cells. If compact spheres were not formed 24 hours later, light trituration was used to break the aggregate apart, and then the plate was respun. For plated assays, 100,000 astrocytes per 100-200 µl were plated onto the glass coverslip of the 35 mm dish (Corning 354077) for two hours. After cell adhesion, an additional 2 ml of AGM media was added to the dish. At times, to aid in adherence, prior to plating the astrocytes, dishes were recoated with 100 µg/ml poly-d-lysine (Sigma P6407) or 100 µg/ml laminin (Life Tech 23017-015). Neurons were plated onto astrospheres or confluent astrocytes 2-4 days after astrocyte dissociation.

Generation of highly defined *de novo* networks

To generate reaggregated neurospheres, differentiated heterogeneous neurospheres were dissociated between days 6 and 11 and specific neuronal subtypes were sorted directly into a well of a 96-well ultra-low adherent u-bottomed plate (Corning – 7007). After sorting, these plates

were spun to pellet the neurons. FACS sheath was removed without disrupting the loose pellet at the bottom of the well and neuronal media was added back. 2 more washes were conducted, combining wells if necessary (some experiments would have caused wells to overflow during FACS if neurons for one network were not split between multiple wells). For sphere assays, the neurons were resuspended and transferred into a well of a u-bottomed 96 well plate that was already filled with an astrosphere. These plates were now spun to increase contact of neurons and astrosphere. The following day, light trituration was used to remove any debris from the main reaggregated neurosphere. A few smaller satellite neurospheres may have also formed, so the plate was spun once more. 24 hours later, all of the neurons and astrocytes formed one coherent neurosphere. All of the media was carefully removed from the cells and new media was added. Unless otherwise noted, the designer spheres were incubated for 3 weeks after FACS before their network activity was imaged, with half of their media being exchanged 3 times a week. For plated networks, the AGM from the 35 mm dish was aspirated sufficiently to dry the plastic surrounding the 10 mm coverslip, and then media on the coverslip was aspirated. Neurons for each network were resuspended in 100-200 µl of neuronal media and plated onto the confluent astrocyte layer. After two hours the neurons had adhered and 2 ml of neuronal media were added to the 35 mm dish. The plated networks were incubated for 2 weeks after FACS before their network activity was imaged, with half of their media being exchanged 3 times a week.

Optical and electrical recording

Calcium signal was recorded using either a ubiquitously expressed GCaMP3 (CAG::GCaMP3) or Oregon Green 488 BAPTA-AM (Life Technologies). For dye application, dye was applied at 10 µM in ACSF (128 mM NaCl; 4 mM KCl; 21 mM $NaHCO_3$; 0.5 mM NaH_2PO_4; 1 mM $MgSO_4$; 30 mM D-glucose; and 2 mM $CaCl_2$) for 1 hour in a 37 °C incubator. Dye was washed out with perfusion of ACSF for 15 minutes prior to recording. Unless otherwise stated, image series were acquired on an upright epifluorescent Olympus microscope (BX51WI) using a Hamamatsu C9100-13 camera and ImageJ plugin: µManager software, capturing 20 frames/second at 128x128 using a 4x 0.28 NA air objective (Olympus) with a 0.63x camera mount, and an X-Cite exacte light source at 2% power. For Figure 2.12d, e, and f, cellular

resolution data of plated networks was acquired at 512x512 using a 20x 1.0 NA water-immersion objective (Olympus) with a 0.63x camera mount. Electrical activity was recorded using a suction electrode with a multiclamp 700B amplifier, filtered at 300 Hz to 1 kHz.

Pharmacology of network activity

Drugs used were in the following final concentrations: 20 μM N-Methyl-DL-aspartic acid (NMA Sigma M2137 – discontinued, 10 μM NMDA M3262 equivalent), 40 μM serotonin creatinine sulfate monohydrate (5-HT, Sigma H7752), 50 μM dihydro-β-erythroidine hydrobromide (DHβE, Tocris 2349), 10 μM mecamylamine hydrochloride (MLA, Tocris 2843), 10 μM CNQX disodium salt (Tocris 1045), 1 μM strychnine hydrochloride (Sigma S8753), and 10 μM picrotoxin (Sigma P1675).

Immunohistochemistry

Neurospheres were fixed in 4% PFA for an hour and then washed in 1x PBS and prepared for cryosectioning. Cryosections (60 μm) were stained in 1x PBS containing 1% BSA and 0.1% triton with NeuroTrace® 640/660 Deep-Red Fluorescent Nissl Stain (Life Technologies N-21483), DAPI, and rabbit anti-GFAP (1:500, Dako).

Data analysis

Data was exported from ImageJ using the ROI manager after manually drawing regions of interest around neurospheres. For plated networks, ROIs were drawn around individual neurons (cellular analysis), or the full or partial field of view (network analysis). Burst detection was carried out by in Igor (TaroTools, Dr Taro Ishikawa, https://sites.google.com/site/tarotoolsregister) or a custom pipeline generated in R.

To analyze network complexity, movies were processed as 8 bit greyscale and resized to 128×128 pixels and saved as TIFF stacks from ImageJ. TIFF stacks were imported into R with the tiff library for analysis. For initial threshold settings a single, randomly drawn 11x11 pixel oval ROI was used. 400 randomly drawn ROIs were used for analysis. The pixels in the ROIs were averaged over time to create intensity versus time signals. All signals were high-pass

filtered at 0.1 Hz and smoothed with a Savitzky-Golay filter with of length 11 samples (about 0.5 seconds). After smoothing signals were z-transformed by normalizing them to their own high-frequency noise by finding the residual variance of the signal after high-pass filtering at 1 Hz (all bursting was at frequencies < 1 Hz). Pre-processed ROIs were blindly filtered to remove signals that appeared to be noise. Intensity versus time signals have very normal distributions in the absence of bursting so signals were tested with the Jarque-Bera test for normality and signals with probability values > 0.05 were discarded. Burst position calling was preformed by convolving signals with an exponential kernel and applying a threshold. Signal to noise levels and bursting patterns were highly variable between movies so a single threshold level was selected manually for each movie using a single random ROI.

Burst positions were identified in 400 random ROIs from each sample. All identified bursts within a sample were collapsed into a single catalog of bursts. Bursts occurring within 1 second of each other were considered the same burst. Each ROI signal was redescribed as a binary vector with 1's indicating which of the catalog bursts were present. A directed graph was constructed from the binary ROI vectors to map out all of the burst-to-burst connections. The vertices of the graph were distinct bursts and edges were valid burst-to-burst occurrences within the signals. Vertices or edges appearing in less than 4% of ROIs were filtered out. The complexity of the graph is proportional to the variability of bursting patterns across the ROI signals so a few simple metrics were extracted from the graph as a base measurement: average number of outgoing edges from each vertex, average number of incoming edges to each vertex, total number of "start" vertices, total number of "end" vertices, ratio of vertices with outgoing edges, ratio of vertices with incoming edges. "Start" and "end" vertices are those that appear to never have incoming or outgoing edges, respectively. Higher numbers of incoming and outgoing edges per vertex imply the presence of variable bursting patterns whereas a graph where all vertices are connected but none have more than 1 incoming or outgoing edge indicates a single bursting pattern.

Graph metrics were collected from all samples and checked for cross correlations. We found that these metrics were highly correlated with one another but to avoid basing the statistical comparison on only one or on all of them, which may be redundant, we instead transformed

them with PCA which revealed a single significant principal component capturing all of the input measurements. A small set of samples had been manually categorized into two groups: those with a single bursting pattern and those with variable bursting patterns across ROIs. Using the manually categorized samples as a training set and the scores for PC1 as predictors we created a logistic regression model to predict variable bursting pattern versus a single bursting pattern on the remaining samples. Response values from the logistic model were compared between groups with the two-sample Kolmogorov-Smirnov test. Each group was compared more than one time so post-hoc correction was applied to all p-values to control for false discovery rate.
All other data was calculated using a student t-test.

Chapter 3 Methods

Kebab

Differentiation of Sim1:Cre;R26/C:LSL:Tomato #2 mESC line was conducted in 400 nM SAG for 6 days. At this time, about 35 neurospheres were threaded onto a wire. For the next 8 days, while being maintained in neural media, the neurospheres fused to form one long network. The network was carefully transferred to a separate 35 mm dish and was covered in calcium indicator dye and then the calcium activity was then imaged (see Chapter 2 methods).

Microislands

Coverslips were coated with 0.02% agarose dissolved in water (Sigma type IIa: #A-9918). A thin layer of agarose was applied to each coverslip and allowed to dry in the hood under the UV-light overnight. Then, using 1:100 collagen (Corning: 354236) and 1:100 poly-D-lysine hydrobromide (Sigma: P6407) were mixed in water. Using a vaporizer this mixture was sprayed onto the agarose coated coverslips and allowed to dry. Astrocytes were then dissociated (see Chapter 2) and 100,000 cells per well were added to the coverslip in a 24-well plate. Two days later, Sim1:Cre;R26/C:LSL:Tomato #6 neurospheres were dissociated after 10 days of differentiation with 1000 nM SAG. From these dissociated neurospheres 100,000 V3 interneurons were sorted into the well. After 20 days, the coverslip was removed from the 24-

well plate, put into a 35 mm petri dish and 200 ul of calcium indicator dye in ACSF was added to the coverslip prior to network activity being imaged (see Chapter 2 methods).

SCI injury

A 2 cm long incision of the skin was made with a scalpel and the skin and underlying tissue retracted to expose the spinal column. A partial laminectomy was made at the level of C4, exposing the spinal cord. Both sides of the dorsal column were cut by lowering the stereotax-mounted wire knife 0.5mm below the dorsal surface and then retracting the knife upward. After making the lesion, cells were injected directly into the spinal cord lesion site through pulled micropipettes (inner diameter 80 µm) using a Picospritzer (general Valve Corp) delivering approximately 20 nl aliquots per pulse. Cells from an Olig2:Cre;R26/C:LSL:Tomato mESC line, after 6 days of differentiation, were dissociated with accutase and then injected into the graft after being resuspended at a concentration of 200,000 cells/µl in a fibrin matrix (25mg/ml fibrinogen and 25U/ml thrombin) containing growth factors to support graft (Lu et al., 2012). Subject was allowed to survive 4 weeks. The animals were then perfused with 4% paraformaldehyde in 0.1M phosphate buffer and the spinal cord was dissected for histology.

References

Azim, E., Jiang, J., Alstermark, B., & Jessell, T. M. (2014). Skilled reaching relies on a V2a propriospinal internal copy circuit. *Nature*, *508*(7496), 357–363. http://doi.org/10.1038/nature13021

Gosgnach, S., Lanuza, G. M., Butt, S. J. B., Saueressig, H., Zhang, Y., Velasquez, T., Riethmacher, D., Callaway, E., Kiehn, O., & Goulding, M. (2006). V1 spinal neurons regulate the speed of vertebrate locomotor outputs. Nature, 440(7081), 215–219. http://doi.org/10.1038/nature04545

Lee, S.-K., Jurata, L. W., Funahashi, J., Ruiz, E. C., & Pfaff, S. L. (2004). Analysis of embryonic motoneuron gene regulation: derepression of general activators function in concert with enhancer factors. *Development*, *131*(14), 3295–3306. http://doi.org/10.1242/dev.01179

Lu, P., Wang, Y., Graham, L., McHale, K., Gao, M., Wu, D., Brock, J., Blesch, A., Rosenzweig, E., Havton, L., Zheng, B., Conner, J., Marsala, M., & Tuszynski, M. H. (2012). Long-distance growth and connectivity of neural stem cells after severe spinal cord injury. Cell, 150(6), 1264–1273. http://doi.org/10.1016/j.cell.2012.08.020

Peljto, M., Dasen, J. S., Mazzoni, E. O., Jessell, T. M., & Wichterle, H. (2010). Functional Diversity of ESC-Derived Motor Neuron Subtypes Revealed through Intraspinal Transplantation. *Cell Stem Cell*, *7*(3), 355–366. http://doi.org/10.1016/j.stem.2010.07.013

Sapir, T., Geiman, E. J., Wang, Z., Velasquez, T., Mitsui, S., Yoshihara, Y., Frank, E., Alvarez, F., & Goulding, M. (2004). Pax6 and engrailed 1 regulate two distinct aspects of renshaw cell development. The Journal of Neuroscience, 24(5), 1255–1264. http://doi.org/10.1523/jneurosci.3187-03.2004

Ullian, E. M., Sapperstein, S. K., Christopherson, K. S., & Barres, B. A. (2001). Control of synapse number by glia. *Science*, *291*(5504), 657–661. http://doi.org/10.1126/science.291.5504.657

Wichterle, H., Lieberam, I., Porter, J. A., & Jessell, T. M. (2002). Directed differentiation of embryonic stem cells into motor neurons. *Cell*, *110*(3), 385–397.

Wichterle, H., & Peljto, M. (2008). Differentiation of mouse embryonic stem cells to spinal motor neurons. *Current Protocols in Stem Cell Biology*, *Chapter 1*(May), Unit 1H.1.1–1H.1.9. http://doi.org/10.1002/9780470151808.sc01h01s5

Zhang, Y., Narayan, S., Geiman, E., Lanuza, G. M., Velasquez, T., Shanks, B., Akay, T., Dyck, J., Pearson, K., Gosgnach, S., Fan, C., & Goulding, M. (2008). V3 spinal neurons establish a robust and balanced locomotor rhythm during walking. Neuron, 60(1), 84–96. http://doi.org/10.1016/j.neuron.2008.09.027